AFIT/GAE/ENY/93D-12

AD-A273 775

DTIC
ELECTE
DEC 16 1993
S A

INFLUENCE OF EMBEDDED OPTICAL FIBERS ON COMPRESSIVE STRENGTH OF ADVANCED COMPOSITES

THESIS

Stefan B. Dosedel
Captain, USAF
AFIT/GAE/ENY/93D-12

93-30409

93 12 15 029

Approved for public release; distribution unlimited

Best
Available
Copy

AFIT/GAE/ENY/93D-12

INFLENCE OF EMBEDDED OPTICAL FIBERS ON COMPRESSIVE STRENGTH OF ADVANCED COMPOSITES

THESIS

Presented to the Faculty of the Graduate School of Engineering

of the Air Force Institute of Technology

Air University

In Partial Fulfillment of the

Requirements for the Degree of

Master of Science in Aeronautial Engineering

Stefan B. Dosedel, B.S.M.E.

Captain, USAF

December 1993

Accesion For	
NTIS CRA&I	☑
DTIC TAB	☐
Unannounced	☐
Justification	
By	
Distribution /	
Availability Codes	
Dist	Avail and / or Special
A-1	

Approved for public release; distribution unlimited

Preface

The primary purpose of this study was to investigate the effects of embedding optical fibers into an advanced composite material. This integrated structure combining the optical fibers and composite materials has been the focus of extensive research in the past ten years and has been termed a "smart structure". This moniker is the result of the optical fibers' ability to successfully sense a multitude of variables within the composite structure including stress, strain, temperature, and damage. The work involved in this study was limited purely to compression testing of an AS4/3501-6 (graphite/epoxy) laminate embedded with several variations of optical fiber size, number, and orientation within the structure. Results showed that it is possible to embed the optical fibers in several different variations so that overall strength of the structure is not effected.

My sponsor, Captain Mike Holl and his assistant Tom Witman, of the Materials Laboratory, provided the mainstay of my information and materials. Mike guided me in the right direction when I got off-track, and Tom was instrumental in laying-up, cutting, and tabbing the six panels (over 150 specimens), and generally helping in any way he could. His eager assistance and helpfulness was always a bright spot on a bad day.

The personnel in the AFIT Laboratory must be recognized for their overwhelming patience and understanding. Mark Derriso, Jacob Roush, and Rob Flinn spent an enormous amount of time showing us over, and over, and over how to run the material test systems, place strain gages on specimens, take pictures, etc. without a single audible complaint. Thanks again, Mark, but when are those strain gages getting in?!

My advisor, Dr. Shankar Mall, always kept me on my toes with his daily visits through the laboratory and must share a great deal of praise for his patience. His understanding and guidance were one of the key ingredients to me completing this

project, while his routine visits kept my feet to the fire. Additional thanks must go to Dr. Torvik, and Major Robinson for their feedback and review of this project.

Although numerous individuals were extremely helpful in assisting me in this project, none were more supportive than my wife Virginia. Although she was undergoing a very stressful and demanding pregnancy for most of this time, her help in keeping me on track and allowing me the time to work unhindered was tremendously generous. I couldn't have gotten this far without her. Happily, she also provided the newest member of our family, Michael, just before this project was completed.

Table of Contents

Preface ii

List of Figures vi

List of Tables viii

Abstract ix

I. Introduction 1

1.1 Background 1
1.2 Problem Statement/Scope 4
1.3 Approach 9

II. Previous Research and Models 11

2.1 Macromechanical Research 12
2.2 Micromechanical Research 15
2.3 Optical Fiber Coatings 18
2.4 Compression Response 19
2.5 Fiber Waviness 21
2.6 Compression Test Fixture 22
2.7 Classical Laminated Plate Theory 23

III. Testing Preparation and Procedures 27

3.1 Specimen Background and Preparation 27
3.2 Test Equipment 41
3.3 Test Procedure 44

IV. Results 47

4.1 Panel 1 - Results and Discussion 50
4.2 Panel 2 - Results and Discussion 56
4.3 Panel 3 - Results and Discussion 62
4.4 Panels 4 and 5 - Results and Discussion 69
4.5 Panel 6 - Results and Discussion 77

V. Discussion 81

5.1 Optical Fiber Parallel to Structural Fibers 81

5.2 Optical Fiber Perpendicular to Structural Fibers 84
5.3 Adhesion 89

VI. Conclusions and Recommendations 92

Appendix A: Calculations for Laminate Euler Buckling Stress 91

Appendix B: Calculations for Classical Laminated Plate Theory 93

Appendix C: Failure Theory Output from GENLAM 98

Appendix D: Test Data 107

Bibliography 115

Vita 119

List of Figures

Figure 1 - Fiber Optic Parallel to Surrounding Fibers 5
Figure 2 - Fiber Optic Perpendicular to Surrounding Fibers 6
Figure 3 - Laminate 1A 32
Figure 4 - Laminate 1B 32
Figure 5 - Laminate 2A 33
Figure 6 - Laminate 2B 33
Figure 7 - Laminate 3A 34
Figure 8 - Laminate 3B 34
Figure 9 - Laminate 4A 35
Figure 10 - Laminate 5A 35
Figure 11 - Laminate 6A 36
Figure 12 - Laminate 6B 36
Figure 13 - Control Laminates (90 Degree Center) 37
Figure 14 - Control Laminates (0 Degree Center) 37
Figure 15 - Autoclave Cure Cycle 38
Figure 16 - Specimen and Laminate Configurations 40
Figure 17 - Test Equipment 42
Figure 18 - IITRI Fixture 43
Figure 19 - Typical Specimen after Compressive Failure 48
Figure 20 - Typical Specimen after Compressive Failure 49
Figure 21 - Panel 1 Test Results 52
Figure 22 - Matrix Crack in 90° Ply 54
Figure 23 - Intact Area surrounding Optical Fiber 54
Figure 24 - Stress-Strain Curve of Panel 1 Control Group 55
Figure 25 - Stress-Strain Curve of Panel 1 Central Fiber Optic Group 55
Figure 26 - Stress-Strain Curve of Panel 1 Outer Fiber Optic Group 56
Figure 27 - Panel 2 Test Results 58

Figure 28 - Failed Outer Plies of Outer Fiber Optic Laminate 60
Figure 29 - Typical Failure Pattern around Optical Fiber 60
Figure 30 - Stress-Strain Curve of Panel 2 Control Group 61
Figure 31 - Stress-Strain Curve of Panel 2 Central Fiber Optic Group 61
Figure 32 - Stress-Strain Curve of Panel 2 Outer Fiber Optic Group 62
Figure 33 - Panel 3 Test Results 64
Figure 34 - Intact Area around Optical Fiber 66
Figure 35 - Failed Area around Optical Fiber 67
Figure 36 - Stress-Strain Curve of Panel 3 Control Group 67
Figure 37 - Stress-Strain Curve of Panel 3 Two Optical Fiber Group 68
Figure 38 - Stress-Strain Curve of Panel 3 Three Optical Fiber Group 68
Figure 39 - Panel 4 Test Results 71
Figure 40 - Panel 5 Test Results 72
Figure 41 - Failed Outer Plies of Two Fiber Group 73
Figure 42 - Failure Progression in "resin eye" around Optical Fiber 74
Figure 43 - Failure Progression in "resin eye" around Optical Fiber 74
Figure 44 - Stress-Strain Curve of Panel 4 Control Group 75
Figure 45 - Stress-Strain Curve of Panel 4 Two Optical Fiber Group 75
Figure 46 - Stress-Strain Curve of Panel 5 Control Group 76
Figure 47 - Stress-Strain Curve of Panel 5 Three Optical Fiber Group 76
Figure 48 - Panel 6 Test Results 78
Figure 49 - Failed Area Surrounding Optical Fiber 79
Figure 50 - Intact Area Surrounding Optical Fiber 80
Figure 51 - Normalized Strength of Parallel Optical Fibers 83
Figure 52 - Normalized Strength of Perpendicular Optical Fibers 85
Figure 53 - Matrix Cracks in "resin eye" 87
Figure 54 - Adhesion of Optical Fiber Coating to Epoxy Matrix 90
Figure 55 - Adhesion of Optical Fiber Coating to Epoxy Matrix 90

List of Tables

Table 1- Testing Configuration 8

Table 2 - Computed Laminate Properties 25

Table 3 - GENLAM Predicted Ultimate Compression Strengths 26

Table 4 - Material Data for AS4/3501-6 Prepreg 27

Table 5A - Laminates Tested 29

Table 5B - Laminates Tested 30

Table 6 - Fiber Volumes of Each Panel 39

Table 7 - Panel 1 Test Data 51

Table 8 - Panel 2 Test Data 57

Table 9 - Panel 3 Test Data 63

Table 10 - Panels 4 and 5 Test Data 70

Table 11 - Panel 6 Test Data 77

Abstract

This study has investigated the effects of embedding optical fibers on the compressive strength of advanced composite materials. A 30-ply lay-up consisting of 40 percent 0° plies, 20 percent 90° plies, and 40 percent ±45° plies was fabricated from Hercules AS4/3501-6 prepreg tape to simulate a structure taken from an actual aircraft. Optical fibers of 125 μm and 240 μm outer diameter and with polyimide coatings were embedded perpendicular to the load, but either parallel or perpendicular to the immediately surrounding structural composite fibers. This latter orientation resulted in what is called a "resin eye" due to the resin rich region produced by bridging the structural composite fibers over the optical fiber.

Six different panels were fabricated with varying number of optical fibers, optical fiber diameters, optical fiber locations, and optical fiber orientations with respect to structural fibers. This resulted in sixteen groups of specimens (ten embedded with optical fibers and six without optical fibers to act as controls). Each group contained ten specimens that were compressively loaded in an IITRI fixture at a constant cross-head displacement of 0.021 mm/s until failure as recommended by ASTM D3410-87. The maximum load obtained was used to calculate the ultimate compressive strength of each specimen. Three specimens from each group were tested to obtain modulus data by placing strain gages on opposite faces of each specimen. This data was collected on a personal computer and used to plot stress-strain curves from which modulus values were calculated.

Results showed that embedding optical fibers can either have no effect or significantly reduce the compressive strength of the structure. No change in modulus was seen in any of the groups. All specimens where the optical fiber was placed parallel to surrounding fibers resulted in no degradation of the average compressive strength of

the specimens. This was the case for one, two, and three 240 μm diameter optical fibers embedded in this orientation. The greatest strength reduction was 27% in specimens where two 240 μm optical fibers were placed across the gage length of the specimen and perpendicular to surrounding structural fibers. In this case, one optical fiber was located in the specimen midplane while the other was located four plies in from an outer surface resulting in an asymmetric condition about the midplane. Other variations of specimens with optical fibers perpendicular to the load resulted in less dramatic results and in some cases did not affect the compressive strength of the specimen.

Adhesion effects of polyimide coatings were seen to contradict some previous findings. Previous studies had reported failure of the coating between the coating/composite matrix interface. In this study, however, all failures occurred between the coating/optical fiber core interface.

The resin rich region in the "resin eye" was seen to develop matrix cracks that presumably led to the delamination of surrounding plies and ultimately led to failure of the specimen.

The results of this study reveal that it is possible to embed optical fibers without affecting either the compressive strength or the modulus of an advanced composite structure.

INFLUENCE OF EMBEDDED OPTICAL FIBERS ON COMPRESSIVE STRENGTH OF ADVANCED COMPOSITES

I. Introduction

1.1 Background

The use of composite materials in the aerospace industry is ever increasing. These materials are quickly overtaking metals as the primary source of new materials in aircraft structures in order to meet performance requirements beyond the capabilities of metals, improve productivity of a system, or reduce the cost of manufacture. In fact, the past three generations of military aircraft have used increasing amounts of composite materials. It is estimated that composites will account for half the structural weight of the Advanced Tactical Fighter (ATF), which represents the next generation [1].

The very high specific strength and stiffness of composite materials can result in significant reductions in aircraft structural weight. The importance of this characteristic cannot be overstated in combat aircraft. It effects all aspects of performance; particularly turn rate, climb rate, acceleration, range, and payload. In general, a 1% reduction in overall aircraft weight can yield an increase in specific excess power of 1%, an increase in subsonic sustained turn rate of 1%, and an increase in supersonic sustained turn rate of .5% [2]. Composite materials can achieve mass savings on the order of 9-30 percent [2]. It is expected that composite materials will eventually replace the more traditional alloys of aluminum, iron and titanium in aircraft structures.

Despite the weight advantages of composite materials, current use in aerospace applications has been limited by several factors: overdesign to compensate for scatter in

material properties, lack of confidence in design analysis methods, and possible undetected damage and delaminations of the composite structure. Current Air Force monitoring of aircraft structures is conducted through the Aircraft Structural Integrity Program (ASIP) in accordance with MIL-STD-1530A and MIL-A-87221. These standards require that composite structures tolerate a certain visible defect, delaminations of a certain minimum area, or impact damage of certain dent size or impact energy. However, failure analysis of these defects is not fully developed or understood [3]. As a result, very conservative designs are employed to account for these unknowns. ASIP requires that the usage of each aircraft be continuously monitored. This information is used to schedule periodic non-destructive evaluations (NDE) of the aircraft structures to ensure that no significant damage has occurred. Current NDE techniques (Ultrasonic C-Scan, X-ray, etc.) are very expensive and not completely accurate methods of testing flight worthiness of composites. There are currently no reliable field test systems for this nondestructive testing. Therefore, this NDE results in reduced readiness, increased life-cycle costs, and longer vehicle turnaround time.

Because of these problems Air Force damage tolerance design methodology requires aircraft to be designed with assumed initial flaws. This results in overdesign, added structural weight, conservative inspection intervals, and labor intensive inspections. This decreases operational readiness, increases costs, and in some cases can even cause damage to the composite structures. Until these problems are resolved, aircraft designers are bound to limit their use of these new, lightweight and high strength composite materials.

In an attempt to resolve the problems of composite design and develop improved material systems, considerable research has been conducted over the past five years in the area of "smart structures." Smart structures have been defined as the

integration of sensors, actuators, processors, and other elements into an architecture of structural materials. This new technology offers the potential to revolutionize composite structures by offering the means to (1) accurately monitor internal environmental properties of composite materials during manufacture, (2) provide sensors for parts and assemblies that will augment nondestructive evaluation techniques, (3) allow health monitoring and damage assessment of composite materials within aerospace and industrial products, and (4) enable control systems to actively monitor and react to changes in a structure's environment.

Smart structures technology will effect all areas of composite material usage. Researchers are currently investigating the use of smart structures in buildings to prevent earthquake damage, in medical prosthesis materials like artificial organs to replace systems operated by external control, and artificial intelligence and robotics applications to replace software and electric circuits [4].

In relation to the aerospace industry, smart materials have the capability for increased strength to weight ratio by reduction in design margins, reduced scheduled maintenance and periodic inspections by continuous monitoring of structural integrity, reduced manufacturing costs by closed loop process control, increased quality by monitoring material properties during manufacture, and added value by multiple uses of the embedded sensors [5]. Once integrated into an aircraft, smart structure systems are envisioned to have the ability to do multiple tasks: determine flight worthiness; measure structural dynamic response, monitor light loads and damage growth, assess battle damage, compute residual strength, advise pilots on flight restrictions, and provide the ground crew with flight load histories, structural integrity and even required repairs [6]. A report published in Australia estimated that implementation of this technology could benefit aircraft with 30% payload increase, 50% longer range, or 30% increase in maneuverability [7].

To date, the most promising results in the smart structures arena have been provided with the embedment of optical fibers into composite materials. Optical fibers are small, light-weight, resistant to corrosion and fatigue, immune to electrical interference, and compatible with composites [8]. Their geometric versatility and small size have meant that they can be easily placed into composite structures. Fiber optics have been shown to effectively measure force, pressure, bending, density change, temperature, electric current, magnetic fields, and changes in chemical composition [4]. Theoretically, they are ideal for eliminating any current doubts and shortcomings about the use of composite materials in aerospace structures.

1.2 Problem Statement/Scope

In order for smart structures to be widely accepted into aircraft structures, it must be shown that the inclusion of the optical fiber does not lead to degradation of the material properties of the composite (tensile and compressive strength, fatigue life, modulus of elasticity, etc.). To date several studies have evaluated the response of simple composite laminates embedded with optical fibers to mechanical loads. However, no experimental data has been published concerning fiber optics embedded in advanced composite materials currently being used in aircraft structures.

Research conducted by Measures [9] shows that particular sensor applications for smart structures have optimal orientations within the composite structure. For strain and temperature sensing, optical fibers should be mounted between two collinear plies and aligned with the reinforcing fibers of the composite. Conversely, damage sensors with the optimum sensitivity should be embedded as close to the surface as possible and be sandwiched orthogonally between a pair of collinear plies. Strain and damage sensing capabilities are two of the most important features that would be used in smart aircraft structures.

In addition to providing the optimal sensing functions for an aircraft structure, the above orientations (optical fiber parallel to surrounding fibers and optical fiber perpendicular to surrounding fibers) also give the least and most obtrusive cases of sensor embedment.

For the optical fiber parallel to the surrounding composite fibers, all fibers are aligned in the same orientation. This allows the fiber optic to be accepted very easily into the framework of the composite structure. During the composite cure cycle, the resin flows around the optical fiber and conforms to its shape. In this case the optical fiber can be seen to act as an inclusion much greater in diameter than the composite fibers (240 μm versus 8 μm). Ply thickness for these laminates was a nominal 210 μm which is sligthly less than the 240 μm diameter optical fiber. Figure 1 shows this optical fiber orientation.

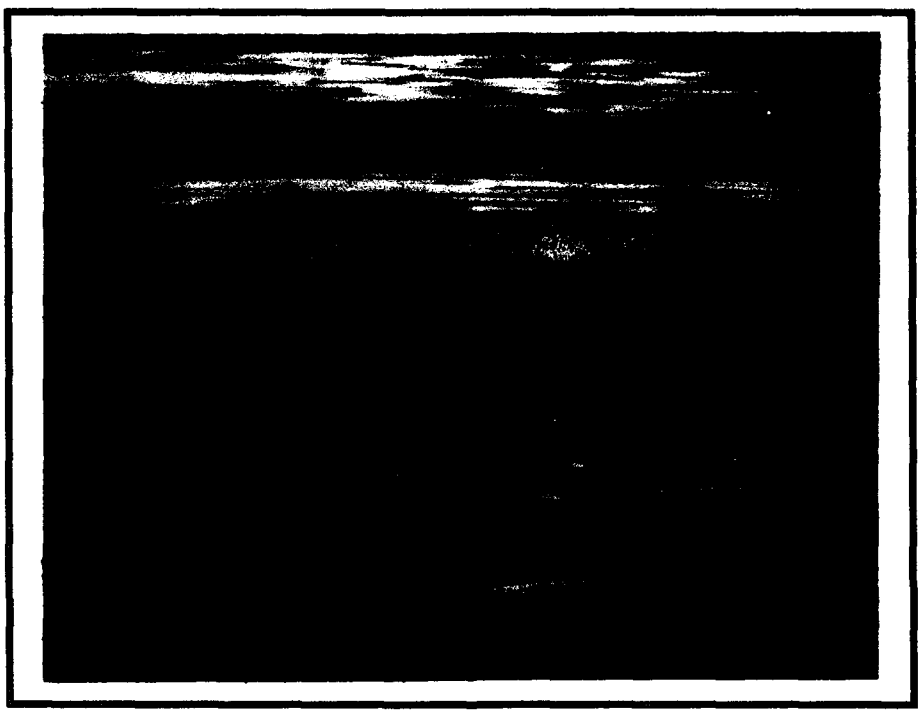

Figure 1 - Fiber Optic Parallel to Surrounding Fibers

When the optical fiber is oriented in a perpendicular fashion to adjacent reinforcing fibers in a composite, a much more obtrusive configuration is developed. A resin rich area ("resin eye") is generated when the reinforcing fibers are forced to bridge over the fiber optic. This not only creates a large area of relatively weak resin but also causes the surrounding reinforcing fibers to be deformed in a wavy pattern in the vicinity of the fiber optic. This initial fiber waviness means that the fibers are essentially prebuckled and could be susceptible to premature compressive failure. Figure 2 shows this resin rich area and fiber waviness.

Figure 2 - Fiber Optic Perpendicular to Surrounding Fibers

There have been very few studies on the effects of this orientation on the compressive strength characteristics of laminates. Studies by Claus [11], Measures [12], Jensen and Pascual [13,14], Roberts and Davidson [15], and Holl and Boyd [16]

have been completed; however all were done under very simple cases of laminate design and generally only used unidirectional or crossply laminates. To date there have been no published reports on compressive strength effects on any quasi-isotropic or advanced composites that are commonly used in aerospace structures. This study was undertaken to fill that void.

The composite laminate modeled in this experiment was taken from an actual aircraft structure flying in the Air Force inventory. It contains 30 plies (layers) of AS4/3501-6 (graphite/epoxy) prepreg material which contains 40 percent 0° plies, 20 percent 90° plies, and 40 percent ±45° plies. Lay-ups containing these orientations of structural fibers are commonly used in aircraft structures to allow the composite to withstand the various flight loading conditions.

Compression response of composite structures is the least understood and most important property of composites. Improvements in tensile strength and stiffness have generally outdistanced compression properties; however, compression loading is the most critical aspect of structural loading. As a result, smart structure technology will provide substantial benefit to the understanding of compression response of composite materials.

In order to provide the most comprehensive test data, several different configurations of specimens were devised. Variables included in this experimental setup included optical fiber diameter, number of optical fibers, optical fiber location within the composite structure, and fiber optic orientation relative to the surrounding composite structural fiber. Table 1 on the following page shows the test configurations used in this study.

Table 1- Testing Configuration

Configuration	Number of Fiber Optics	F.O. Direction Relative to Load	F.O. Direction Relative to Graphite Fiber	F.O. Size (μm)	F.O. Location
1-Control	0	N/A	N/A	N/A	N/A
1-Center	1	Perpendicular	Perpendicular	240	Center
1-Outer	1	Perpendicular	Perpendicular	240	Outer
2-Control	0	N/A	N/A	N/A	N/A
2-Center	1	Perpendicular	Parallel	240	Center
2-Outer	1	Perpendicular	Parallel	240	Outer
3-Control	0	N/A	N/A	N/A	N/A
3-Two Fiber	2	Perpendicular	Perpendicular	240	Cen/Out
3-Three Fiber	3	Perpendicular	Perpendicular	240	O/C/O
4-Control	0	N/A	N/A	N/A	N/A
4-Two Fiber	2	Perpendicular	Parallel	240	Cen/Out
4-Three Fiber	3	Perpendicular	Parallel	240	O/C/O
5-Control	0	N/A	N/A	N/A	N/A
5-Two Fiber	2	Perpendicular	Parallel	125	Cen/Out
5-Three Fiber	3	Perpendicular	Parallel	125	O/C/O

Remarks:

1. Fiber Optic locations for configurations with two fibers were placed eccentrically about the midplane of the laminate. One fiber was located between two collinear outer plies while the other fiber was placed between two collinear plies in the midplane of the laminate.

2. Fiber Optic locations for configurations with three fibers were placed symmetrically about the midplane of the laminate. One fiber was located in the midplane of the laminate while the remaining two fibers were placed on either side of the midplane in outer plies.

1.3 Approach

Optical fibers of 125μm and 240μm diameter were embedded into a 30 ply lay-up of AS4/3501-6 (graphite/epoxy) composite panel. Five different panels with different optical fiber orientations, locations, densities, and sizes were fabricated and cut into 114.3 mm x 6.35 mm (length x width) specimens for compression testing. The gage section of each specimen was 12.7 mm to preclude Euler buckling. Each panel generated three groups of specimens (two with optical fibers and one without to act as a control group) for a total of fifteen specimen groups (ten fiber optic and five control). Fiberglass tabs were placed with epoxy to each of the specimens.

An Illinois Institute of Technology Research Institute (IITRI) compression fixture was used to conduct the static compression testing. Each group had a minimum of ten specimens that were compressively loaded in the IITRI fixture until failure. The load at failure was obtained for each test to determine the ultimate compressive strength of each specimen.

Strain gages were placed on a minimum of three specimens in each group to collect stress-strain data. Data obtained from the strain gages was used to calculate the longitudinal modulus of elasticity of the specimen. The gages were placed on both sides of the specimen to determine if fiber optic location, orientation, or density had any effect on the modulus of elasticity. This data was also used to determine if global Euler buckling was occurring. In determining the modulus of elasticity only the initial linear loading portion of the curve was used (0.1 to 0.3 percent strain).

Several additional specimens from each group were polished to obtain micro-photographs of the test section. These specimens were then incrementally loaded and viewed under a microscope to determine where crack initiation and initial damage

occurred. Specimens were loaded until failure and again micro-photographed to assist in determining the modes of failure.

Systematic investigation of the results obtained from these different analyses were used to explain and substantiate the observed effects of the optical fibers on the compressive response of a practical laminate employed in the aerospace industry.

II. Previous Research and Models

Investigation into mechanical and material aspects of embedding optical fibers into composite materials has essentially fallen into two areas: trying to understand the effects from a macromechanical (laminate) viewpoint, and trying to model the system via a micromechanical method. This chapter will review previous studies in both these areas of smart structure analysis. For more in-depth analysis covering a very broad realm of research conducted on smart structures, a recent article by Carmen and Sendeckyj [10] is recommended. This paper covers a comprehensive review of research conducted in the area of optical fiber embedment into composite materials and is recommended to provide information not fully pertinent to the research conducted by this study.

The macromechanical approach studies the structural behavior of the smart structure using laminated plate theory (discussed in Section 2.7). In this method, the properties of the structural fiber, matrix, and optical fiber are combined to form the laminate properties. Results are concerned with the smart structure's overall properties and do not identify any interactions between the composite material and the embedded optical fiber.

Micromechanical studies, on the other hand, have focused on establishing the local interaction of host composite and embedded optical fiber. This method utilizes effective ply properties as functions of the structural fiber, matrix, and optical fiber properties. Finite element method (FEM) analysis and Moiré Interferometry are often used to predict stress and strain concentrations within the composite and especially at the interface between the composite and optical fibers.

Compression testing of composite materials is the least understood of the material properties. In compression testing there are so many variables that effect the

overall strength of a specimen that the failure mode is often impossible to characterize. In addition, there are several different compression test fixtures and methods that are utilized to conduct these tests, each with their own method of load application to achieve compression failure. There has been extensive research in this area to attempt the understanding of compression failure, but it is still far from being completely explored. Several pertinent research efforts will be reviewed to give a general background into compression failure and testing techniques associated with this study.

Finally, this chapter will use laminated plate theory to attempt to predict the material properties of the composite specimens used in this experiment. This analysis will assist in analyzing data from the tests and will be correlated with the test data to further study the failure modes. A commercially available computer program, GENLAM, will also be used to predict the overall strength of the specimens, and, again compared with the test data.

2.1 Macromechanical Research

Several research efforts have been undertaken using the macromechanical approach to determine the effects of embedding optical fibers into composite materials. The two most common tests that have been employed for these composites are determining ultimate tensile strength and ultimate compressive strength of the fiber optic embedded structure. Tensile testing has generally produced consistent results, whereby, the smart structure has shown little or no degradation regardless of optical fiber size, orientation, or number of optical fibers embedded. Compression testing, on the other hand, has produced widely differing results depending on the optical fiber's diameter, coating material, orientation, and density. A review of these previous studies follows.

One of the first documented smart structure mechanical tests was conducted by Claus et al [11]. They reported an increase in the longitudinal strain to failure and a decrease in transverse strain to failure of graphite/epoxy specimens with different numbers of 125 μm optical fibers. The optical fiber was embedded parallel to the loading direction; however, the other test information (methods, stacking sequence, and optical fiber coating material) was not discussed.

Measures et al [12] conducted both tensile and compressive testing of Kevlar/epoxy laminates. Both test setups used 125 μm optical fibers perpendicular to surrounding fibers. Tension tests on 4 ply, 0° laminates indicated that the tensile strength is not compromised by the presence of embedded optical fibers. Compression tests on 8 ply, 90° laminates with 3 optical fibers also gave similar results. Measures concluded that the presence of embedded optical fibers had a negligible influence on the strength of the material.

Jensen and Pascual [13, 14] have conducted several series of tests in both tension and compression. Various configurations were fabricated with different quantities of optical fibers and locations relative to surrounding composite fibers. Graphite/Bismaleimide (Gr/BMI) composite prepreg tape was used with 250 μm acrylate coated optical fibers. In tension, strength and stiffness reductions of less than 5% were observed for every case but one. Results fell within the standard deviations except for the configuration with 2 optical fibers perpendicular to both the load and surrounding fibers. They concluded that optical fibers embedded at various orientations and low volume fractions only slightly reduce the tensile mechanical properties. In compression, strength and stiffness reductions ranged up to 70% and 20% respectively. Standard deviations for these tests were as high as 24% for the strength data. From this, Jensen and Pascual determined that compressive strength is sensitive to optical fiber orientation with respect to the loading direction. The greatest sensitivity and

strength reduction was determined to be when the optical fiber was placed perpendicular to both the load and the surrounding fibers.

Roberts and Davidson [15] did comprehensive testing on carbon/epoxy laminates and studied the effects of optical fibers on longitudinal and transverse tension, longitudinal compression, and interlaminar and in-plane shear. These studies concluded that small fibers (less that 100 μm) have little or no effect on longitudinal and transverse tension or in-plane and interlaminar shear. However, longitudinal compression strengths of two fiber optics placed perpendicular to the load are reduced by approximately 26%.

Holl and Boyd [16] presented studies on AS4/3501-6 with embedded optical fibers to provide corroborating evidence to the study Roberts and Davidson [15]. Optical fibers with 125 μm and 240 μm diameter and polyimide coatings were embedded in 0° compression, 90° tension, 8-ply quasi-isotropic tension, and first ply failure of cross-ply specimens. The optical fibers were placed in the midplane of the specimens both parallel and perpendicular to the loading direction. Tension tests on the 90° laminates showed a decrease in strength of up to 15% for the 125 μm fiber optic and a 14% decrease for the 240 μm fiber optic. Quasi-isotropic laminate strengths were not affected by either the size or the orientation of the fiber optic. Compression tests were inconclusive since the specimens did not fail in the gage sections. However, it was noted that all fracture surfaces were far from the fiber optic in the gage length.

As shown, the few studies that have been completed in this area are relatively inconclusive. The testing that will be completed in this document is meant to further the research that has already been accomplished and determine whether it is possible to embed optical fibers into advanced structural composites without degrading the material's strength characteristics.

2.2 Micromechanical Research

Micromechanical studies of smart structures have covered very diverse effects of the embedment of optical fibers into composite structures. Researchers have examined the distortions caused in the composite due to various orientations of the optical fiber relative to the surrounding structural fibers ("resin-eyes"). They have also investigated the local stress and strain concentrations introduced by placing the fiber optic in the host composite material through the use of Moiré Interferometry and finite element methods (FEM). Some research has been confined to the local interaction of the optical fiber properties and has concentrated on the adhesion between the optical fiber and the surrounding composite, effects of different optical fiber coating materials, and cure temperature effects on optical fibers.

As discussed in Chapter I, the orientation of the optical fiber relative to the surrounding structure can cause significant deformation of the composite. Since the optical fibers are significantly larger than the structural fibers (240 μm and 125 μm versus 8 μm in this case) this effect has been investigated by several researchers. The most comprehensive study to determine the size of the deformation was conducted by Dasgupta et al. [17]. They developed an analytical model to determine the length of the "resin eye" as a function of optical fiber diameter, embedment angle relative to the structural fibers, laminate stacking sequence, laminate stiffness, and processing parameters. The analytical model showed good agreement with experimental results, and, as would be expected, the largest deformation occurred for large diameter optical fibers oriented perpendicular to the surrounding fibers.

Leka and Bayo [18] investigated the waviness of structural fibers caused by the introduction of the optical fiber into a composite. Their results show that embedding an optical fiber parallel to structural fibers causes no local material perturbations. However, for an optical fiber oriented perpendicular to structural fibers, severe

perturbations in the geometry of the structural fibers occurred. Depending on the size of the optical fiber, this can cause perturbations that extend well into other plies.

Knowing that the introduction of the optical fiber affects the local geometry of the composite, several researchers have attempted to quantify the effects in terms of local stress and strain concentrations. These studies are discussed in the following paragraphs.

Czarnek [19] studied the surface strains on the edge of a cross-ply laminate subjected to uniaxial tension using Moiré Interferometry. Optical fibers were placed both perpendicular and parallel to surrounding fibers but always perpendicular to the load. It was demonstrated that a local strain concentration of approximately 4 times the far field values was seen on the optical fiber parallel to the surrounding fibers (no "resin eye"). Optical fibers perpendicular to surrounding fibers showed strain concentrations as great as 14.2 in the direction perpendicular to loading. However, as pointed out by Carmen and Sendeckyj [10], this high strain concentration is probably due to an extremely compliant coating on the optical fiber, which suggests that the stress concentration is actually small. Also, failure initiation occurs at the location parallel to the load where the measured strain is only 3.6 times that of the far field strain.

Salehi et al. [20] applied both Moiré Interferometry and the finite element method (FEM) to five graphite/epoxy laminates. One unidirectional and four cross-ply laminates were used with an optical fiber at the midplane of the laminate and perpendicular to the loading direction. For strain components parallel to the load, results generally agreed with those obtained by Czarnek and ranged from 2 to 4. Finite element method analysis strain concentrations of from 12.3 to 17.8 were measured for the case where the optical fiber was perpendicular to surrounding fibers. However, Moiré Interferometry analysis failed to provide similar results for this case. It was

suggested that the highest strain concentrations in the composite occurred in the optical fiber coating.

Singh et al. [21] investigated the strain distributions around optical fibers in a unidirectional laminate subjected to compression loading. Using Moiré Interferometry and several different optical fiber diameters and coatings, they obtained similar results to Salehi. Stress concentrations were shown to be a function of the optical fiber diameter.

Davidson and Roberts [22] conducted finite element analysis to predict stress concentrations around optical fibers embedded transversely to the reinforcement in unidirectional and cross-ply laminates. High strain concentrations were seen in the resin-rich area of the "resin eye" where the plies try to move apart in bending. In this area, peak stresses of 34% above applied stress occurs close to the fiber coating at the horizontal midplane. An area that extends over 3 fiber diameters away from this location has an increase in stress greater than 10%. Shear stresses resulting from compression loading are maximized along the region between the resin rich area and the composite fibers. It was shown that the physical size of the fiber and coating affect the stress concentration in the composite. The greater the separation between plies around the optical fiber, the greater are the bending moments experienced by the plies due to longitudinal loads. For an applied longitudinal compressive load, the longitudinal strain is low in the optical fiber in the resin rich area. The transverse strain, however, is dependent on the resin and fiber which act to bond the plies together. In general, stress concentrations in the composite are reduced for small optical fibers and stiff resins and are not significantly affected by the construction of the laminate lay-up.

2.3 Optical Fiber Coatings

Optical fibers are typically manufactured with glass cores and cladding of similar composition and with a protective coating of either metallic or organic composition. These coatings are generally used to prevent moisture absorption and improve ease of handling of the fibers. Once embedded in composites, however, these coatings introduce an added dimension to micromechanical analysis. Several studies have been conducted that concentrate solely on the optical fiber coating materials and how this effects local performance of the smart structure.

Coatings used on optical fibers embedded in composites are typically polyimide or acrylate organic materials. These coatings have a wide range of property values depending on the particular type used. Several studies [23, 24, 25] have shown that some of these coatings begin to decompose at the elevated temperatures needed to cure composites. Polyimide coatings were seen to have the most resistance to high temperature cure cycles of the composites.

The optical fiber coating must not only survive the composite cure cycle, but, once embedded, must be able to transfer the desired sensing function (strain, stress, temperature, etc.) from the composite to the optical fiber. This requires good adhesion, not only between the composites and coating material, but also between the coating and optical fiber. DiFranca and Claus [26] attempted to study adhesion related issues between optical fibers and epoxy resins. They suggested that debonding could occur at either the matrix/coating interface or the coating/optical fiber interface. They also noted that matrix cracking occurred around the optical fiber. Roberts and Davidson [15] investigated adhesion properties of both acrylate and polyimide coatings. It appeared that acrylate coatings did not adhere well to the optical fibers as compared to the polyimide coatings. Failure in the acrylate was between the coating and the optical fiber while failure in the polyimide was between the coating and the matrix. It was also

suggested that the stiffer polyimide coating had a greater potential to degrade the overall strength of the composite when compared to the more compliant acrylate coating.

2.4 Compression Response

Compression response of composites is the least understood phenomenon associated with these materials. Even though it has been the subject of investigation since the development of these materials, the usually instantaneous fracture has hampered efforts to completely identify the basic compression failure mechanisms.

It has been shown that many factors influence the compressive response of composite materials [27] which, acting together, can trigger a variety of failure modes. These factors occur at the structural level (coupon geometry), macrostructural level (lamina), and microstructural level (fiber/matrix). Local inhomogeneities and defects, manufacturing, lamina thickness, constituent properties, laminate orientations, specimen geometry, method of load introduction, fiber waviness, voids, and stress concentrations have all been shown to play a role in determining the predominant failure mode of composites in compression. Failure modes that have been identified include global Euler buckling, microbuckling, transverse tension, fiber kinking, fiber compression, matrix compression, and delaminations.

As shown above, compression failures can occur in a variety of ways and can be caused by a number of factors. This leads to an immense number of combinations that are far beyond the scope of this paper to explore. In order to limit the discussion to pertinent issues, several papers on compression testing of graphite/epoxy systems will be covered.

Colvin and Swanson [28] studied the compressive strength and failure of graphite/epoxy (AS4/3501-6) laminates. Seven different laminates representing 0°

dominated lay-ups, axial bias lay-ups, and quasi-isotropic lay-ups were tested. Non-linear stress-strain behavior became evident at high failure strains; however, when specimens were repetitively loaded and unloaded, the stress-strain response was determined to be elastic. Fiber kinking was observed in the failure zones which leads to the conclusion that fiber microbuckling is the governing failure. These tests were conducted using a cylindrical diameter test specimen which provided inherent resistance to global buckling failure modes.

Ha and Nairn [29] used several different graphite/epoxy material systems to test the compression failure mechanisms of single-ply unidirectional composites. The failure modes observed for most specimens were longitudinal splitting leading to fiber kinking. These kink bands were seen to propagate throughout the specimens to cause failure. However, since the failure of AS4/3501-6 was too rapid to allow observation of the earliest stages of compression damage, it could only be hypothesized that similar failure patterns occurred.

Sohi et al. [30] determined the failure initiation mechanism that governed all seven quasi-isotropic composite systems tested. This mechanism was determined to be fiber kinking in the 0° plies. They established a sequence of events that lead to final failure of quasi-isotropic graphite/epoxy laminates:

1. As compressive load increases, fiber kinking occurs in a 0° ply at an edge and propagates inward. The rotation of broken fiber segments in a kink band is both in and out of the plane of the 0° ply.

2. Failure of a 0° ply not only transfers the load to other plies but also results in load eccentricity since the specimen loses stiffness on the side of the failed ply. This enhances a sequential rather than random failure of the remaining 0° plies starting with the one closest to the failed ply and propagating inward.

3. A 0° ply with fiber kinking may move relative to neighboring angle plies. This brings about delamination between the failed 0° ply and the angle plies.

4. After delamination, the sublaminates are more susceptible to buckling than the original laminate because of thinner thickness and load eccentricity. The global buckling of sublaminates leads to final failure.

2.5 Fiber Waviness

Fiber waviness was discussed earlier as one of the factors that can initiate compressive failure. This has been a concern of researchers due to the inherent waviness of graphite fibers in composite structures. This waviness is significantly magnified when these structural fibers are forced to bridge around an optical fiber placed perpendicular to their direction.

Telegades and Hyer [31] studied the effects of fiber waviness on the compressive response of 27 cases of carbon/epoxy cross-ply cylinders. They determined that the wave causes an increase in the fiber compressive stress directly above the midplane of the wave. This waviness and associated increased stress level always caused a decrease in the predicted failure strength of the cylinder in all but the most benign cases. As the severity of the flaw increased (wavelength shortened and amplitude increased), the strength of the material decreased.

Adams and Hyer [32] reported on the effects of fiber waviness on specimens compressively loaded in an IITRI fixture. Laminates of carbon/polysulfone prepreg (T300/P1700) were made with wavy 0° plies at the midplane. Layer waviness was shown to produce strength reductions up to 36% although the wavy layers accounted for only 20% of the load carrying capacity of the laminate. Two parameters, wavelength divided by wave amplitude and maximum angle of fiber rotation are shown to characterize the severity of layer waviness.

2.6 Compression Test Fixture

ASTM Standard D3410-87 (Standard Test Method for Compressive Properties of Unidirectional or Crossply Fiber-Resin Composites) [33] suggests three allowable test fixtures for compression testing. These are the Celanese, the Illinois Institute of Technology Research Institute (IITRI), and the four point loading of a sandwich beam. The first two fixtures are two of the most commonly used for compression testing, however, researchers have shown that each fixture has its own advantages and disadvantages. The IITRI fixture was used in this testing due to its availability at AFIT.

The IITRI fixture applies compressive load through wedge grips that introduce shear loading through tabs adhesively bonded to the specimen. A gage length of 12.7 mm is recommended by ASTM D3410-87 to preclude failure by structural column buckling (Euler buckling). A test specimen of excessive slenderness ratio will fail by this method which is one of the drawbacks of using the IITRI fixture.

In order to determine the critical buckling stress for the specimens used in this testing, we must use a modification of the Euler buckling equation for an anisotropic material [34] :

$$P_{cr} = \frac{(\pi / L)^2 D_{11}}{1 + \frac{n(\pi / L)^2}{AG_{12}}} \tag{1}$$

In this equation, D_{11} is the flexural stiffness of the material, L is the gage length, A the cross-sectional area, G_{12} the shear stiffness in the direction of buckling, and n is a constant depending on the cross-section geometry (n = 1.2 in this case since the specimen has a rectangular cross-section). Using this equation a conservative buckling stress of 1151 MPa was calculated. (Appendix A). This is the stress that is required to cause global Euler buckling of the specimen and will be compared to the failure stress of the specimen calculated in the next section.

2.7 Classical Laminated Plate Theory

In laminated plate theory [35, 36, 37], the properties of the fiber and matrix are combined to give effective properties of individual layers (laminas). These layers are bonded together to form composite structures (laminates). In this study, 30 layers of prepreg tape are bonded together to form the laminate. There are a number of assumptions associated with classical laminated plate theory:

-- Individual layers are assumed to be homogeneous, orthotropic, elastic materials
-- Individual layers are assumed to be in a state of plane stress
-- Displacements follow a restrictive class according to Kirchoff assumptions, and
-- Individual layers are perfectly bonded to adjacent layers.

Equations of lamination theory relate in-plane forces and bending moments to midplane strains and curvatures of the laminate. This is done by defining material properties of the lamina, layer fiber orientation, layer thickness, and stacking sequence.

Since individual layers of a laminate are assumed to be homogeneous, elastic, and orthotropic materials, the following constitutive equation is defined:

$$\{\varepsilon\}_1 = [S]\{\sigma\}_1 \quad \text{where} \quad [S] = \begin{bmatrix} S_{11} & S_{12} & 0 \\ S_{21} & S_{22} & 0 \\ 0 & 0 & S_{66} \end{bmatrix} \tag{2}$$

where $\{\varepsilon\}_1$ is the strain in the principal material direction of the fibers, [S] is the compliance matrix, and $\{\sigma\}_1$ is the stress in the principal material direction of the fibers. This equation can be inverted to define the stiffness matrix, [Q], where $[Q]=[S]^{-1}$.

Individual terms of [S] can be expressed in terms of the material properties E_1, E_2, ν_{12}, and G_{12}. This results in the following equations:

$$S_{11} = \frac{1}{E_1}, \quad S_{12} = S_{21} = \frac{-\nu_{12}}{E_1}, \quad S_{22} = \frac{1}{E_2}, \text{ and } \quad S_{66} = \frac{1}{G_{12}}. \tag{3}$$

Components of [Q] can be expressed in terms of these same properties by inverting the compliance matrix, [S].

Stresses, strains and stiffness coefficients can be transformed into any arbitrary coordinate system related to the fiber orientation through any angle orientation. This generates a transformation matrix:

$$T = \begin{bmatrix} \cos^2\theta & \sin^2\theta & 2\cos\theta\sin\theta \\ \sin^2\theta & \cos^2\theta & -2\cos\theta\sin\theta \\ -\cos\theta\sin\theta & \cos\theta\sin\theta & \cos^2\theta - \sin^2\theta \end{bmatrix} \tag{4}$$

This allows us to obtain stress-strain relationships in the arbitrary coordinate system and yields:

$$\{\sigma\}_x = [\overline{Q}]\{\varepsilon\}_x \quad \text{where} \quad [\overline{Q}] = [T]^{-1}[Q][T]. \tag{5}$$

Applying forces and moments to a laminate generates both strains and curvature relationships. These are the fundamental equations of laminated plate theory:

$$\begin{Bmatrix} N \\ M \end{Bmatrix} = \begin{bmatrix} A & B \\ B & D \end{bmatrix} \begin{Bmatrix} \varepsilon^0 \\ \kappa \end{Bmatrix} \tag{6}$$

where N and M are applied forces and moments, ε^0 and κ are midplane strains and plate curvatures, and

$$[A] = \sum_{1}^{30} [\overline{Q}](z_k - z_{k-1}) \tag{7}$$

$$[B] = \frac{1}{2}\sum_{1}^{30} [\overline{Q}](z_k^2 - z_{k-1}^2) \tag{8}$$

$$[D] = \frac{1}{3}\sum_{1}^{30} [\overline{Q}](z_k^3 - z_{k-1}^3) \tag{9}$$

where z_k is the thickness of each ply.

For symmetric laminates about the mid plane, [B] is identically zero and there is no bending associated with applied loads. Therefore, as we are only applying loads and not moments in this testing:

$$\{N\} = [A]\{\varepsilon^0\} \tag{10}$$

This relationship can now provide expressions for the laminate material properties by applying the stress-strain relationship to obtain:

$$E_1 = \frac{A_{11} - A_{12}}{A_{22}h}\ ,\quad E_1 = \frac{A_{11}A_{22} - A_{12}}{A_{11}h}\ ,\quad \nu_{12} = \frac{A_{12}}{A_{22}}\ ,\text{ and }\ G_{12} = \frac{A_{66}}{h} \tag{11}$$

Using the properties given for AS-4/3501-6 given from Table 4 (Chapter III), the laminate material properties were computed using the preceding information. (Appendix B) and are shown in Table 2.

Table 2 - Computed Laminate Properties

Longitudinal Modulus(GPa)	E_1	74.10
Transverse Modulus (GPa)	E_2	49.67
Major Poisson Ratio	ν_{12}	.288
Minor Poisson Ratio	ν_{21}	.193
Shear Modulus (GPa)	G_{12}	19.33

A commercially available software package, which computes laminate properties and estimates failure strengths based on CLPT principles was also used for comparison with the above calculations. Printout from the GENeral purpose LAMinate program (GENLAM) [38] is contained in Appendix C. This program uses through-the-thickness point stress analysis for composite laminates and computes the stiffness and strength of symmetric and unsymmetric hybrid laminates subjected to complex in-plane loads and bending moments. As expected, results for the laminate stiffness properties are exactly the same as computed above. GENLAM has the capability to compute estimated ultimate strengths using three failure theories: Quadratic, Maximum Strain, and Fiber Failure. These calculations are done using an empirically derived matrix degradation model rather than the total discount method frequently used for this analysis. Tsai [38] recommends the use of the Quadratic Failure Theory as it gives easy application,

continuous extension to a last-ply-failure prediction, and systematic incorporation of residual stresses and hygrothermal stress. Results from all three failure theories are given in Table 3.

Table 3 - GENLAM Predicted Ultimate Compression Strengths

Quadratic Ultimate Compression Strength (MPa)	708.31
Maximum Strain Ultimate Compression Strength (MPa)	899.51
Fiber Failure Ultimate Compression Strength (MPa)	899.51

As can be seen from these predicted strength values, they are all well below the critical buckling stress (1151 MPa) computed in Section 2.6. This means that global Euler buckling should not be a concern in determining the initial mode of compression failure.

III. Testing Preparation and Procedures

The specimen preparation and test procedures are the most important aspects of this testing. Unless these factors are done within rigorous guidelines and repetitious procedures, accurate and uniform data will not be taken. As a result, a great deal of caution was taken in preparing the specimens and completing the testing procedures. This chapter outlines the steps taken to complete these efforts.

3.1 Specimen Background and Preparation

The material used was commercially available AS4/3501-6 (graphite/epoxy) prepreg tape from Hercules Inc. of Magna, Utah. Material data for this prepreg is shown in Table 4 [39].

Table 4 - Material Data for AS4/3501-6 Prepreg

Longitudinal Modulus of Elasticity (GPa)	E_1	145
Transverse Modulus of Elasticity (GPa)	E_2	10.6
Shear Modulus (GPa)	G_{12}	7.6
Poisson Ratio	ν_{12}	.27
Longitudinal Compressive Strength (MPa)	F_{1c}^u	1440
Transverse Compressive Strength (MPa)	F_{2c}^u	228
Shear Compressive Strength (MPa)	F_{12}^u	71
Longitudinal Compressive Strain (%)	ε_{1c}^u	1.41
Transverse Compressive Strain (%)	ε_{2c}^u	2.39
Shear Compressive Strain (%)	ε_{12}^u	.75

Optical fibers made by Polymicro Industries were used as the embedded fiber within the composite laminate. The optical fibers had been fabricated with a silica glass core, a germanium doped cladding, and a polyimide coating. Two different sizes of optical fibers were used in this testing: 125 μm and 240 μm nominal diameters. The larger fiber core had a nominal diameter of 200 μm, the cladding 220 μm , and the coating 240 μm. The smaller fiber core had a nominal diameter of 100 μm, the cladding 112 μm, and the coating 125 μm. The fibers were encased within the graphite/epoxy laminate to simulate possible sensor applications.

In order to get the most practical and usable results, several laminates were manufactured that would feasibly be used in a smart structure to measure desired stress and strain conditions or to sense whether damage had occurred in the structure. These two cases represent the two extremes of optical fiber embedment. The first case is the least obtrusive since the optical fiber is embedded parallel to structural fibers in the composite, while the second case is the most obtrusive where the optical fiber is embedded perpendicular to the structural fibers. This second case represents the case of "resin eyes" and structural fiber waviness in the area of the optical fiber. For smart structures with multiple sensing capabilities, several optical fibers would need to be placed in the cross-section. In order to simulate this condition, two and three optical fibers were embedded in the gage length. Other factors taken into consideration in this testing were size of the optical fiber and location relative to the midplane of the laminate. The two different sizes used represent the most likely application and availability of optical fibers for single and multi-mode sensing, while the location of the optical fiber was varied in the laminate to determine whether asymmetric effects of optical fiber placement would result. This resulted in six different laminates, with each laminate consisting of three groups of specimens. Each laminate had a control group that did not contain an optical fiber to act as a baseline for comparison to the optical

fiber groups. The laminates and optical fiber orientations, locations, sizes, and number of optical fibers are identified in Tables 5A and 5B.

Table 5A - Laminates Tested

Laminate	Lay-up
Control 1	$[0_2/+45/90_2/-45/0_2/\pm45/0/+45/0/-45/90]_s$
1A	$[0_2/+45/90_2/-45/0_2/\pm45/0/+45/0/-45/90/\{FO\}]_s$
1B	$[0_2/+45/90/\{FO\}/90/-45/0_2/\pm45/0/+45/0/-45/90]_s$
Control 2	$[0_2/+45/0_2/-45/90_2/\pm45/0/+45/90/-45/0]_s$
2A	$[0_2/+45/0_2/-45/90_2/\pm45/0/+45/90/-45/0/\{FO\}]_s$
2B	$[0_2/+45/0/\{FO\}/0/-45/90_2/\pm45/0/+45/90/-45/0]_s$
Control 3	$[0_2/+45/90_2/-45/0_2/\pm45/0/+45/0/-45/90]_s$
3A	$[0_2/+45/90/\{FO\}/90/-45/0_2/\pm45/0/+45/0/-45/90/\{FO\}]_s$
3B	$[0_2/+45/90/\{FO\}/90/-45/0_2/\pm45/0/+45/0/-45/90/\{FO\}]_s$
Control 4	$[0_2/+45/0_2/-45/90_2/\pm45/0/+45/90/-45/0]_s$
4A	$[0_2/+45/0/\{FO\}/0/-45/90_2/\pm45/0/+45/90/-45/0/\{FO\}]_s$
Control 5	$[0_2/+45/0_2/-45/90_2/\pm45/0/+45/90/-45/0]_s$
5A	$[0_2/+45/0/\{FO\}/0/-45/90_2/\pm45/0/+45/90/-45/0/\{FO\}]_s$
Control 6	$[0_2/+45/0_2/-45/90_2/\pm45/0/+45/90/-45/0]_s$
6A	$[0_2/+45/0/\{FO\}/0/-45/90_2/\pm45/0/+45/90/-45/0/\{FO\}]_s$
6B	$[0_2/+45/0/\{FO\}/0/-45/90_2/\pm45/0/+45/90/-45/0/\{FO\}]_s$

Remarks:

1. Laminates 4 and 5 in this table are equivalent to Configuration 4 in Table 1. This resulted from fiber misalignment during the cure cycle and necessitated that an additional panel be fabricated to alleviate this problem.

2. All panels that are embedded with outer optical fibers and two optical fibers are not completely symmetric about the midplane. This results from optical fiber asymmetry.

Table 5B - Laminates Tested

Laminate	F.O. Size (μm)	# of F.O.	F.O. Location	F.O. Direction
Control 1	N/A	N/A	N/A	N/A
1A	240	1	Center	Parallel
1B	240	1	Outer	Parallel
Control 2	N/A	N/A	N/A	N/A
2A	240	1	Center	Perpendicular
2B	240	1	Outer	Perpendicular
Control 3	N/A	N/A	N/A	N/A
3A	240	2	Out / Cen	Parallel
3B	240	3	Out / Cen / Cen	Parallel
Control 4	N/A	N/A	N/A	N/A
4A	240	2	Out / Cen	Perpendicular
Control 5	N/A	N/A	N/A	N/A
5A	240	3	Out / Cen / Out	Perpendicular
Control 6	N/A	N/A	N/A	N/A
6A	125	2	Out / Cen	Perpendicular
6B	125	3	Out / Cen / Out	Perpendicular

The various laminates were each laid up by hand by placing layers of prepreg tape in the required laminate directions. Fiber optics were placed in the stacking sequence after first being cleaned with acetone and handled with clean surgical gloves to prevent contamination of the bonding surfaces between prepreg layers as well as the optical fiber. The fiber optic was placed across the stack and temporarily taped into

place on both ends of the laminate. The next layer of prepreg tape was then placed on the stack with care being taken not to misalign the optical fiber but yet to get a good bond between the adjoining layers of prepreg tape.

Once the stacking sequence had been completed, the lay-up was cut down into a 30 cm x 30 cm plate to prepare it for curing. During this cutting process, care was taken to minimize fiber misalignment; however, occasional shifting of the fiber within the plate did occur. This misalignment resulted in having to make another panel as significant shifting occurred in the original Panel 4 (240 μm optical fiber perpendicular to the surrounding graphite fibers). The control group and group with two optical fibers were acceptable; however, the group with three optical fibers was unacceptable due to significant floating of the optical fibers during the cure cycle. This resulted in having to fabricate another panel (Panel 5) from which the three fiber group was obtained. A control group was also taken from this panel to act as the baseline for the three fiber group. Microphotographs of each group are shown in Figures 3-14 and give a representative view of all specimens tested in this study.

Almost all groups with multiple optical fibers had some original placement misalignment or floating of the optical fiber during cure. This is readily apparent in the microphotographs, where the cross-sectional plane containing the optical fibers does not always contain all of the fibers. In some instances, the distance separating the optical fibers is as great as three or four optical fiber diameters (approximately 1 mm). This misalignment turned out to be a problem that had to be accepted as part of the problem of embedment. As stated previously, care was taken during placement of the fibers to maintain symmetry, however, during the cure cycle, floating of the fibers within the structure was beyond experimental control. This is a problem that has not been addressed in previous research, and requires future examination to ensure proper placement of optical fibers in a composite environment.

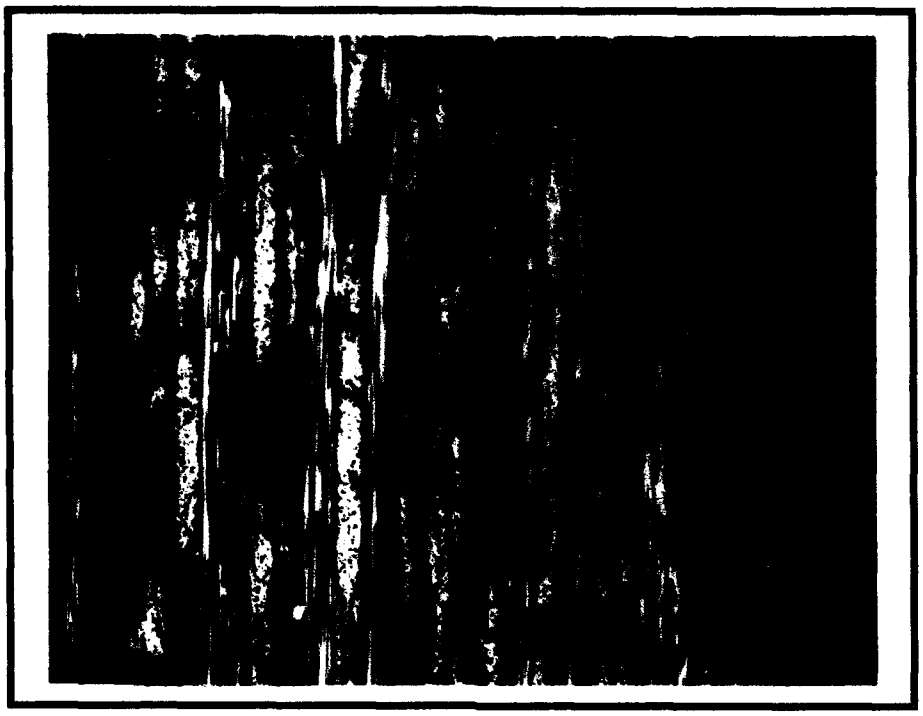

Figure 3 - Laminate 1A

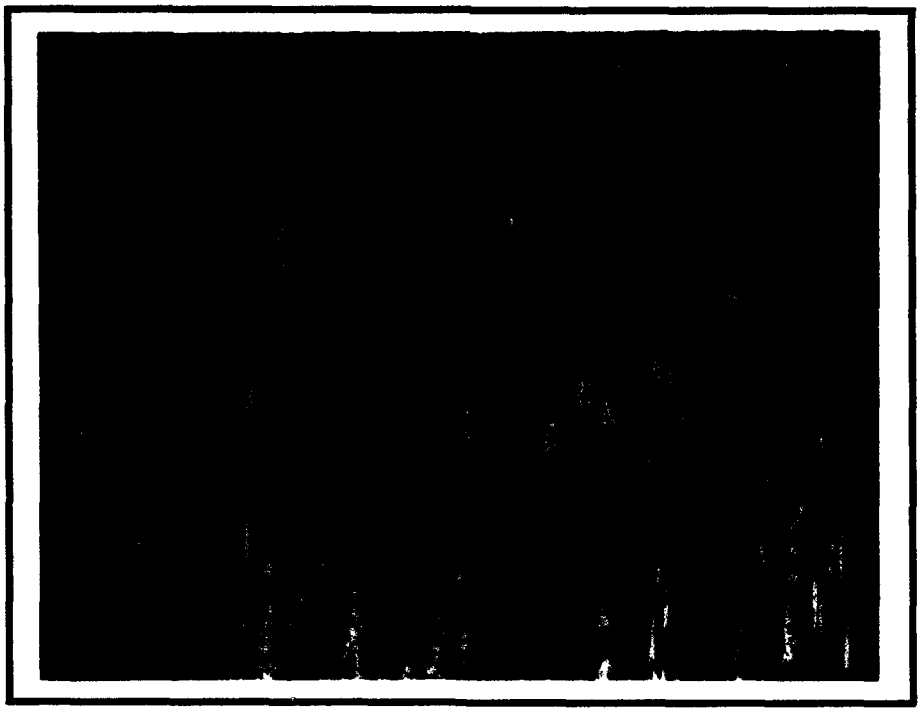

Figure 4 - Laminate 1B

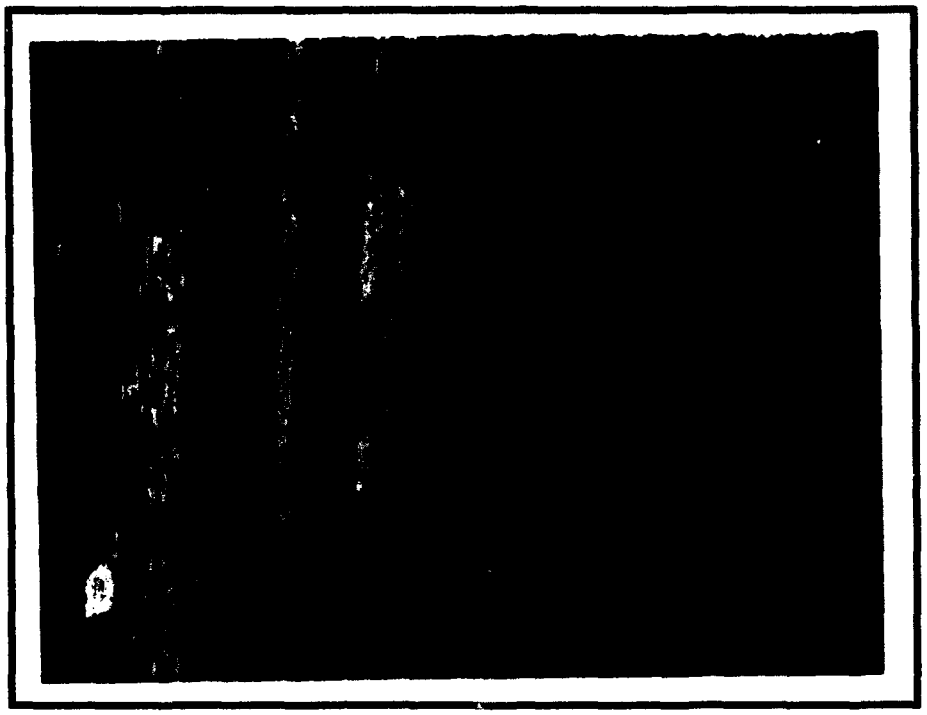

Figure 5 - Laminate 2A

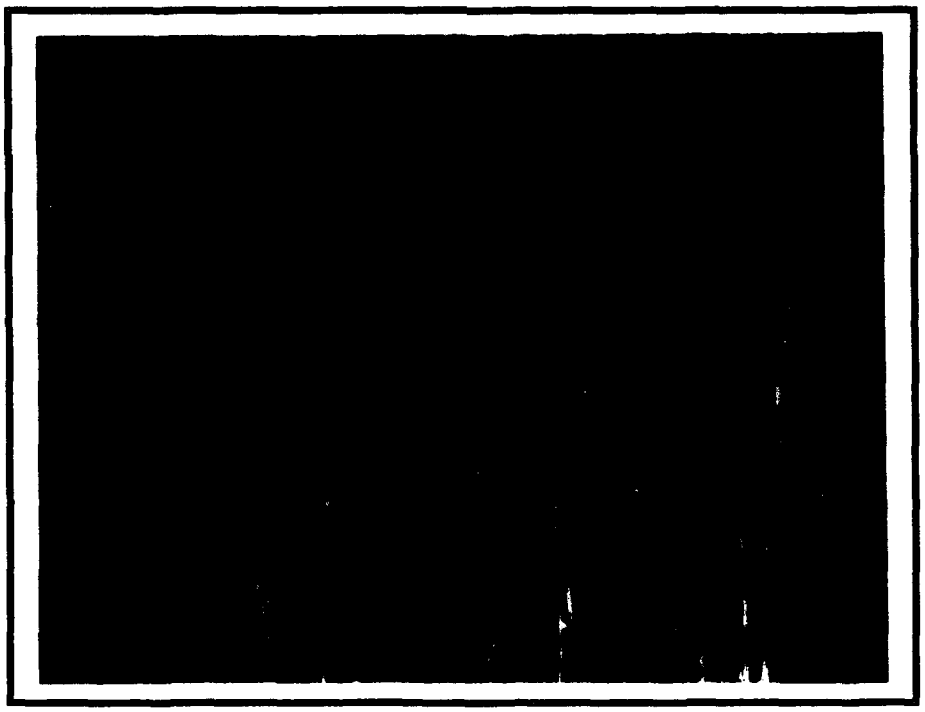

Figure 6 - Laminate 2B

Figure 7 - Laminate 3A

Figure 8 - Laminate 3B

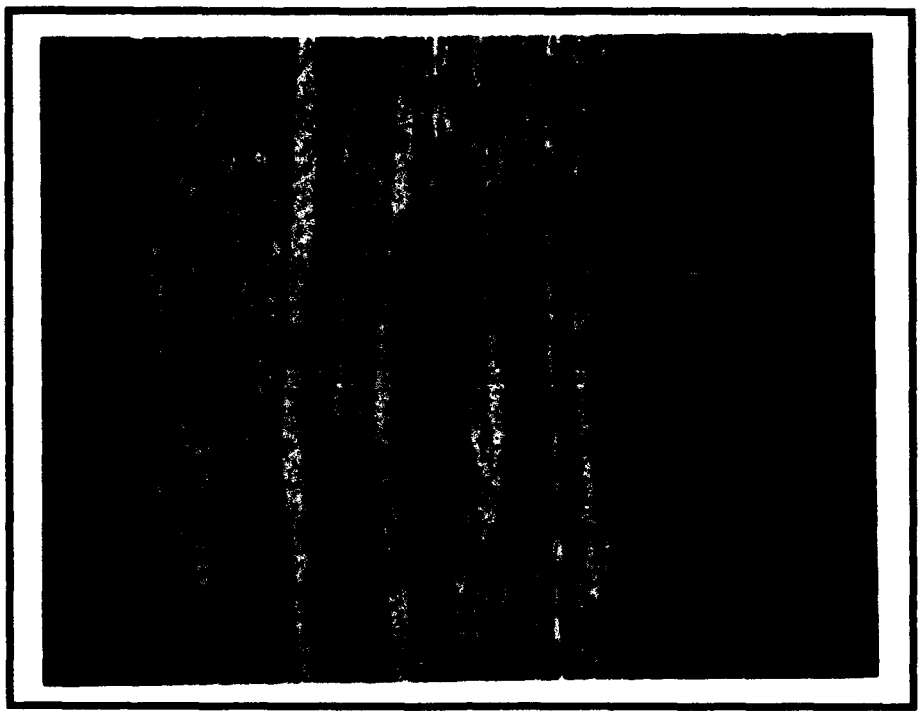

Figure 9 - Laminate 4A

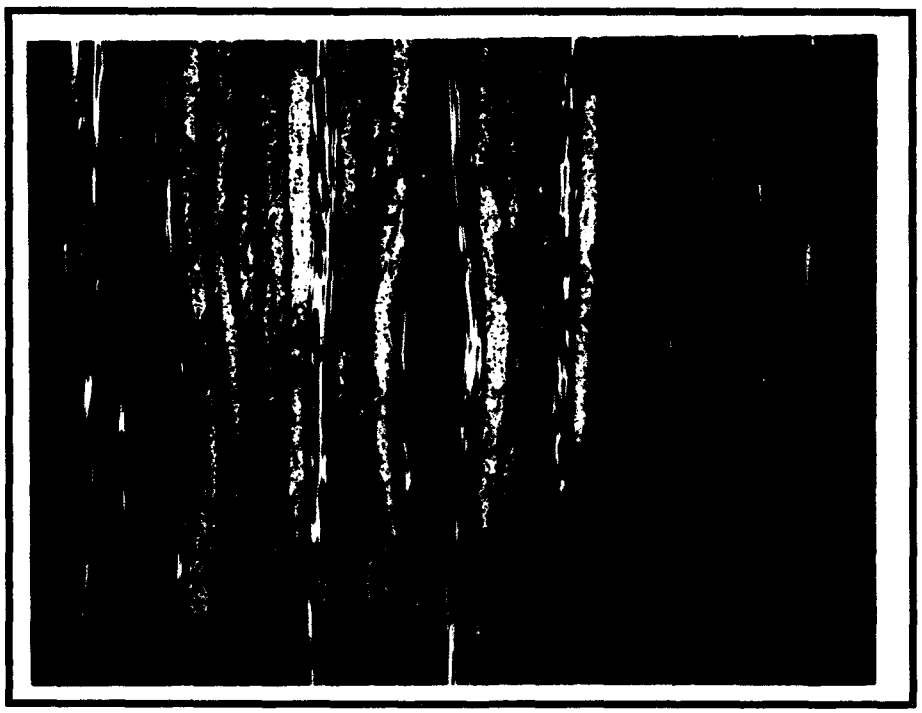

Figure 10 - Laminate 5A

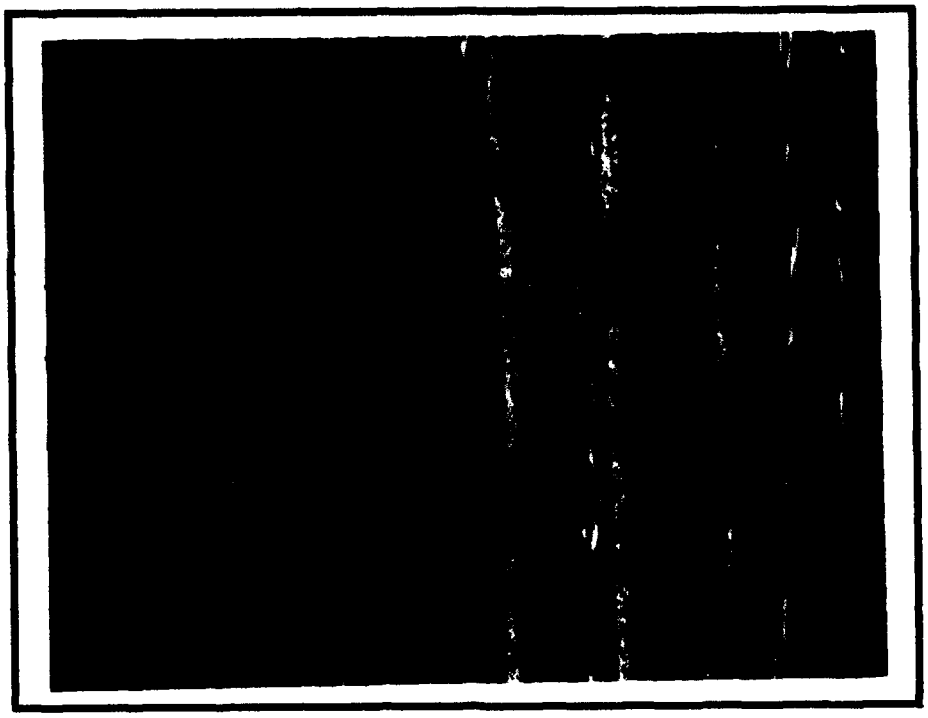

Figure 11 - Laminate 6A

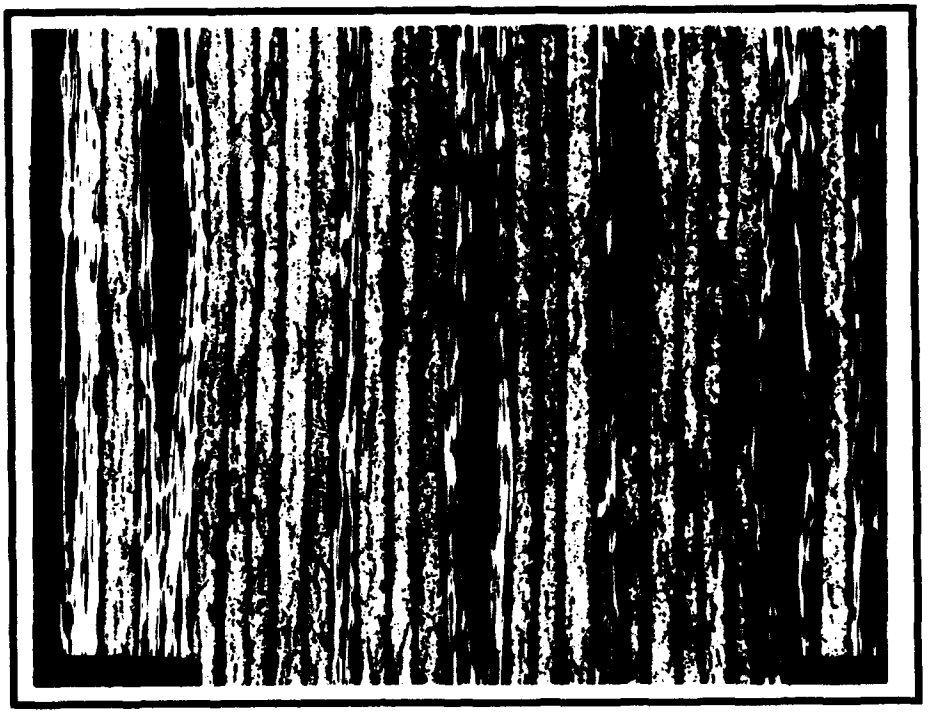

Figure 12 - Laminate 6B

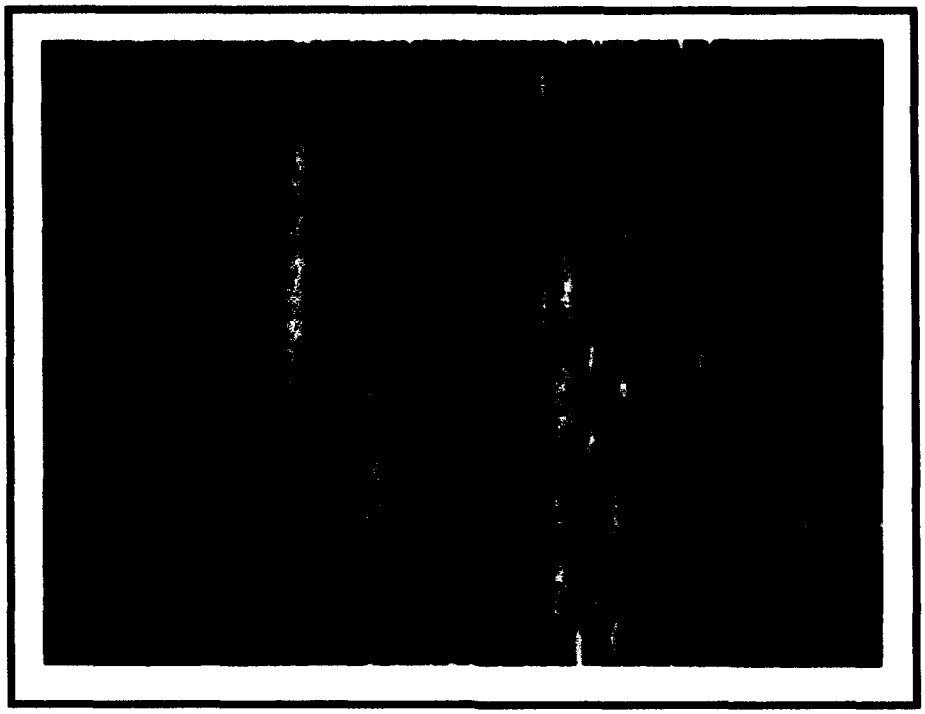

Figure 13 - Control Laminates (90 Degree Center)

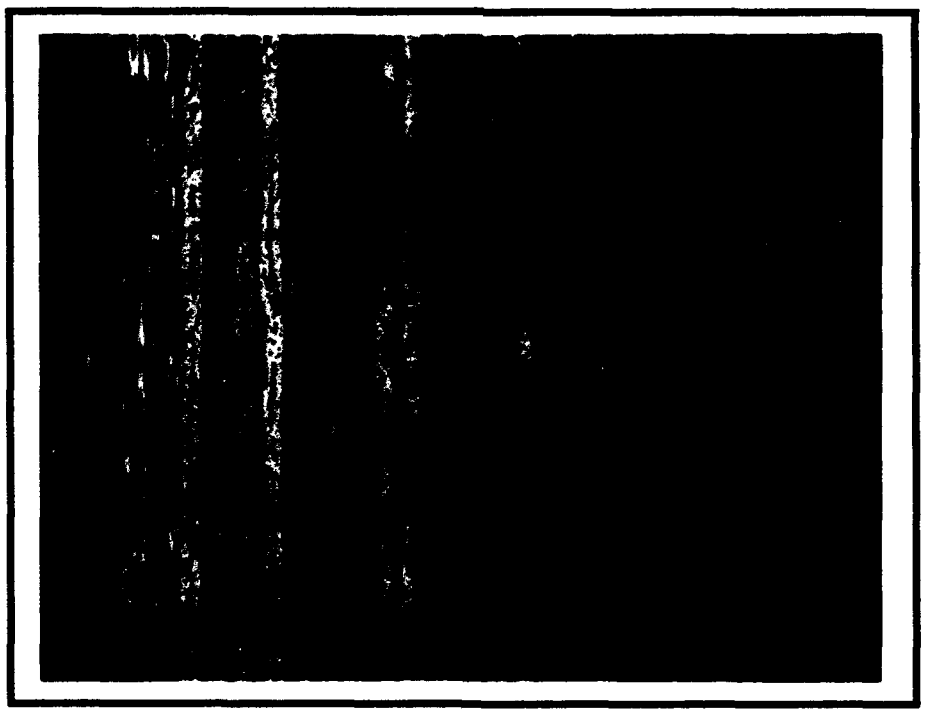

Figure 14 - Control Laminates (0 Degree Center)

The panel was cured using the manufacturer's recommended cure cycle which requires one hour at 115 degrees Celsius and two hours at 177 degrees Celsius. The cure process is shown in Figure 15.

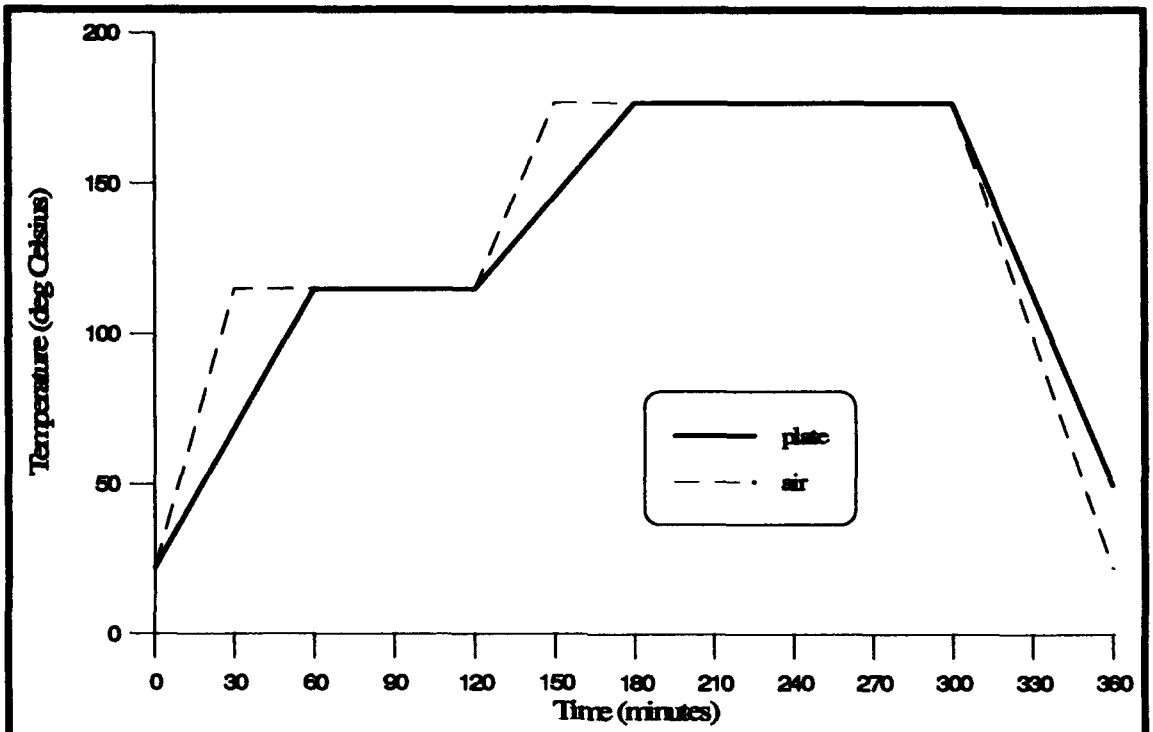

Cure Cycle B-240-T

1. Apply full vacuum, 25" Hg. minimum and 85 psi internal pressure to the autoclave
2. Heat air to 115° ± 5° C in 30 minutes
3. Hold the plate at 115° ± 5° C, 85 psi and full vacuum for 60 minutes
4. Increase the pressure to 100 psi and vent the vacuum
5. Heat air to 177° ± 5° C in 30 ± 5 minutes
6. Hold the plate at 177° ± 5° C and 100 psi for 120 minutes
7. Cool the plate below 65° C in 120 minutes while maintaining 100 psi
8. Vent the pressure and open the autoclave

Figure 15 - Autoclave Cure Cycle

The fiber volume fraction of each panel was determined at two locations on each panel using the methods prescribed by ASTM-D3171 (acid digestion) [40]. Results were averaged and are given in Table 6.

Table 6 - Fiber Volumes of Each Panel

Panel	V_f (First Test)	V_f (Second Test)	Average V_f
1	54.14%	54.18%	54.16%
2	54.88%	54.38%	54.63%
3	53.48%	53.26%	53.37%
4	59.69%	59.76%	59.73%
5	54.39%	55.98%	55.19%
6	53.74%	53.44%	53.59%

Although there was no evident damage to any of the panels, still up to 2.5 cm was cut from each edge with a water cooled diamond edge saw to remove any possible flaws or delaminations. The remaining panels were then cut into nominal strips of .635 cm (.25") to obtain specimens as close to ASTM D3410-87 [33] as possible. That specification recommends for coupons to be 12.7 cm x .635 cm (5" x .25"). Unfortunately, to accommodate the panel cutting diagram outlined in Figure 16, specimens were cut into nominal 11.43 cm (4.5") lengths. However, as this has no effect on the overall gage length of the test section, it was not considered to be a problem.

As many coupons as possible were cut from each panel and numbered according to their location on the panel. A minimum of fifteen specimens were obtained from each panel to meet the test program requirements. Glass/epoxy tabs of 5.08 cm (2")

length were attached with two stage epoxy glue to ten of the specimens to be used as data specimens for the ultimate compression failure strengths. Figure 16 shows the panel and specimen configurations.

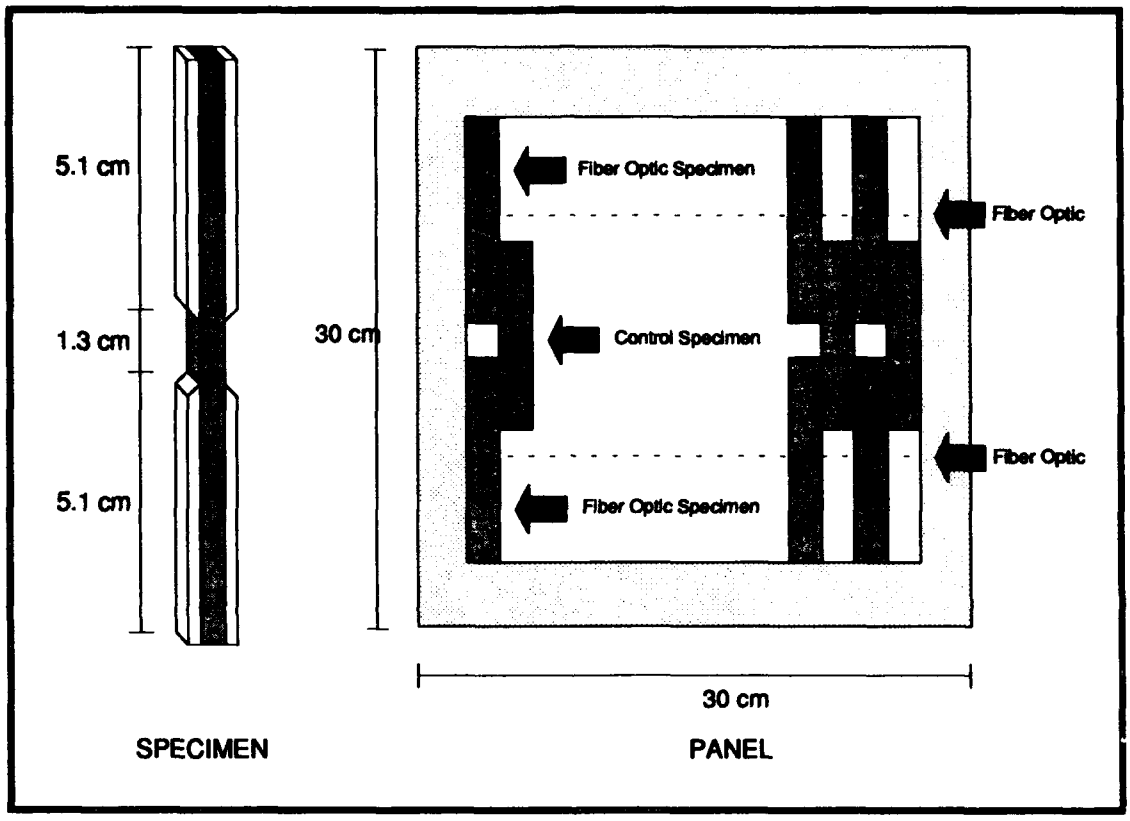

Figure 16 - Specimen and Laminate Configurations

The remaining specimens were polished to obtain microphotographs of the specimens prior to testing and during compressive loading. The specimens were initially rough polished with several stages of a Buehler Handimet II Roll Grinder. Each specimen was subjected to successive grades of silicon carbide paper (240, 320, 400, and 600 grit) which was applied until a smooth level surface was obtained and a clear, unpitted optical fiber was seen under the microscope. Once rough polishing was completed, the specimens were fine polished with Buehler Alpha Micropolish II (1

micron Deagglomerated Alumina) and Microcloth on a Buehler Polimet I Polisher with a variable speed wheel. After a minimum of 30 minutes, the specimens were viewed under the microscope to observe the progress. Once ready, the final polish was applied with Buehler Gamma Micropolish II (.03 micron Deagglomerated Alumina). After this stage was complete, the specimen had a smooth, lustrous finish across the entire surface. These specimens were dried at ambient temperature overnight before applying fiberglass/epoxy tabs as described previously.

A considerable amount of time was spent trying various polishing techniques to provide the best possible surface on both the composite and the optical fiber. Unfortunately, one thing that worked well for one of the components generally did damage to the other. As a result, the final technique that was used did provide an excellent interfacial polish between the optical fiber and composite but, in many cases, did not completely polish the optical fiber core.

3.2 Test Equipment

The major test components used in this testing included a 110 Kip servo-hydraulic Materials Test System (MTS), a Rockland Series 2000 Filter, two strain gage conditioning amplifiers, a Zenith personal computer with data acquisition capabilities, and an Illinois Institute of Technology Research Institute (IITRI) compression test fixture. The entire setup is displayed in Figure 17.

The MTS is a system with the capability to control the testing via transducers, a microprofiler, a 458.20 MicroConsole with digital display, and DC output voltages that correspond to load, displacement, and strain. The load and displacement transducers output a specific voltage for physical changes in the system. The MicroConsole converts the voltages received from the transducers to an actual engineering quantity that is displayed digitally. It also gives the capability to output the transducer DC

voltages directly to a Quatech Analog to Digital (A/D) board. The function of the microprofiler is to enable the user to define the type of displacement or load profile required in the testing.

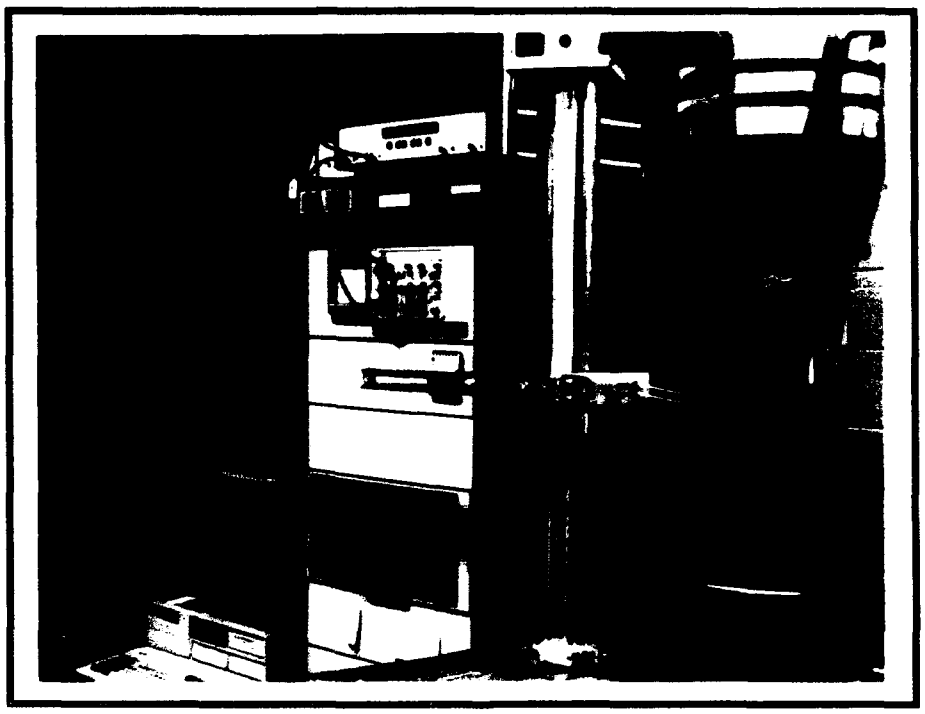

Figure 17 - Test Equipment

The Rockland Series 2000 Filter was implemented to filter out undesirable noise in the system. The filter incorporates a low pass filter which was used to filter out frequencies above 200 Hz.

Strain gage conditioning amplifiers were necessary to amplify output voltages from the back to back strain gages to levels compatible with the data acquisition system. The amplifiers were calibrated to the system requirements prior to testing. Gain and offset variables were used to maximize the resolution of the amplifier to meet particular test requirements.

A Zenith 286 personal computer with data acquisition capabilities was employed for the collection of data. This was accomplished through the Quatech A/D board which received output voltages from the MicroConsole and amplifiers. Software developed for this purpose converts these input voltages into physical quantities (load, strain, displacement) using calibration equations. Output data files were then generated by the software.

The IITRI fixture used for specimen testing had been previously fabricated by the AFIT Model Shop to specifications given in ASTM 3410-87 [33]. The main block of the fixture were made from Titanium, the alignment pins of stainless steel, and the grips and wedges of D2 Tool Steel. An additional set of wedges had to be fabricated to accommodate the overall thickness of the specimens tested. The fixture alignment had been verified previously using two mild steel coupons and fell well within ASTM standards [41]. Figure 18 shows the IITRI fixture.

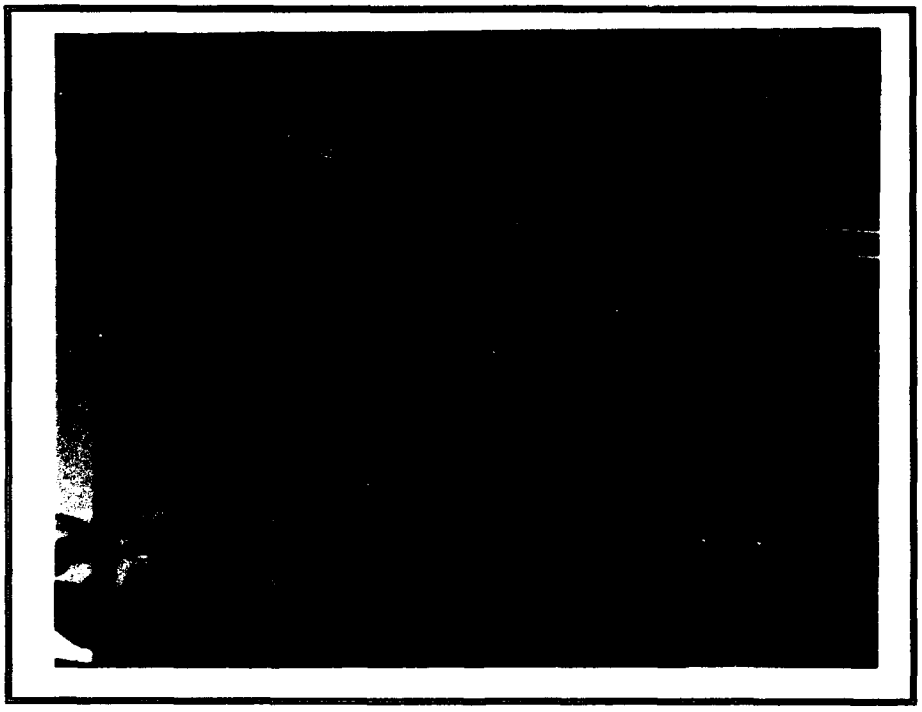

Figure 18 - IITRI Fixture

3.3 Test Procedure

Each specimen was marked with an identification number during specimen preparation to assure specimen inventory and configuration control. Once a specimen was selected for testing, its gage area was determined using a micrometer. Each dimension (width and thickness) was measured in three places in the gage length and the minimum area was determined from these locations. This area was recorded in specimen data sheets.

The specimen was then placed into the IITRI grips and centered in this fixture using an aluminum alignment jig. Before tightening the grips, a small level was applied to the gage section of the specimen to ensure that it was correctly aligned in the grips. Silicon grease was applied to all edges of the IITRI fixture prior to inserting the grips. This assisted in limiting friction build-up and allowed smooth load transfer in the fixture.

Once the top half of the IITRII fixture was carefully lowered into place, the specimen was ready for testing.

The top head of the MTS was lowered down onto the fixture and a preload of approximately 444 N was applied to minimize shifting of the grips during testing. The microprofiler was programmed to cause a constant crosshead speed of .021 mm/s as recommended by ASTM 3410-87 [33]. This program was run until ultimate failure of the specimen was achieved. The MicroConsole displayed the maximum applied load to the specimen, and this was recorded in data sheets as the ultimate load.

Micro-Measurements CEA-06-032UW-120 Strain Gages were applied to three specimens in each group. This was done for all groups except for those in Plate 6 (125 μm Fiber Optic). Plate 6 was not used to obtain strain gage data due to limited time available for testing and the large cost already incurred for the previous testing with strain gages.

The strain gages were applied using standard techniques called for by the manufacturer. Strain gages were centrally located on both faces of the specimen and care was taken to assure alignment of the gage with the zero degree fibers on the specimen. The strain gage outputs were recorded on the data acquisition system and shown graphically during each test. The data was later used to find the initial modulus of the specimens.

Polished specimens were tested using the same techniques as above, although no strain gages were applied. The original intent was to use these specimens to obtain acetate/acetone replicas of failure progression. However, the small size of the graphite fibers (6-8 μm) did not provide clear replicas of the gage section. Additionally, the confined area of the IITRI fixture and high load at failure led to safety considerations ruling out this technique. As a result, the specimens had to be incrementally loaded, taken out of the fixture, and viewed under a microscope to detect damage. This cyclic loading was minimized by using dummy specimens (not fully polished) to determine the range of first ply failure and estimate the required incremental loads. This allowed a polished specimen to be loaded to this range without multiple loadings/unloadings. Microphotographs were taken of damage initiation sites and will be discussed in detail in the coming chapters.

The ultimate compression strength of each specimen was calculated from the data with the following equation:

$$\sigma_{UC} = \frac{Ultimate\ Load}{Initial\ Area} \tag{12}$$

The initial modulus of elasticity was found from the initial, straight line portion of the stress-strain curve of each specimen. A constant range of 0.1 to 0.3 percent strain was used for all specimens. This allowed for any settling of the grips in the IITRI

fixture and provided consistency for data manipulation. The calculated modulus for both strain gages were averaged to give a single value for the specimen modulus.

$$E = \frac{\Delta\sigma}{\Delta\varepsilon} \tag{13}$$

For each group of specimens the average value, standard deviation, and coefficient of variation for ultimate compression strength and initial modulus of elasticity were found:

$$\overline{X} = \sum_{i=1}^{n} X_i / n \tag{14}$$

$$S = \sqrt{\sum_{i=1}^{n} (X_i - \overline{X})^2 / (n-1)} \tag{15}$$

$$\nu = S / \overline{X} \tag{16}$$

IV. Results

As mentioned in Chapter 3, different groups of specimens were obtained from the same panel. Therefore, the results will be presented in this chapter for each panel separately along with comparisons between individual groups of specimens from each panel. General discussion will be given for each panel, however, overall discussion and comparisons for the entire study will be presented in the next chapter. The results comprise the data for each group's average strength and average longitudinal modulus of elasticity, bar charts showing strength data for each specimen, and stress-strain curves obtained using strain gages. Microphotographs of failed and partially failed polished specimens are also included to show crack propagation and failure modes.

In general, all specimens for this study failed in a similar manner. As is common for the type of lay-up employed in this study, which somewhat resembles quasi-isotropic laminates in unidirectional loading, the failure was sudden and catastrophic. For the majority of the laminates, there was no obvious indication of first ply failure (observable delamination, noise, etc.) and the failure was immediate. However, a few of the laminates underwent partial failure of individual plies prior to complete specimen failure. All specimens for these tests failed in the gage section. The failure patterns will be discussed in further detail for each panel.

Figures 19 and 20 show typical failure patterns of specimens in this study. As described in Chapter 2, several studies have been completed that describe the failure pattern of quasi-isotropic graphite/epoxy laminates. Of these, Sohi et al. [30] gave a complete failure sequence of these laminates which describes fiber kinking of the 0° plies as the primary failure mechanism. The four step process begins with kinking of the 0° plies at an edge which propagates inward into other plies. The outer kinked fibers begin to fail which leads to load eccentricity and failure of subsequent fibers in the

interior of the laminate. When these plies fail, they move relative to neighboring angle plies and delamination results. This delamination results in multiple sublaminates that are more susceptible to buckling than the original laminate. The global buckling of sublaminates leads to final failure of the specimen.

Because of the sudden nature of failure in the specimens tested in this study, no fiber kinking was noted during loading. However, as can clearly be seen in Figures 19 and 20, the specimens contain multiple delaminations that have resulted in global buckling of the specimen which ultimately led to final failure of the specimen. As was common for the specimens tested, the sublaminates buckled outwardly on each side of the specimen so that global buckling of the total laminate did not occur in any one direction.

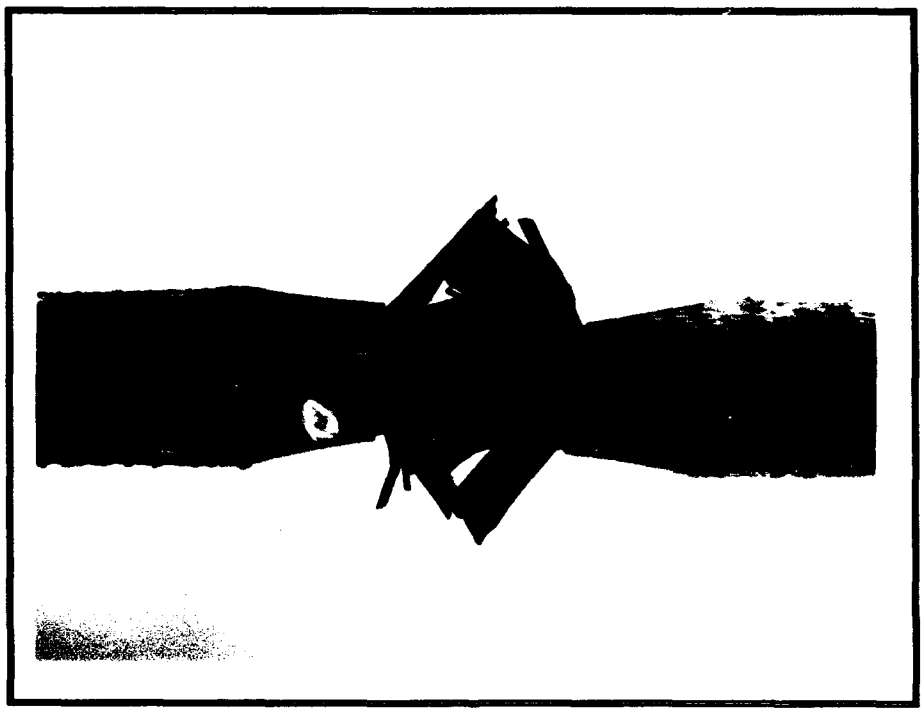

Figure 19 - Typical Specimen after Compressive Failure

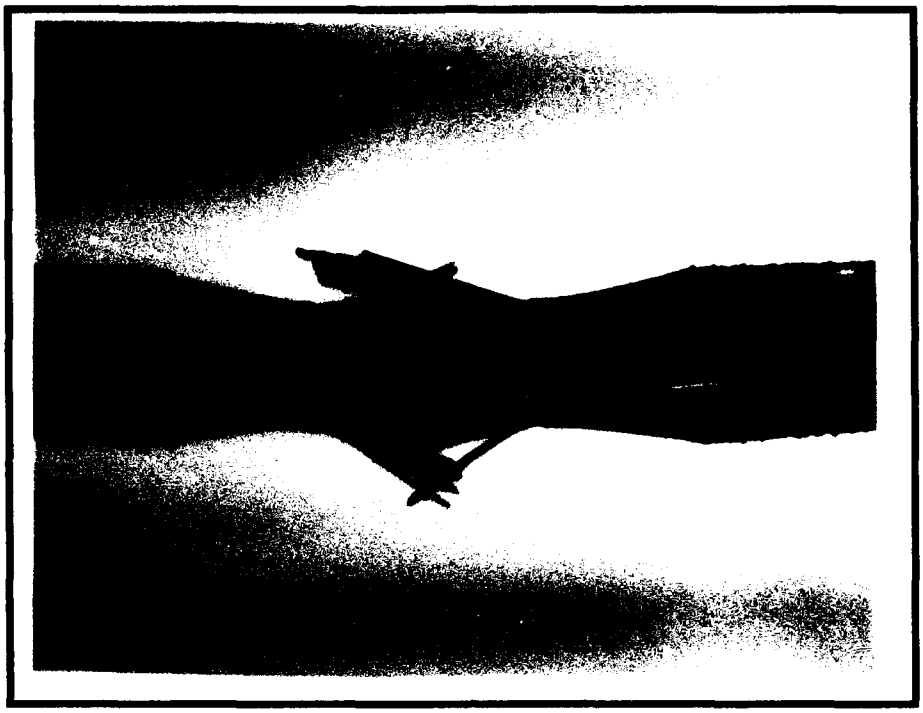

Figure 20 - Typical Specimen after Compressive Failure

Included in the results for each panel are typical stress-strain curves of each group of specimens from that panel. They are included to show that the specimens did not undergo global Euler buckling as evidenced by the initial parallel response and linearity of both strain gages when placed back to back on specimens. Even though each specimen showed a different response beyond the initial linear portion of the curve, the curves can be said to be typical of all specimens of that particular group because each specimen failed at essentially the same level of strain and had similar stress-strain data during the elastic portion of the curve.

The variance beyond the linear portion of the curve is easily explained by referring back to Chapter 2 when it was shown that several variables in a specimen can affect its response to compressive loading. Even though attempts were made to ensure similarity between all specimens, even small voids or minor changes in structural fiber

orientation will create significant changes in stress-strain response. One significant aspect that will be discussed further in the next chapter is the apparent buckling of most specimens after they had first been damaged through different mechanisms of compressive failure. This phenomenon is apparent at elevated stress levels where the readings from the strain gages diverge rapidly until specimen failure occurs.

4.1 Panel 1 - Results and Discussion

Panel 1 is characterized by a single 240 μm optical fiber laid up in parallel to the surrounding composite fibers. The optical fibers were located at either the midplane of the composite or at an outer ply as indicated in previous discussion. There were three groups of specimens obtained from this panel: control (with no fiber optic), central fiber optic, and outer fiber optic. Photomicrographs of these lay-ups have already been presented in Figures 3, 4, and 13 of Chapter III.

The data obtained from the testing of each group are presented in Table 7 and Figure 21. The strength data represents testing of ten specimens for each group, while the modulus of elasticity data is taken from three of the ten specimens tested with strain gages.

As Table 7 shows, the reduction of strength for the groups containing optical fibers is relatively small or negligible and is essentially the same as the percent deviation for each group. These values suggest that the overall compressive strength of the laminate is not affected by the presence of the optical fiber. Modulus values also suggest similar results. A slight degradation of the modulus values is seen for the centrally located fiber optic, while a slight increase is seen for the outer fiber optic. Again, these values were very close to each other and within few percent deviations and can be considered to be negligible changes compared to the control values.

Table 7 - Panel 1 Test Data

PANEL 1	Control	Central F.O.	Outer F.O.
Average Strength (MPa)	745.77	712.93	720.21
Standard Deviation	31.91	25.94	26.33
% Deviation	4.28%	3.64%	3.66%
% Strength Reduction	-----	-4.40%	-3.43%
Average Modulus (GPa)	55.86	54.64	56.35
Standard Deviation	2.24	0.85	1.31
% Deviation	4.00%	1.55%	2.32 %
% Modulus Change	-----	-2.19 %	0.86 %

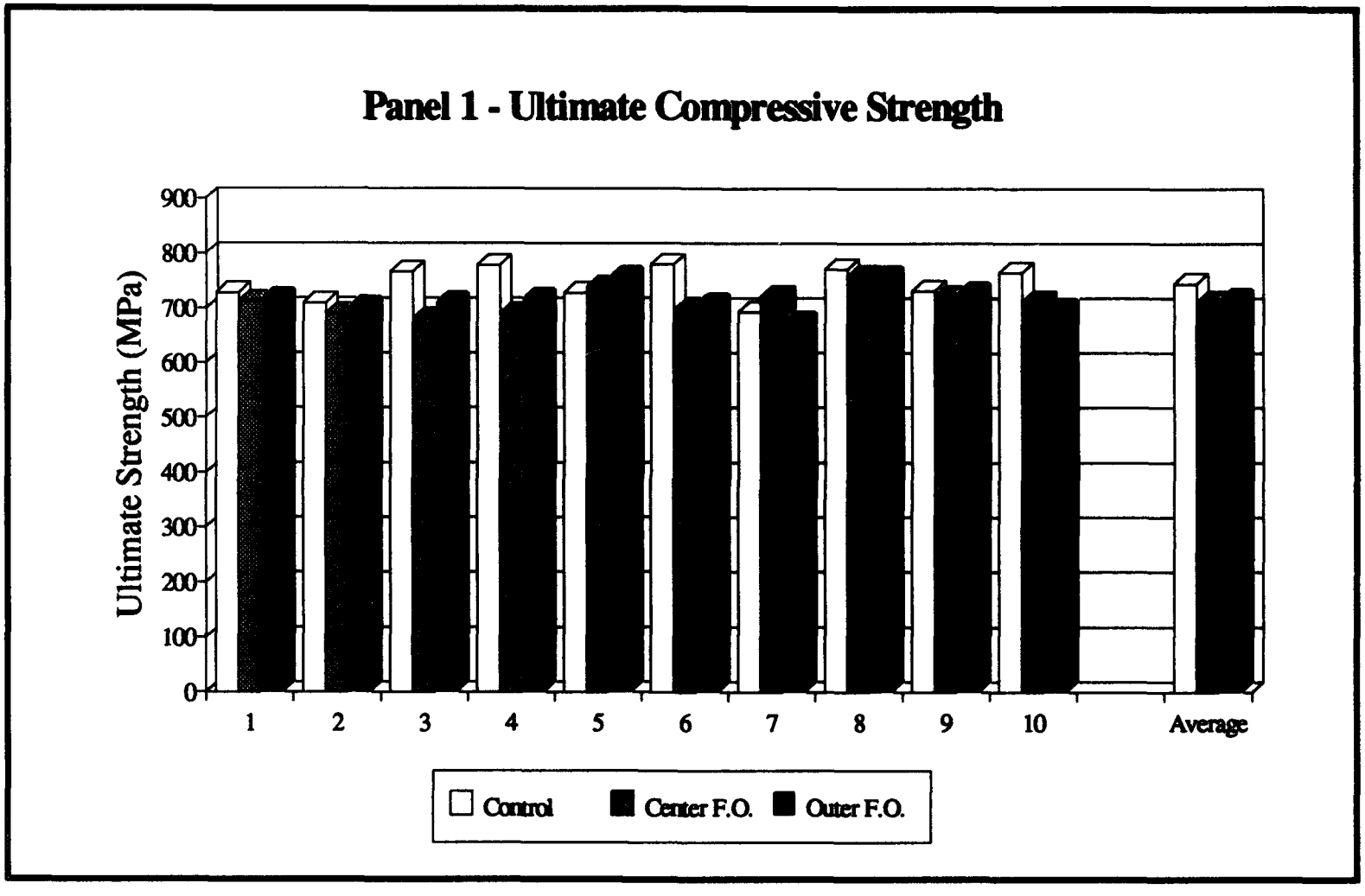

Figure 21 - Panel 1 Test Results

There was no discernible difference in failure characteristics of any of the three groups tested in Panel 1. All specimens failed in the gage section with a sudden and violent failure. No visible damage indicators were typically given prior to this catastrophic event. In only one or two cases did obvious delamination of outer plies occur. This delamination, however, did not effect the measured strength of the specimen. Several specimens emitted audible noises that indicated some damage occurring prior to failure, however, as stated earlier, this damage was not visible, and could not be associated with lower failure strengths of these specimens.

Several specimens that had been polished, as indicated in Chapter 3, were loaded with progressively higher loads until failure. In these specimens, matrix cracks began to develop at approximately 90% of the ultimate load. These cracks were only seen to occur in the 90° plies and were arrested by the surrounding 45° plies. At most, one or two cracks were observed prior to complete specimen failure. Similar cracks were observed for both the control and the fiber optic specimens. Figure 22 shows a typical matrix crack in a 90° ply.

After specimen failure, all specimens were observed under a microscope to determine whether the failure affected the area surrounding the optical fiber. In all cases observed for this panel, none of the immediate areas surrounding the optical fiber were affected by the failure. This can be seen in Figure 23 where the area around the fiber optic remains intact.

Stress-strain curves of one specimen from each of these three groups are shown in Figures 24, 25, and 26. These curves were used to calculate the modulus values given in Table 7. Note that all are similar in that they failed at approximately the same level of strain. The stress-strain response at the maximum load is due to catastrophic failure of the specimen where it fails in buckling. This is evidenced by the rapid divergence of the strain gage readings at this level.

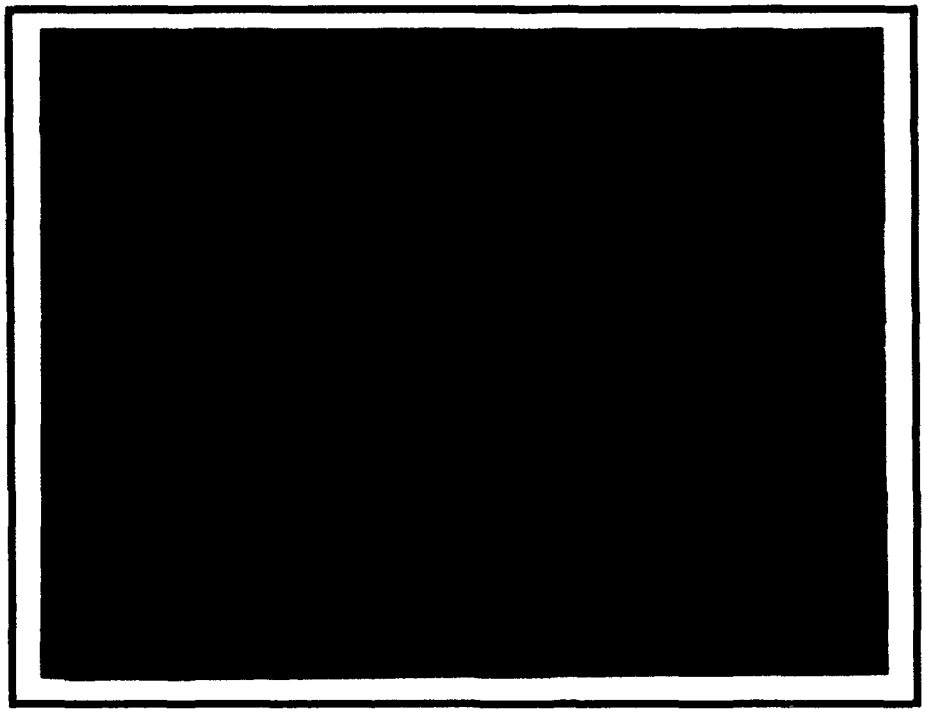

Figure 22 - Matrix Crack in 90° Ply

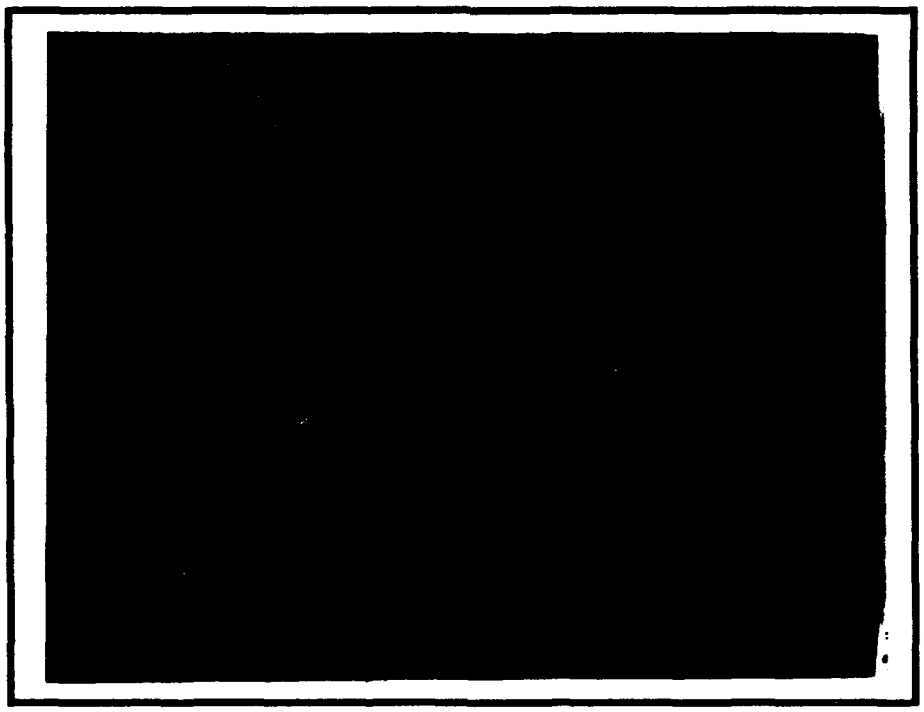

Figure 23 - Intact Area surrounding Optical Fiber

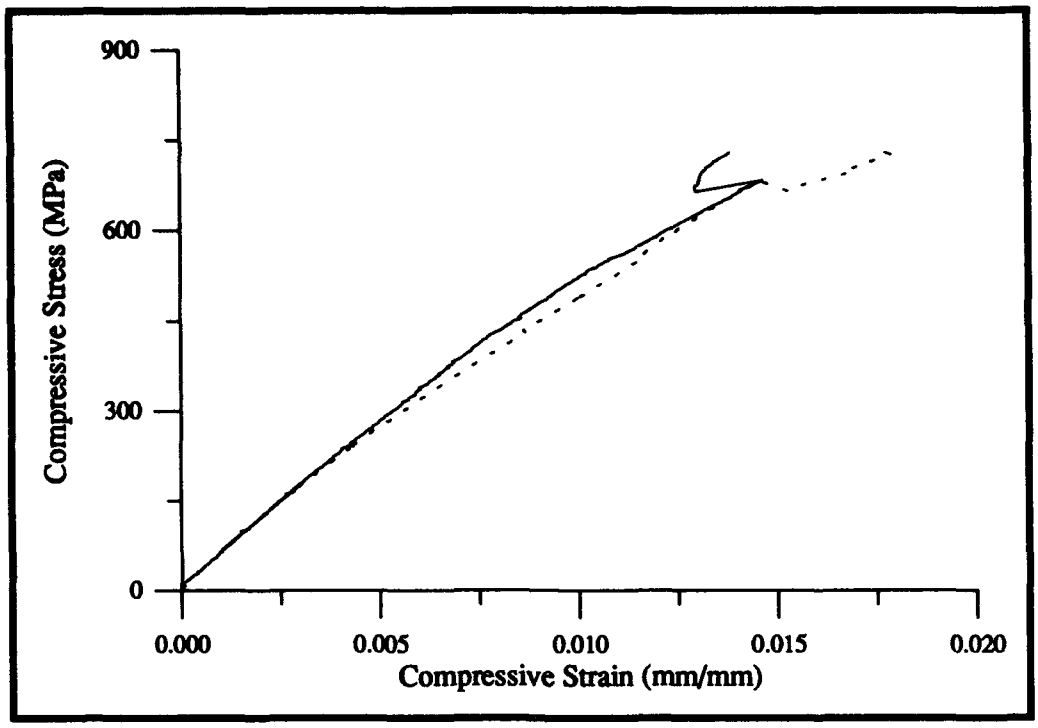

Figure 24 - Stress-Strain Curve of Panel 1 Control Group

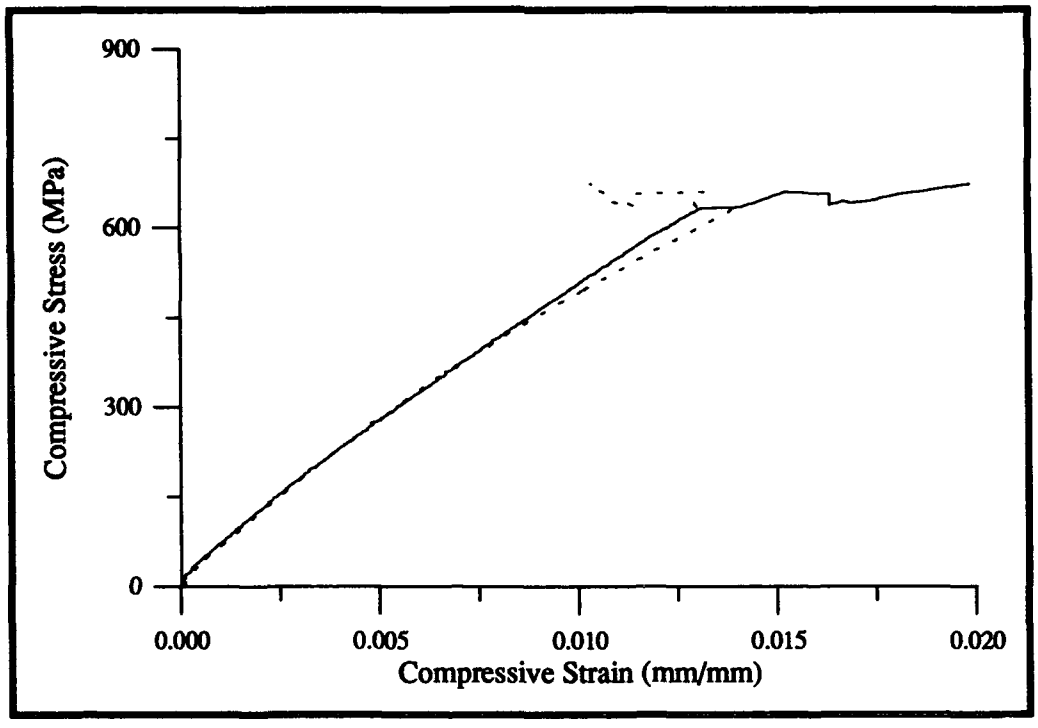

Figure 25 - Stress-Strain Curve of Panel 1 Central Fiber Optic Group

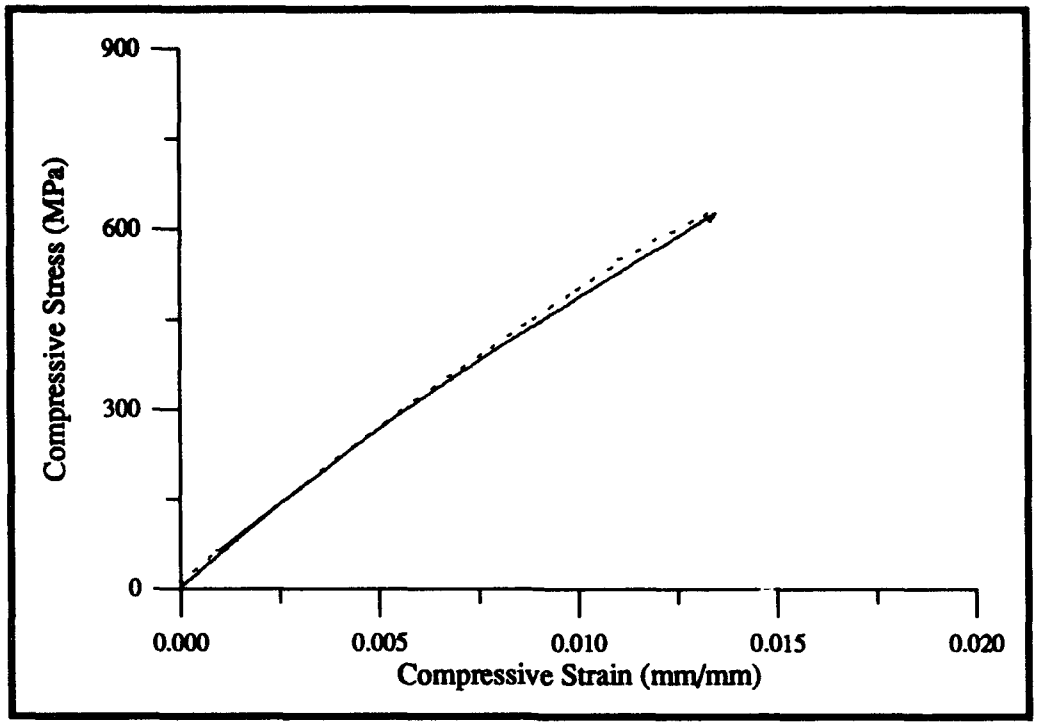

Figure 26 - Stress-Strain Curve of Panel 1 Outer Fiber Optic Group

4.2 Panel 2 - Results and Discussion

Panel 2 is characterized by a single 240 μm optical fiber lay-up perpendicular to the surrounding composite fibers. This orientation generates a single "resin eye" in the specimen. The optical fibers were located at either the midplane of the laminate or at an outer ply. There were three groups for this panel: control, central fiber optic, and outer fiber optic. Photomicrographs of these lay-ups have already been presented in Figures 5, 6, and 14.

The average compressive strength and longitudinal modulus values for this panel are shown in Table 8. Individual specimen strength values are shown in Figure 27.

Table 8 - Panel 2 Test Data

PANEL 2	Control	Central F.O.	Outer F.O.
Average Strength (MPa)	730.71	714.22	641.95
Standard Deviation	46.03	46.92	46.72
% Deviation	6.30%	6.57%	7.28%
% Strength Reduction	-----	-2.26%	-12.15%
Average Modulus (GPa)	54.91	55.41	55.10
Standard Deviation	0.47	1.20	3.97
% Deviation	0.85%	2.16%	7.21%
% Modulus Change	-----	0.91%	0.35%

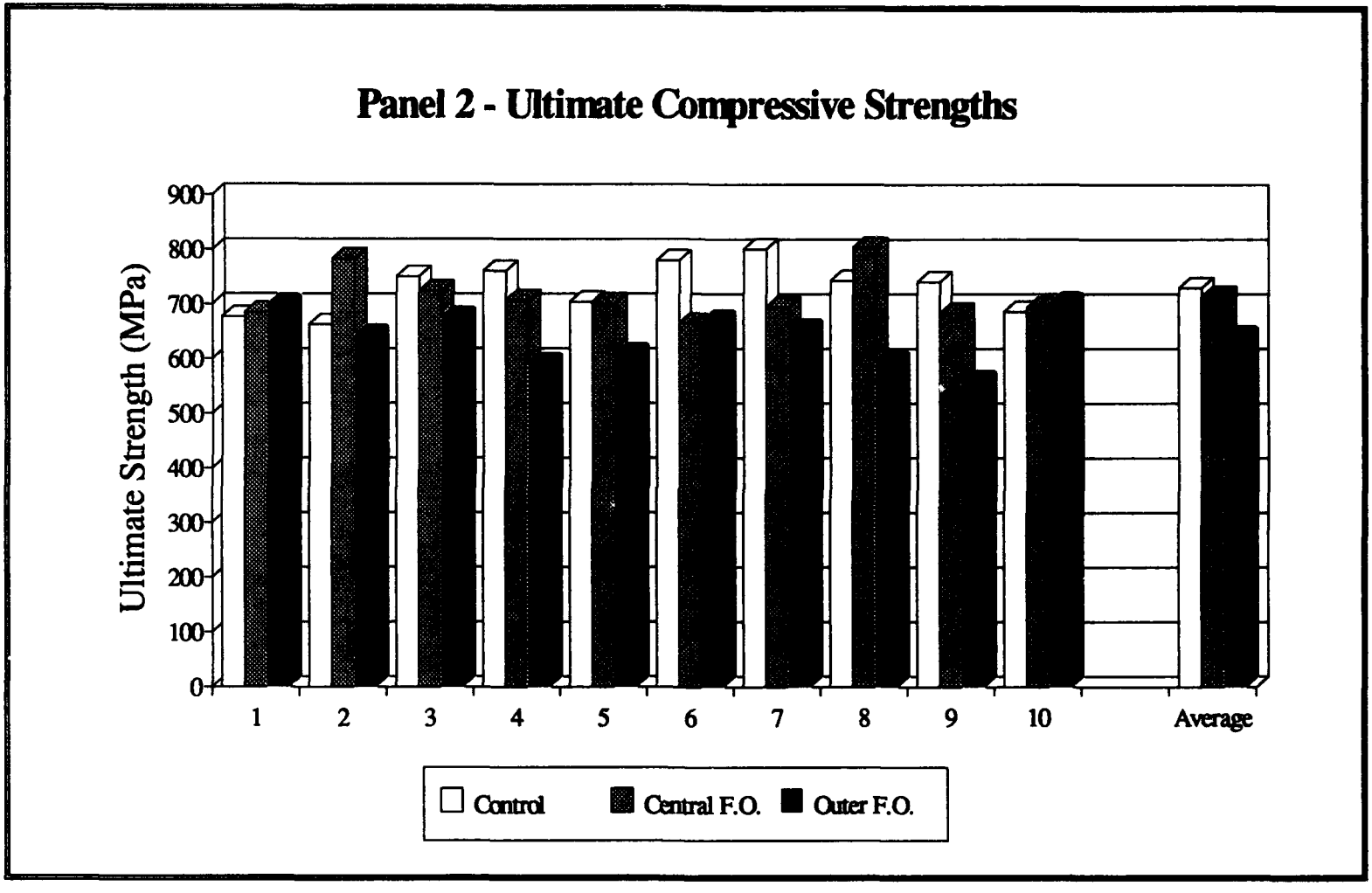

Figure 27 - Panel 2 Test Results

The percent variations in strength within each group were all approximately 7%, which is very common in compression testing where so many variables affect the overall specimen strengths. Relative to the control group, the group with the central optical fiber had only a 2% strength reduction, while the group with the outer optical fiber a strength reduction of just over 12%. The modulus values for optical fiber groups did not show any deviation from the values obtained from the control group. Percent deviations for this data varied from 1% for the control to 7% for the outer fiber optic.

Unlike Panel 1, where there was no discernible difference of failure progression between the groups, this panel showed readily apparent differences. The control group and central fiber optic failed in the same manner as described for Panel 1 where there was usually no indication of damage prior to sudden, catastrophic failure. However, the specimens with an optical fiber located in outer plies gave obvious visible and audible indication of damage prior to complete failure of each specimen. In this case, at approximately 95% of the ultimate load, the side of the specimen where the optical fiber was located fractured in the vicinity of the optical fiber. Upon examination under a microscope, it was seen that this fracture occurred in the five outermost plies on the fiber optic side of the specimen and was centered around the optical fiber. This fracture surface is shown in Figure 28.

Examination of failed specimens showed that all failures affected the resin rich zone around the fiber optic. This was the case for both center and outer locations of the fiber optic. Whereas Panel 1 showed no damage around optical fibers, this panel showed fiber optic areas were affected in both cases, with center and outer locations. Figure 29 shows typical failure surfaces around the optical fiber.

Stress-Strain curves for one of each of the laminates are shown in Figures 30, 31, and 32. These curves were one of three for each specimen from which the modulus data was taken in the initial portion of the curve (0.1 to 0.3 percent strain).

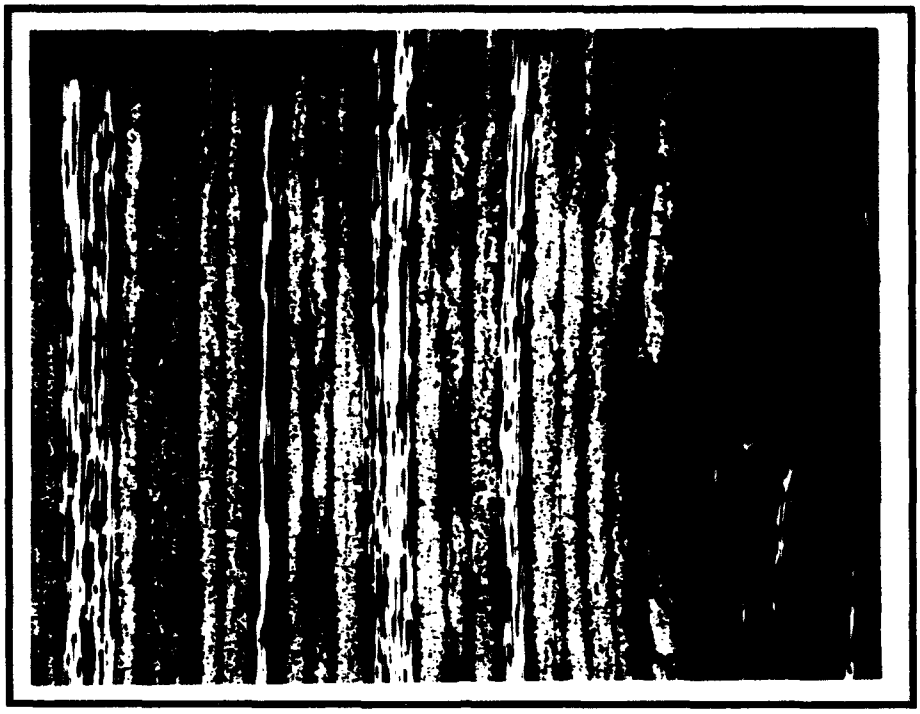

Figure 28 - Failed Outer Plies of Outer Fiber Optic Laminate

Figure 29 - Typical Failure Pattern around Optical Fiber

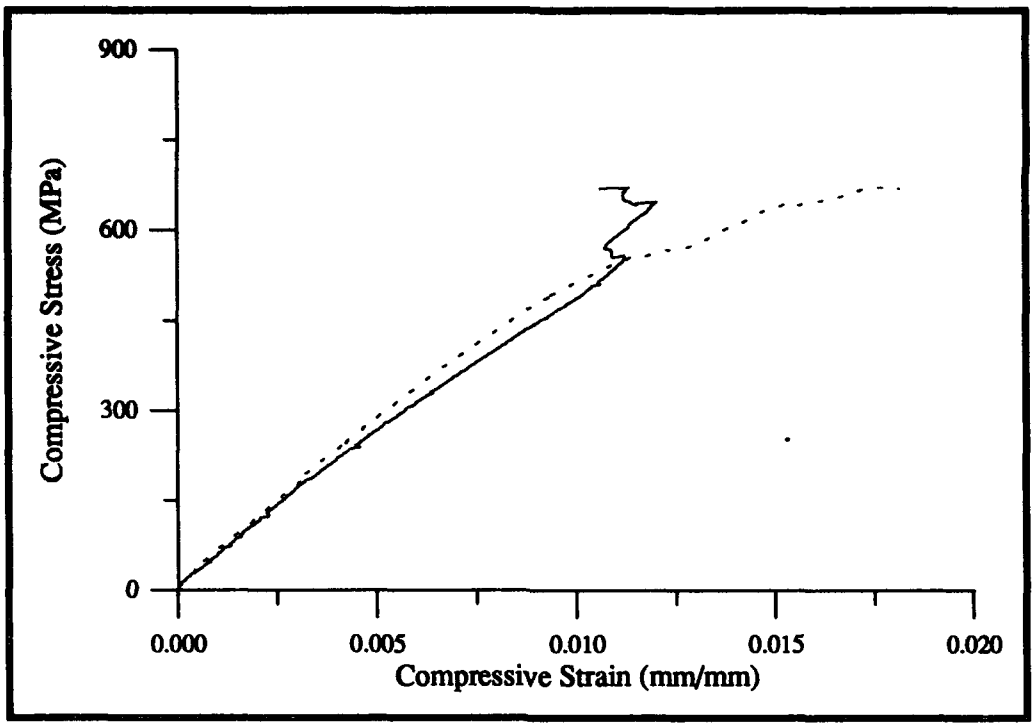

Figure 30 - Stress-Strain Curve of Panel 2 Control Group

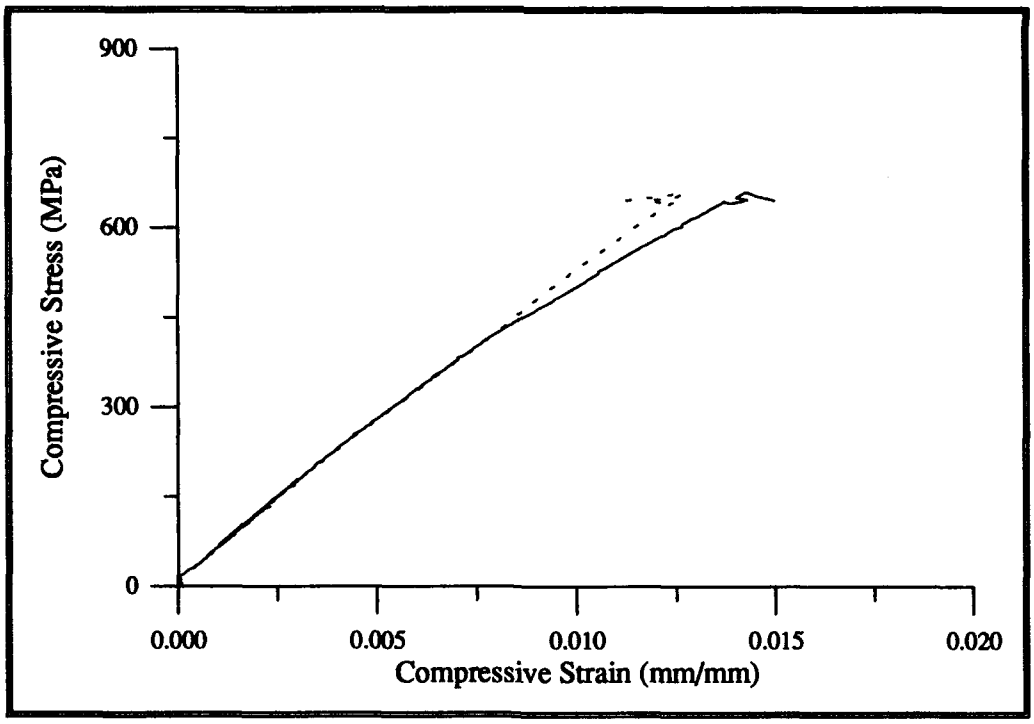

Figure 31 - Stress-Strain Curve of Panel 2 Central Fiber Optic Group

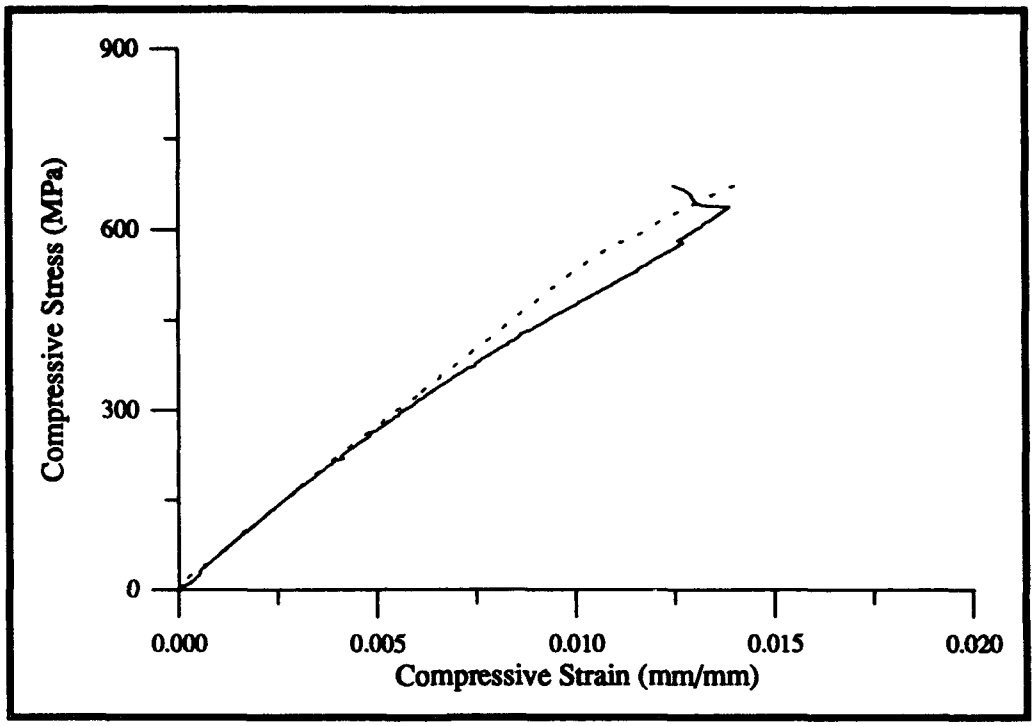

Figure 32 - Stress-Strain Curve of Panel 2 Outer Fiber Optic Group

4.3 Panel 3 - Results and Discussion

Panel 3 is characterized by groups of two and three 240 μm optical fibers parallel to the composite fibers. The specimens with two optical fibers were located at the midplane and at an outer location three plies in from the specimen surface. The specimens with three optical fibers were located symmetrically about the midplane (outer, center, outer) and placed at the same outer location as described above. As with all other panels, these two groups were tested against a control group taken from the same panel. Photomicrographs are located in Figures 7, 8, and 13. Average compressive strengths and longitudinal modulus values for these three groups are shown in Table 9. Individual strength of each specimen is shown in Figure 33.

Table 9 - Panel 3 Test Data

PANEL 3	Control	Two F.O.	Three F.O.
Average Strength (MPa)	784.60	778.06	782.99
Standard Deviation	39.96	44.02	27.31
% Deviation	5.09%	5.66%	3.49%
% Strength Reduction	-----	-0.83%	-0.21%
Average Modulus (GPa)	56.17	57.36	55.55
Standard Deviation	1.47	1.39	2.35
% Deviation	2.62%	2.43%	4.23%
% Modulus Change	-----	2.11%	-1.10%

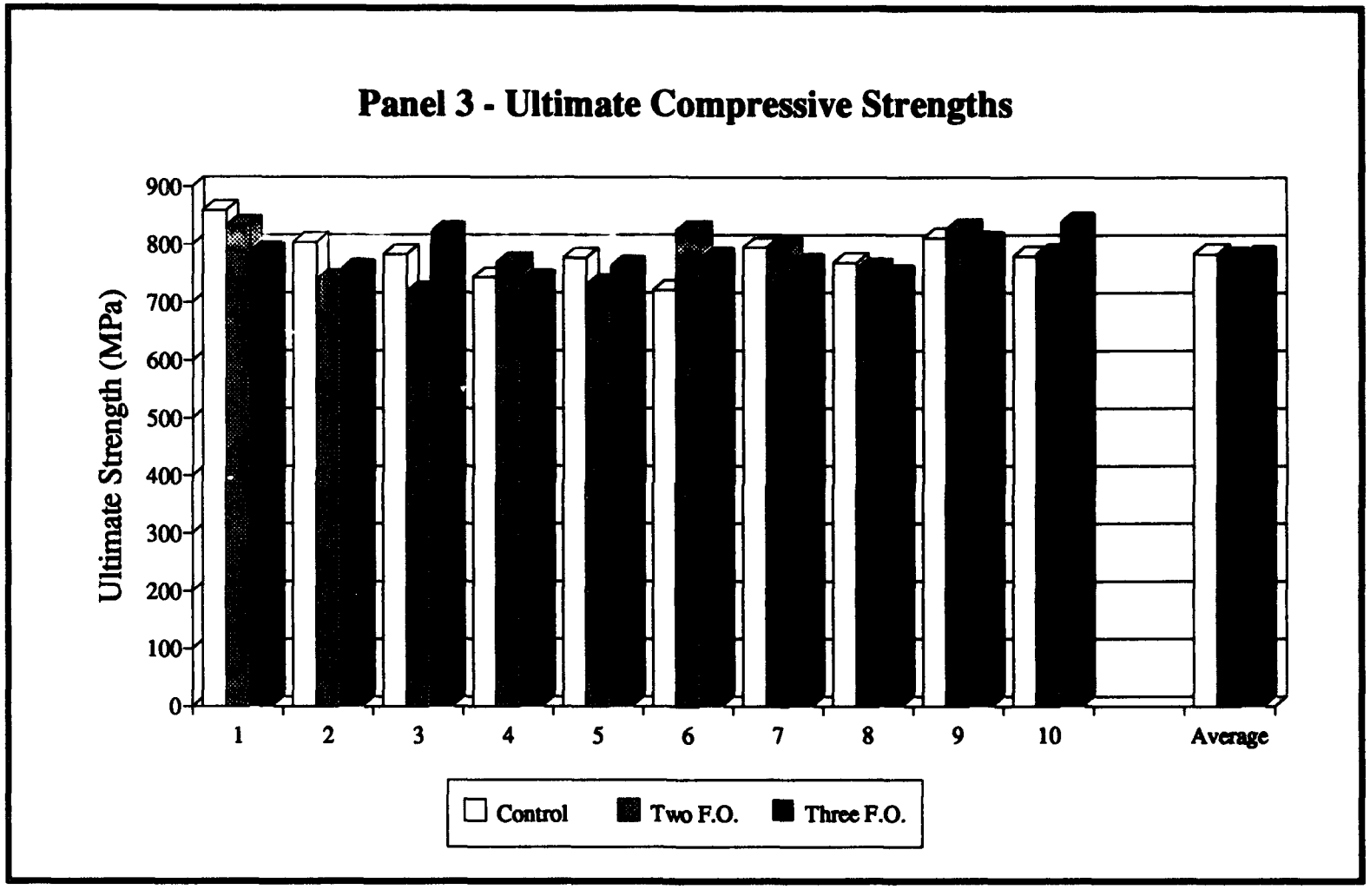

Figure 33 - Panel 3 Test Results

As it can be seen, no quantifiable reduction in average strength for both the fiber optic groups is observed. These values are within 1% of the control values and have percent variations of approximately 5%. Therefore, it can be concluded that these configurations of the fiber optic embedment has no apparent effect on the compressive strength of the specimens. Modulus values showed an increase of 2.1% for the two fiber optic group, while a decrease of 1.1% was shown for the three fiber optic group. Percent variations were all under 5% for this data. As with the compressive strength data for this panel, these values show no evidence of effective modulus change due to the optical fiber embedment.

Failure patterns were similar to Panel 1 with all groups giving an immediate failure without indication of damage. However, several polished specimens were tested with progressive incremental loads until failure. In these specimens, matrix cracks began to appear in the 90° plies at approximately 90% of the ultimate load. When observed, these cracks were minimal (2 or 3 per ply) and were arrested by the surrounding 45° plies. However, in the six specimens observed with matrix cracks, none of the cracks occurred in the 90° plies containing optical fibers. Once this phenomenon was observed for this panel, specimens from Panel 1 (similar optical fiber orientation within the composite) were examined and similar results were seen for these specimens. Even though optical fibers seemingly prevented matrix cracks from occurring in their own plies, no correlating change in strength could be made. This phenomenon will be discussed in further detail in the next chapter.

Failed specimens did not typically show failure around the fiber optic. In most cases, the immediate area surrounding the optical fiber was intact after complete specimen failure. In only two cases, the optical fiber was damaged during failure. Microphotographs of both cases (failed and unfailed areas) are shown in Figures 34 and 35 to indicate the extent of damage to the specimens and optical fibers. As can be seen

in these figures, the laminate has undergone catastrophic failure. Both figures show extensive delaminations and matrix cracks. Figure 35 identifies the failed area around an optical fiber and shows the intact optical fiber coating that has adhered to the composite matrix around the failure zone.

Figures 36, 37, and 38 relate the stress-strain data that was used to compute the modulus for these specimens. Again, as has been seen for other stress-strain curves, the strain gage readings at the failure load diverge rapidly to indicate the global buckling occurring in the sublaminates of the specimen. Figure 37 is the only curve obtained in this study that shows non-linear response in the usual elastic region of the specimen. This response is probably a result of improper specimen alignment in the test fixture, but as explained in Chapter 2, it could be the result of any number of factors affecting the compressive stress of this specimen.

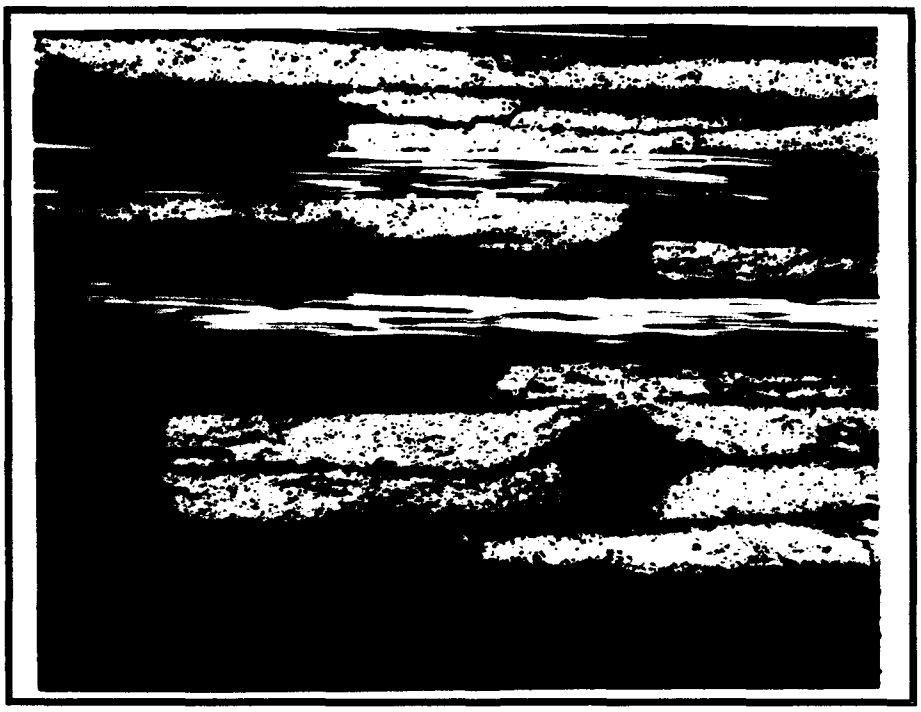

Figure 34 - Intact Area around Optical Fiber

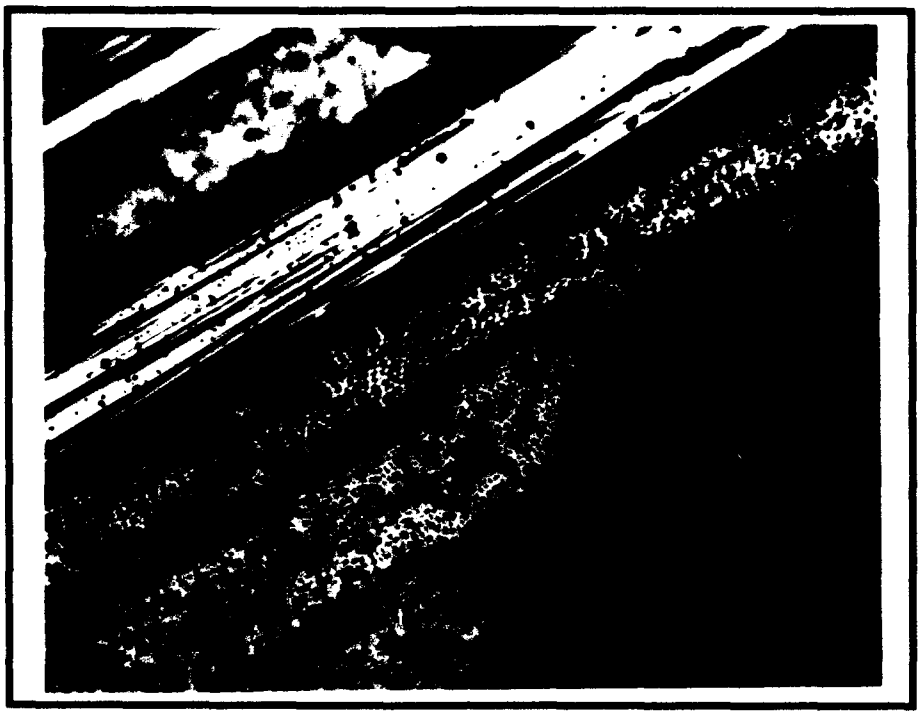

Figure 35 - Failed Area around Optical Fiber

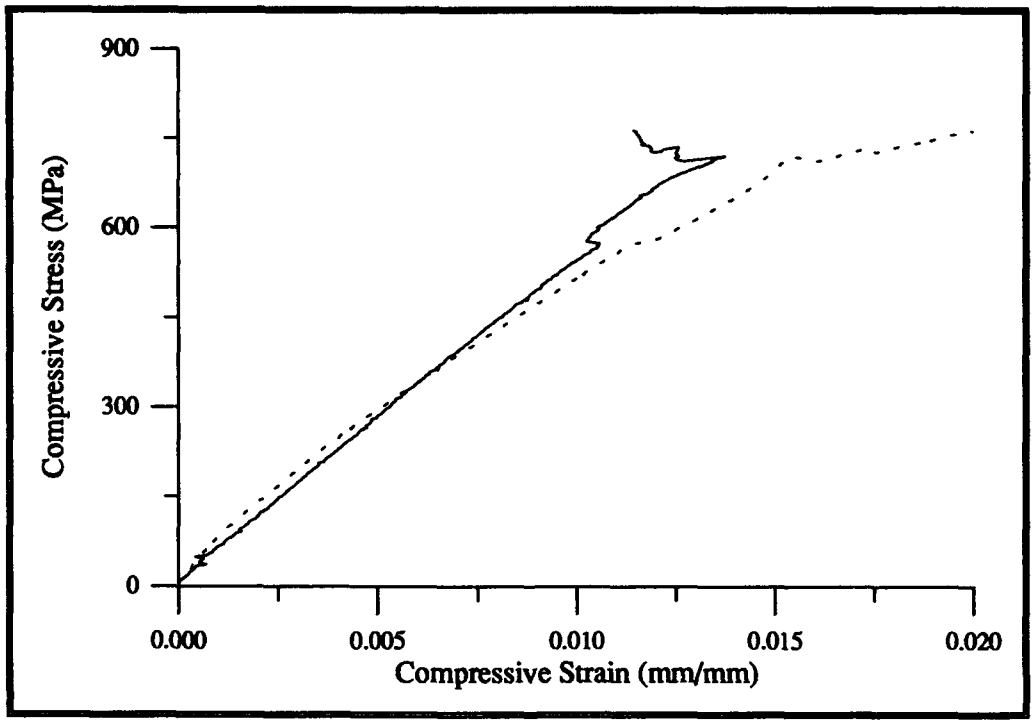

Figure 36 - Stress-Strain Curve of Panel 3 Control Group

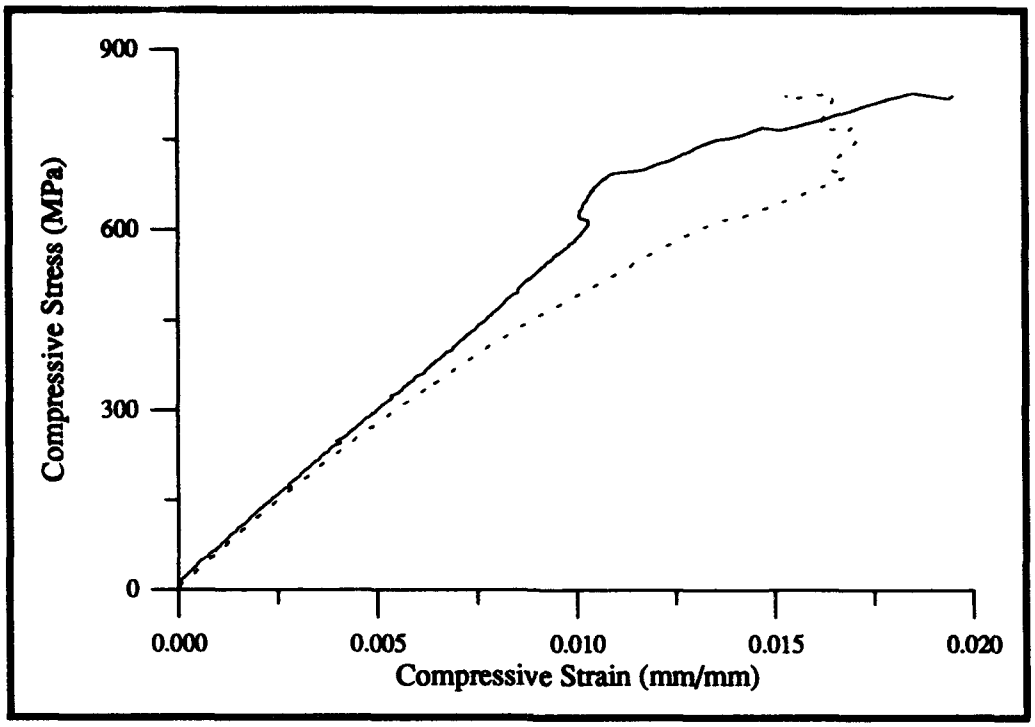

Figure 37 - Stress-Strain Curve of Panel 3 Two Optical Fiber Group

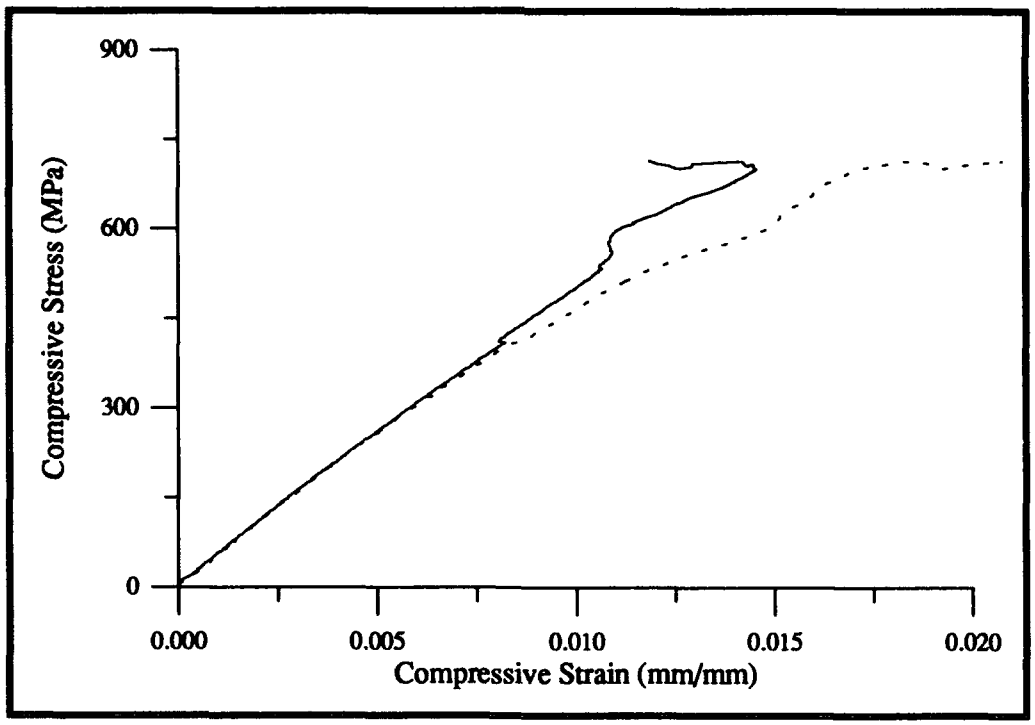

Figure 38 - Stress-Strain Curve of Panel 3 Three Optical Fiber Group

4.4 Panels 4 and 5 - Results and Discussion

Panel 4 contained two 240 μm optical fibers perpendicular to the surrounding composite fibers (two "resin eyes"), while Panel 5 contained three 240 μm optical fibers perpendicular to the surrounding fibers (three "resin eyes"). Each panel contained a control group. These panels will be discussed in tandem in this and subsequent sections as the original intent was to have both fiber optic groups from the same panel. However, during fabrication of the initial panel (Panel 4), the optical fibers in the group containing three fibers underwent significant shifting of the fibers during the cure cycle, and did not remain in the original co-planar location. This resulted in the fabrication of Panel 5 to give a more uniform group of three optical fiber specimens. A control group was also taken from this panel to ensure good correlation of data between optical fiber and control groups. Microphotographs of these laminates have already been shown in Figures 9, 10, and 14.

Average strength and modulus data of both panels is shown in Table 10. Individual strength values for each specimen are shown in Figures 39 and 40 for Panels 4 and 5 respectively. These panels showed the greatest strength reduction of any groups in this study. The group with two optical fibers embedded perpendicular to the composite fibers had a strength reduction of almost 27%, while the group with three optical fibers had a strength reduction of over 19%. The percent deviations were all within the norm and ranged from 3% to 7% for the four groups tested in these two panels. Modulus data was similar to all other groups where no significant change was noted. The two optical fiber group had a strength increase of just over 1%, while the group with three optical fibers showed a decrease of just over 1%. Percent deviations for both the fiber optic and control groups were all under 4%. This confirms the negligible effect of embedding optical fibers on the compressive modulus of smart structures.

Table 10 - Panels 4 and 5 Test Data

PANELS 4 and 5	Control 4	Two F.O.	Control 5	Three F.O.
Average Strength (MPa)	772.06	564.14	773.30	624.28
Standard Deviation	41.54	35.02	24.52	44.17
% Deviation	5.38%	6.21%	3.17%	7.08%
% Strength Reduction	-----	-26.93%	-----	-19.27%
Average Modulus (GPa)	58.28	59.04	56.07	55.44
Standard Deviation	1.42	2.24	1.31%	0.76
% Deviation	2.44%	3.79%	2.34%	1.37%
% Modulus Change	-----	1.32%	-----	-1.13%

Failure patterns were very similar to those described for Panel 2, where "resin eyes" were present in the structure. The group with two optical fibers failed in almost exactly the same manner as described for the outer optical fiber group of Panel 2. In this group, the plies surrounding the outer fiber optic failed at approximately 95% of the ultimate load. As with the Panel 2 specimen, this failure effected the 5 outer most plies. A typical failure is shown in Figure 41.

The group with three optical fibers failed in almost the same manner as described for other groups, where no prior indication of a sudden failure was observed. The only discernible difference between this and other groups was the lower strength at

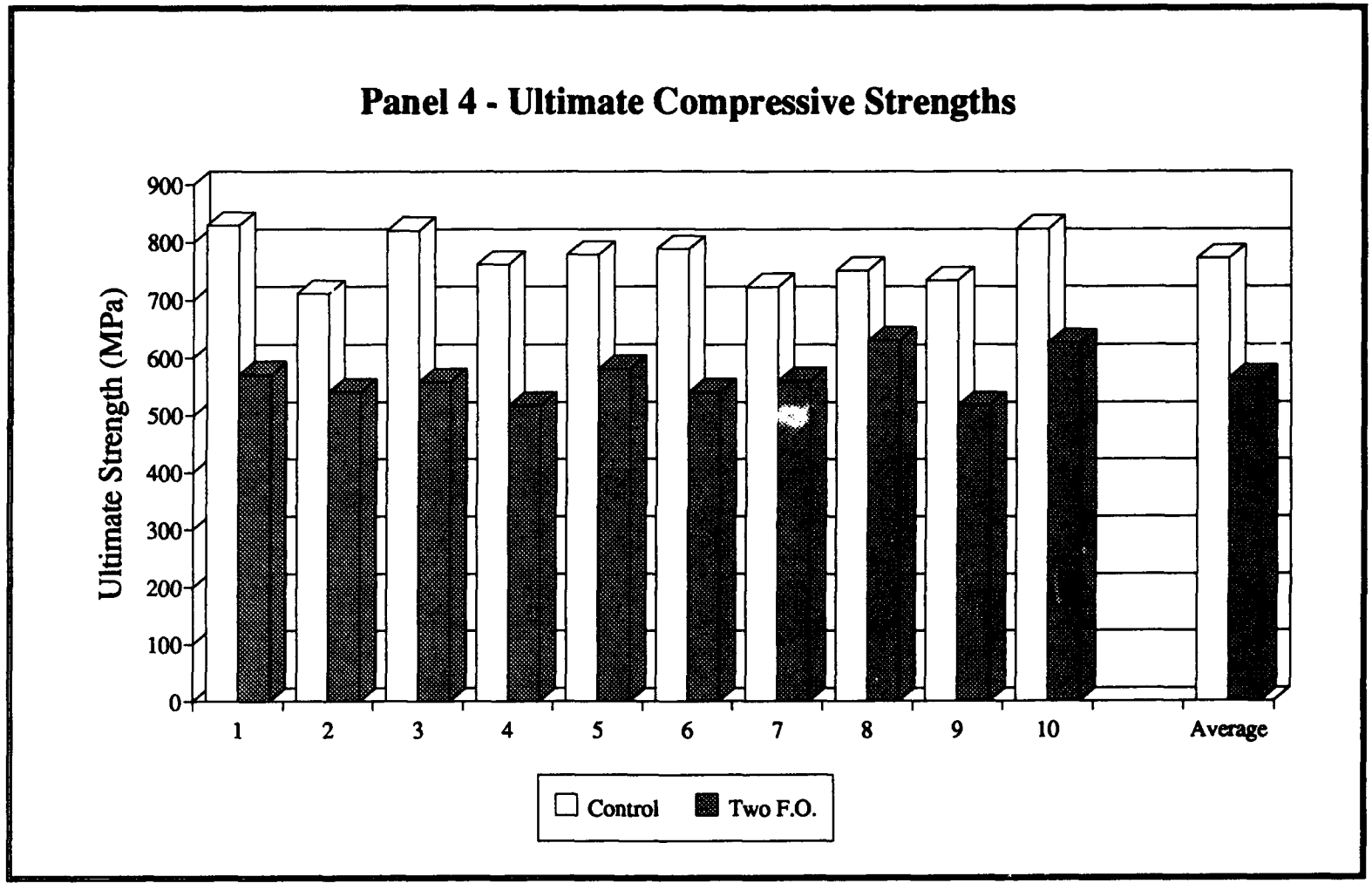

Figure 39 - Panel 4 Test Results

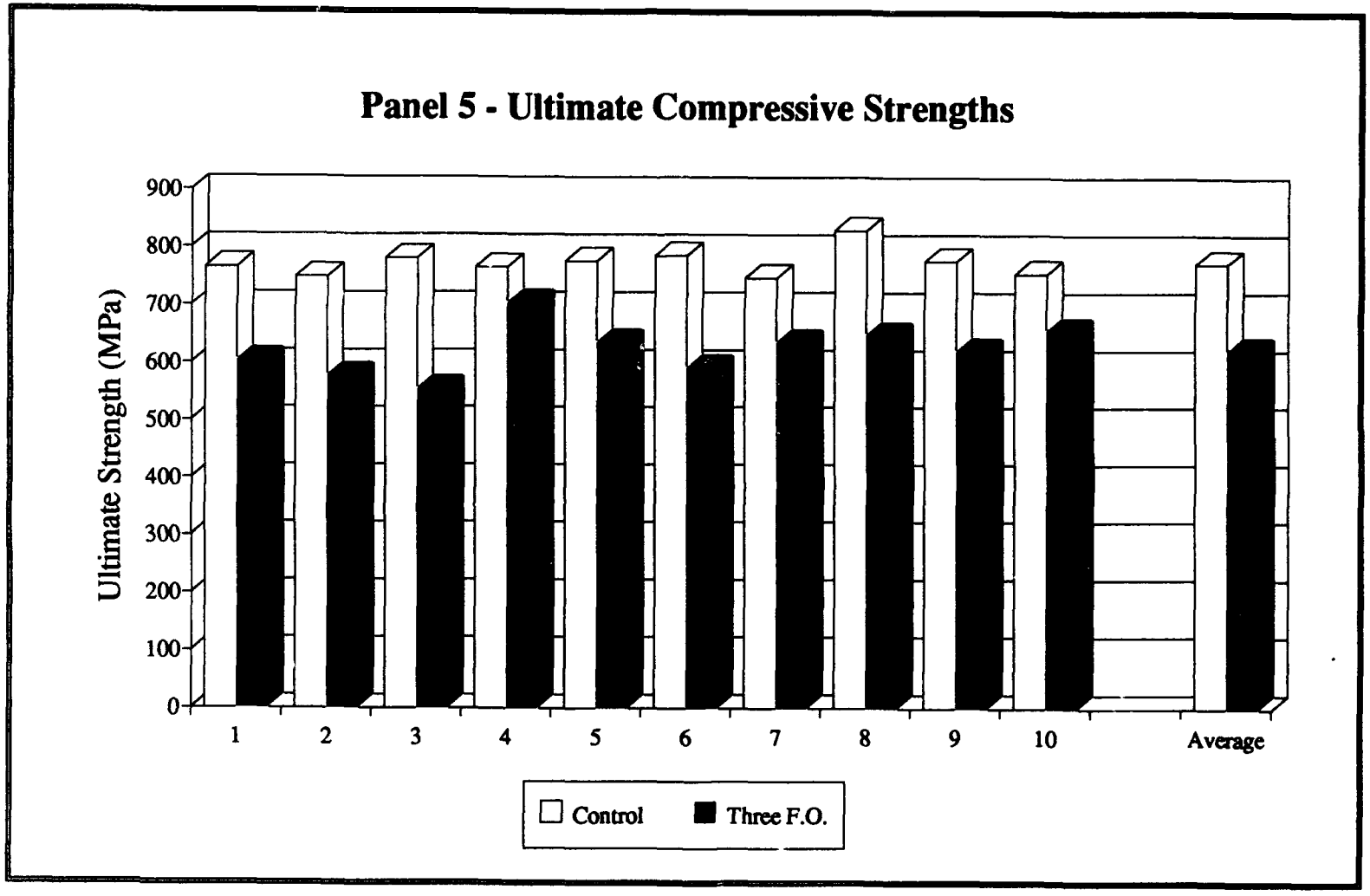

Figure 40 - Panel 5 Test Results

which the failure occurred. This was confirmed by the data in Table 10, where this group showed a strength decrease of almost 20% over the control group.

Figure 41 - Failed Outer Plies of Two Fiber Group

Failure propagated through the optical fibers for this case. In both the two and three optical fiber groups, all resin rich areas surrounding the optical fibers were seen to have cracks propagating through their length. These failure zones can be seen in Figures 42 and 43 which are typical of these failed "resin eyes".

Stress-strain curves of one of the specimens from each group is shown in Figures 44, 45, 46, and 47. These figures were among those used to calculate the initial modulus of elasticity for each of the groups.

Figure 42 - Failure Progression in "resin eye" around Optical Fiber

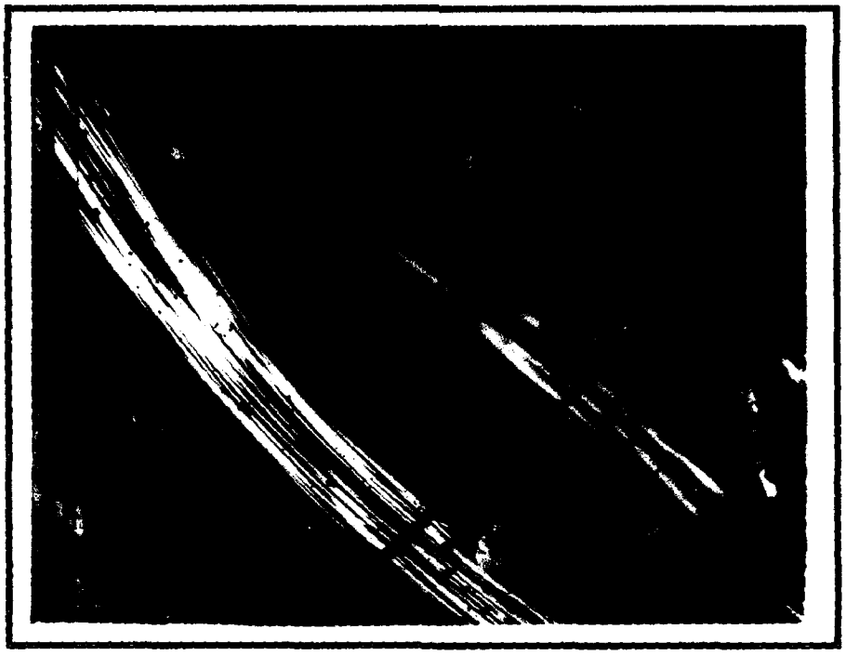

Figure 43 - Failure Progression in "resin eye" around Optical Fiber

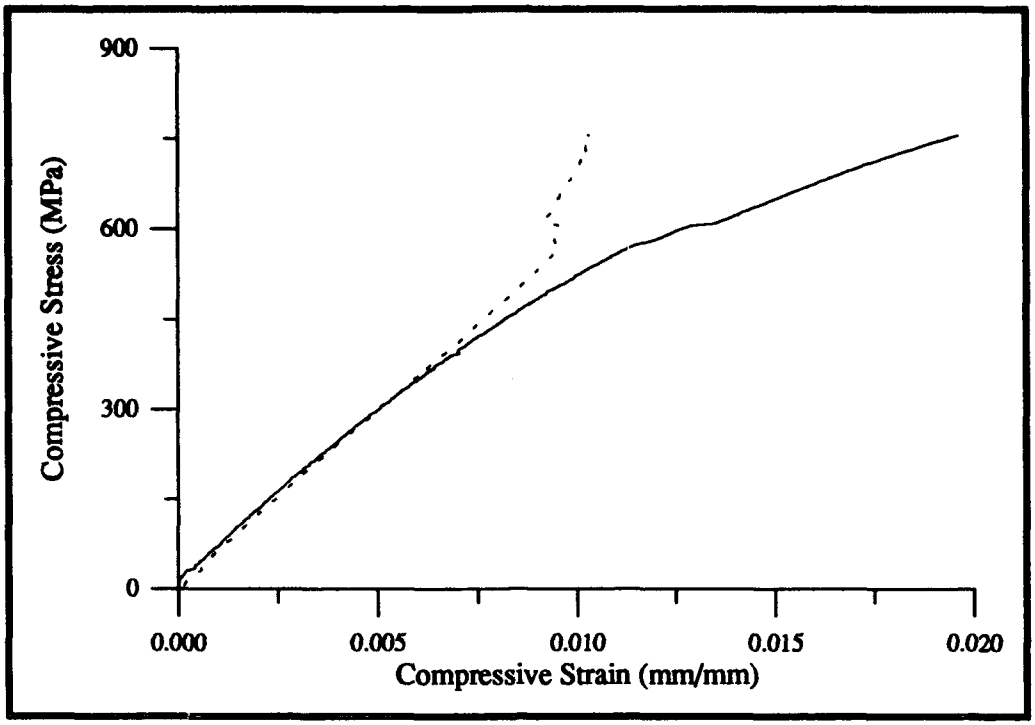

Figure 44 - Stress-Strain Curve of Panel 4 Control Group

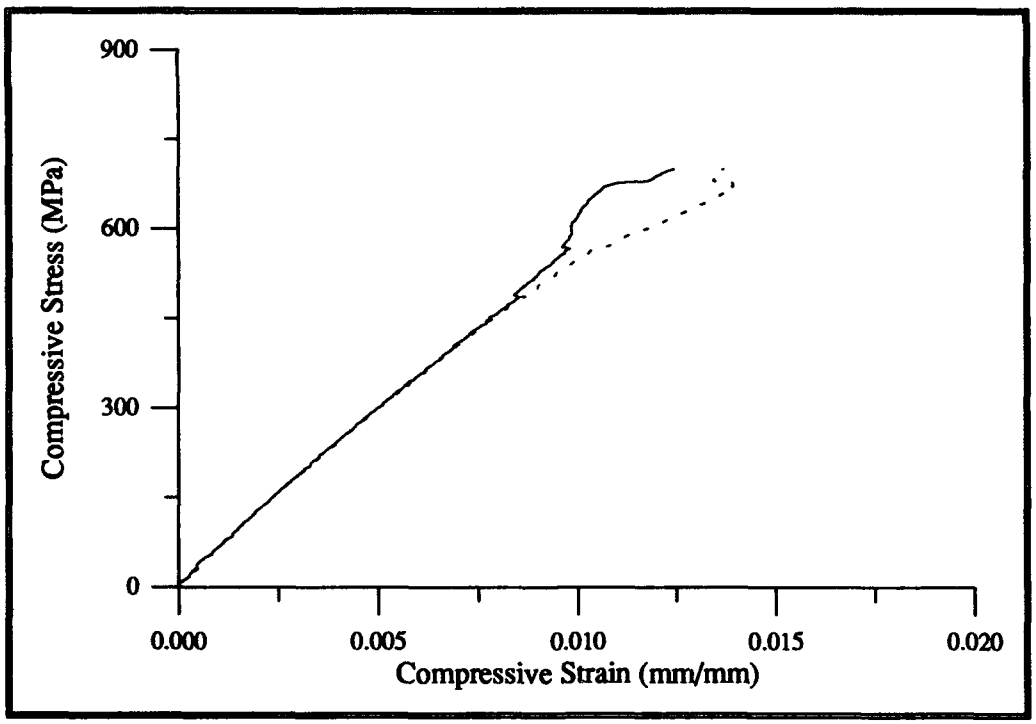

Figure 45 - Stress-Strain Curve of Panel 4 Two Optical Fiber Group

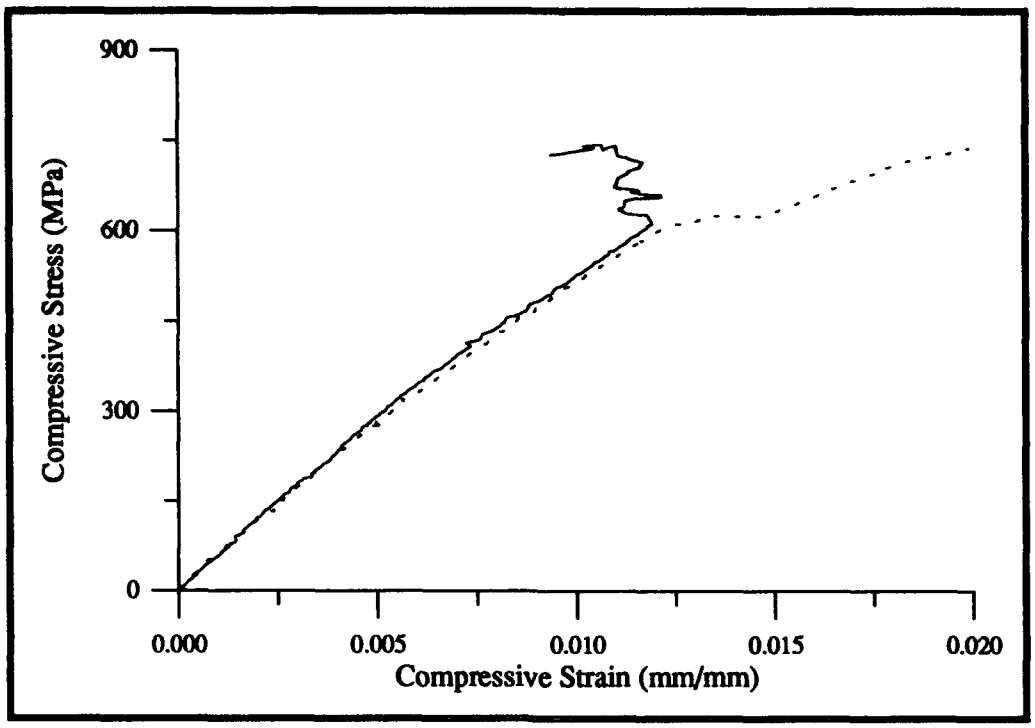

Figure 46 - Stress-Strain Curve of Panel 5 Control Group

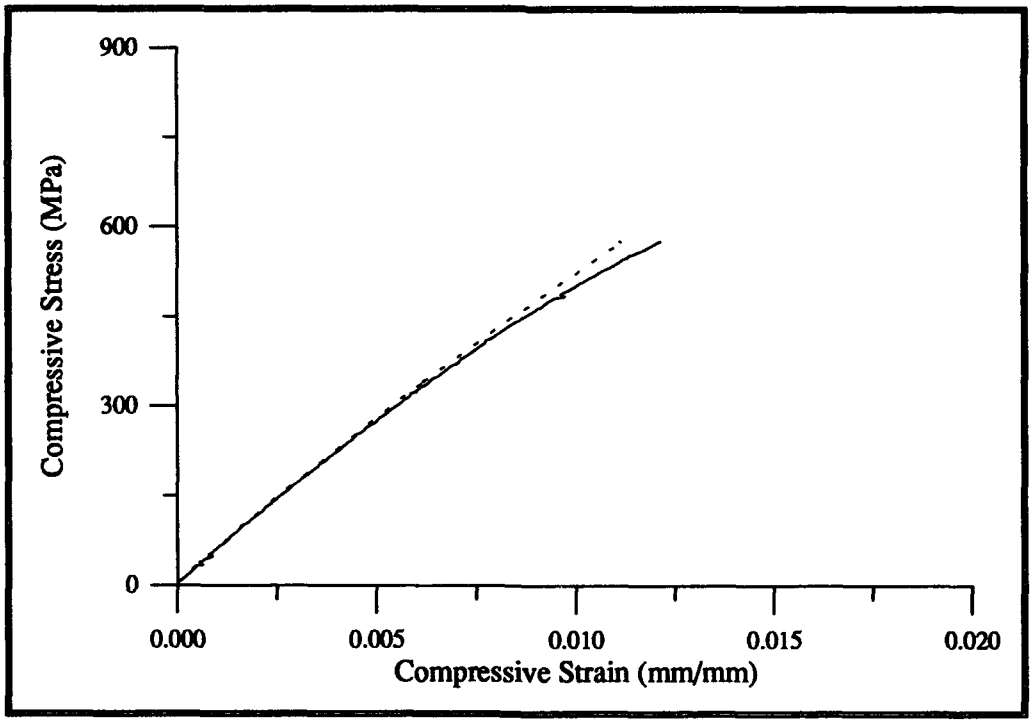

Figure 47 - Stress-Strain Curve of Panel 5 Three Optical Fiber Group

4.5 Panel 6 - Results and Discussion

This panel was fabricated with a control group, a group with two 125 μm optical fibers, and a group with three 125 μm optical fibers. All optical fibers were placed perpendicular to the surrounding structural fibers of the composite. This resulted in the "resin eyes" common to this type of lay-up. Relative to the previous groups with these type of lay-ups (Panels 4 and 5), the resin rich areas surrounding the optical fibers in Panel 6 are much smaller due to the smaller diameter optical fiber. Microphotographs of these groups can be seen in Figures 11, 12, and 14 of Chapter 3.

Only compressive strength data for this panel was obtained and is shown in Table 11 and Figure 48. No stress-strain curves were taken for this panel due to the previous results showing no change in modulus; even for laminates fabricated with three 240 μm diameter optical fibers.

Table 11 - Panel 6 Test Data

PANEL 6	Control	Two F.O.	Three F.O.
Average Strength (MPa)	752.09	767.55	736.74
Standard Deviation	26.36	37.48	19.53
% Deviation	3.50%	4.88%	2.65%
% Strength Reduction	-----	2.06%	-4.01%

The strength data showed that the smaller optical fiber (240 μm versus 125 μm) had a much different effect on strength reduction. Two optical fibers showed an increase in

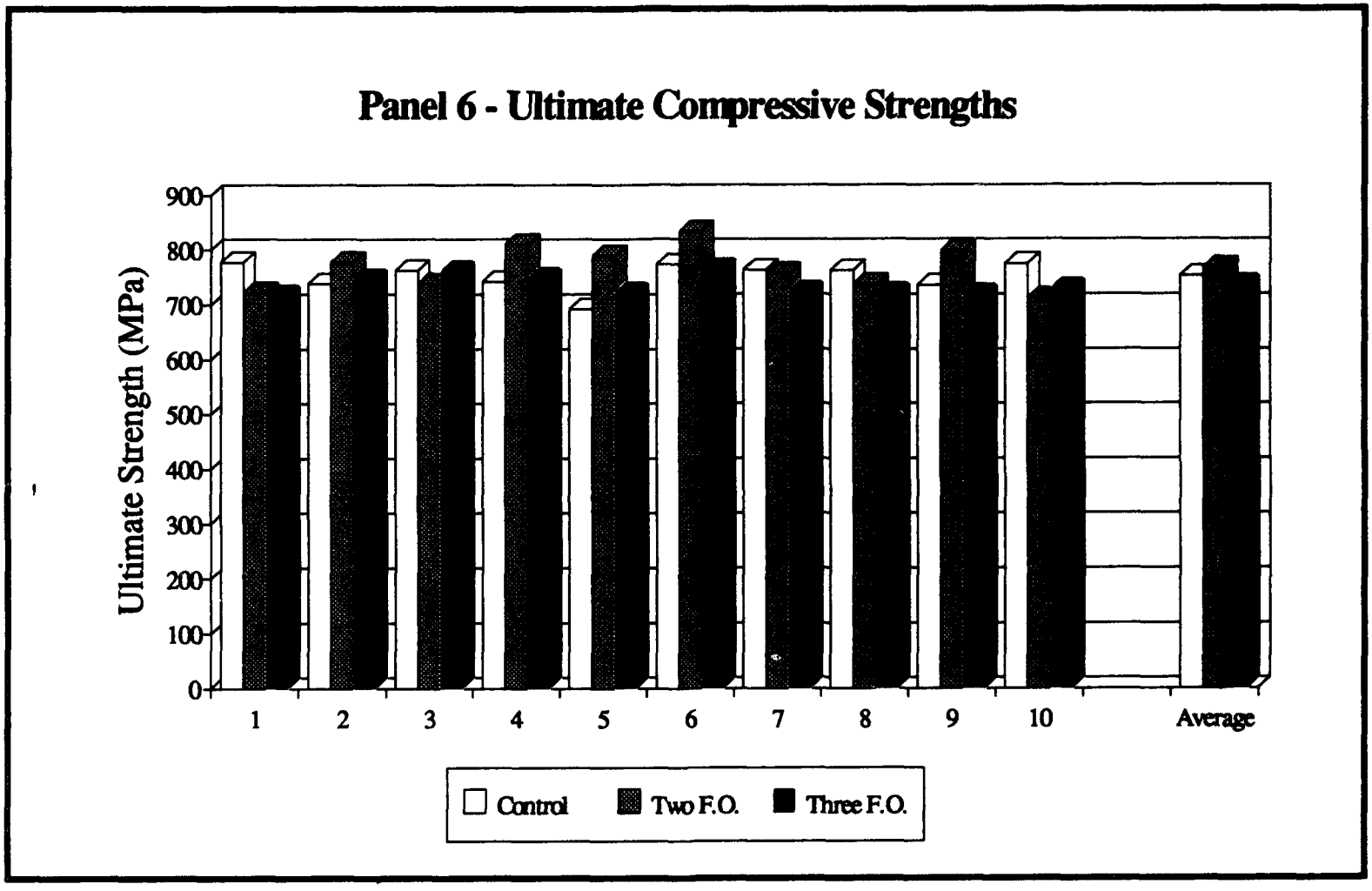

Figure 48 - Panel 6 Test Results

strength by just over 2%, while three optical fibers reduced strength by slightly over 4%. The percent deviations were all under 5% for all groups in this panel.

Failure modes were similar to the majority of other groups where no indication of onset of failure was indicated through visible or audible methods. Unlike other resin rich areas around the optical fiber (Panels 2, 4, and 5) where all "resin eyes" were damaged, only approximately 50% of the "resin eyes" in these groups showed observable damage at failure. Both failed and unfailed "resin eyes" can be seen in Figures 49 and 50.

Figure 49 - Failed Area Surrounding Optical Fiber

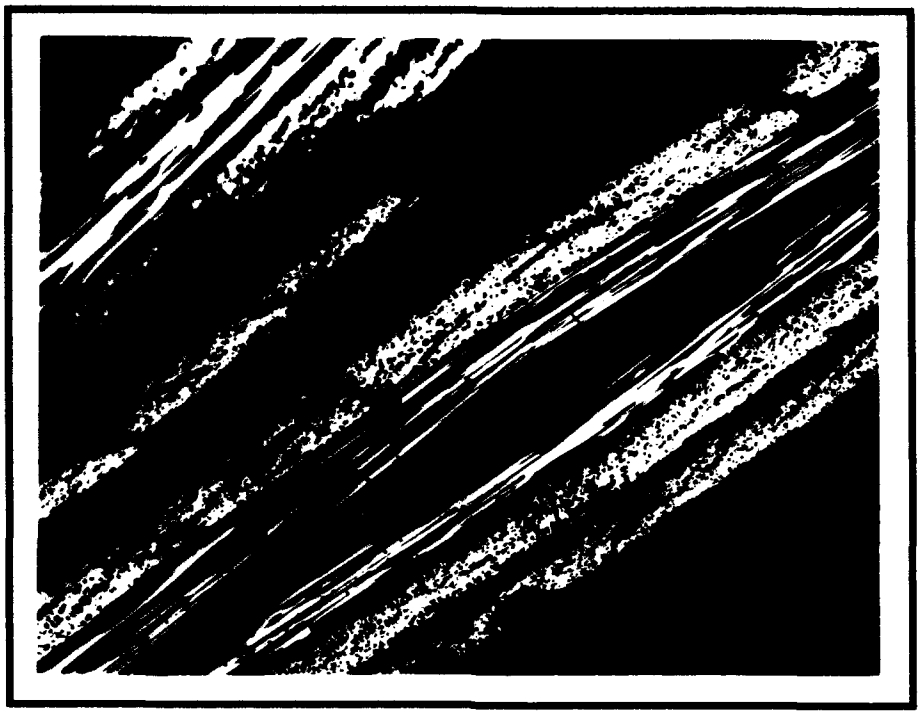

Figure 50 - Intact Area Surrounding Optical Fiber

V. Discussion

This chapter will provide a comprehensive review of the results from this study as they pertain to general embedment issues of optical fibers in composite structures. While the previous chapter discussed results from individual panels and the groups within each panel, this chapter will provide an overall review that correlates the data for all cases. This will be done by relating results to fiber optic orientation with regard to the composite structural fibers, location of the fibers in the structure, number of optical fibers embedded, and diameter of the optical fibers. The results will be discussed in correlation with previous studies already described in Chapter II. Specifically, this will deal with stress and strain concentrations around the optical fiber, fiber waviness, and adhesion of the optical fiber to the composite material.

5.1 Optical Fiber Parallel to Structural Fibers

This study identified the two extremes of optical fiber embedment in the composite structure. The least obtrusive orientation was shown to be where the optical fiber and structural fibers lay parallel to each other in the immediate area surrounding the optical fiber. In this case, the optical fiber is accepted into the composite structure with the minimum perturbation of the composite plies. The most obtrusive case was where the optical fiber was surrounded by perpendicular structural fibers. This latter case resulted in the resin rich area around the optical fiber where the structural fibers had to bridge around it, and has been termed a "resin eye". Both of these configurations were tested using different permutations of optical fiber size, location, and number.

In all cases where the optical fiber was oriented parallel to surrounding composite structural fibers, no effective change in overall compressive strength or

modulus was observed. This was seen for all four groups of specimens with optical fibers taken from panels 1 and 3. In these two panels, only optical fibers with 240 μm diameter were used, and the number of optical fibers embedded ranged from one to three. The optical fibers had different locations within the composite structure which resulted in both symmetric and asymmetric lay-ups about the specimen midplane. These results indicate that even with relatively large optical fibers and multiple embedments, a composite structure's overall strength will not be affected. Figure 51 shows the normalized average stresses for these four groups where they have been normalized by the average stresses of the control groups which contained no optical fibers. As can be seen from this chart, all four groups have retained over 96% of the control group's strength. Additionally, an average of the four groups show a strength retention of over 98%.

This orientation warrants additional discussion regarding observed crack inhibition in the plies containing optical fibers. As briefly discussed in Chapter 4, 90° plies containing optical fibers did not exhibit any matrix cracks up to 95% of the ultimate load. This was in contrast to 90° plies without optical fibers that regularly contained matrix cracks at the same loading. From this, it appears that the optical fiber reduced the effective strain in its 90° plies which caused cracks in the other 90° plies. This can be attributed to the compliant polyimide coating on the optical fiber. This low modulus material would undergo a greater strain than the surrounding stiffer 90° plies and thus absorb enough strain energy to inhibit cracks in these plies. In a review of previous research concerning optical fiber embedment issues, Sirkis and Dasgupta [42] state that several researchers have already shown that the compliant polyimide coating undergoes significantly greater strain concentrations than the surrounding composite material. This would justify the explanation given above. However, this crack arresting feature of the optical fibers did not affect the overall strength of the specimens since the

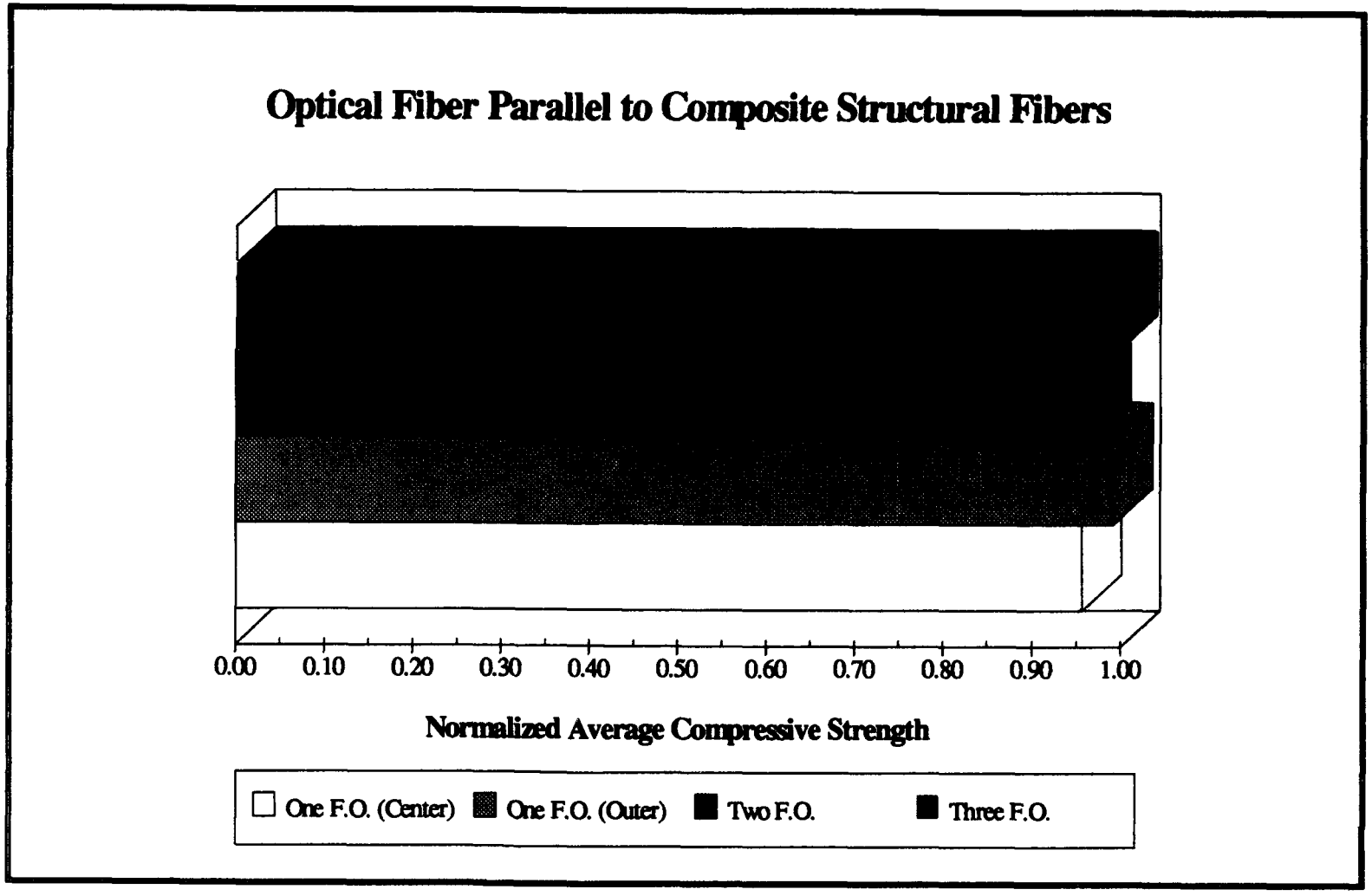

Figure 51 - Normalized Strength of Parallel Optical Fibers

final failure probably initiated from the other 90° plies which did not contain optical fibers.

5.2 Optical Fiber Perpendicular to Structural Fibers

When the optical fiber is placed perpendicular to surrounding structural fibers, results showed that compressive strength can be unaffected or be reduced by as much as 27%. Panels 2, 4, 5, and 6 each carried optical fibers in this orientation. Optical fibers varied in number from one to three, were placed both symmetrically and asymmetrically about the midplane, and had diameters of either 240 μm or 125 μm. As it would be expected, the greatest strength reductions were seen for the larger, multiply embedded optical fibers. Figure 52 shows normalized compressive strengths for each of these groups, where they have been normalized by the strengths of their respective control groups which contained no optical fibers.

The variance in the results for these groups with optical fibers perpendicular to the structural fibers can be explained by reviewing some of the studies presented in Chapter 2. The pertinent investigations for this analysis relate the results on stress concentrations around optical fibers, fiber waviness, and failure patterns in quasi-isotropic graphite/epoxy laminates.

As described in Chapter 4, the failure patterns for all of these laminates was seen to generally follow that described by Sohi et al. [30] where fiber kinking in 0° plies led to multiple delaminations and final failure of the laminate by global buckling of sublaminates. Thus, the 0° plies have the greatest impact on the laminate's strength, as expected.

This fiber kinking in 0° plies was exacerbated by the presence of optical fibers that caused fiber waviness in the 0° plies immediately surrounding the optical fiber. As expected, this waviness was observed to be a function of optical fiber diameter,

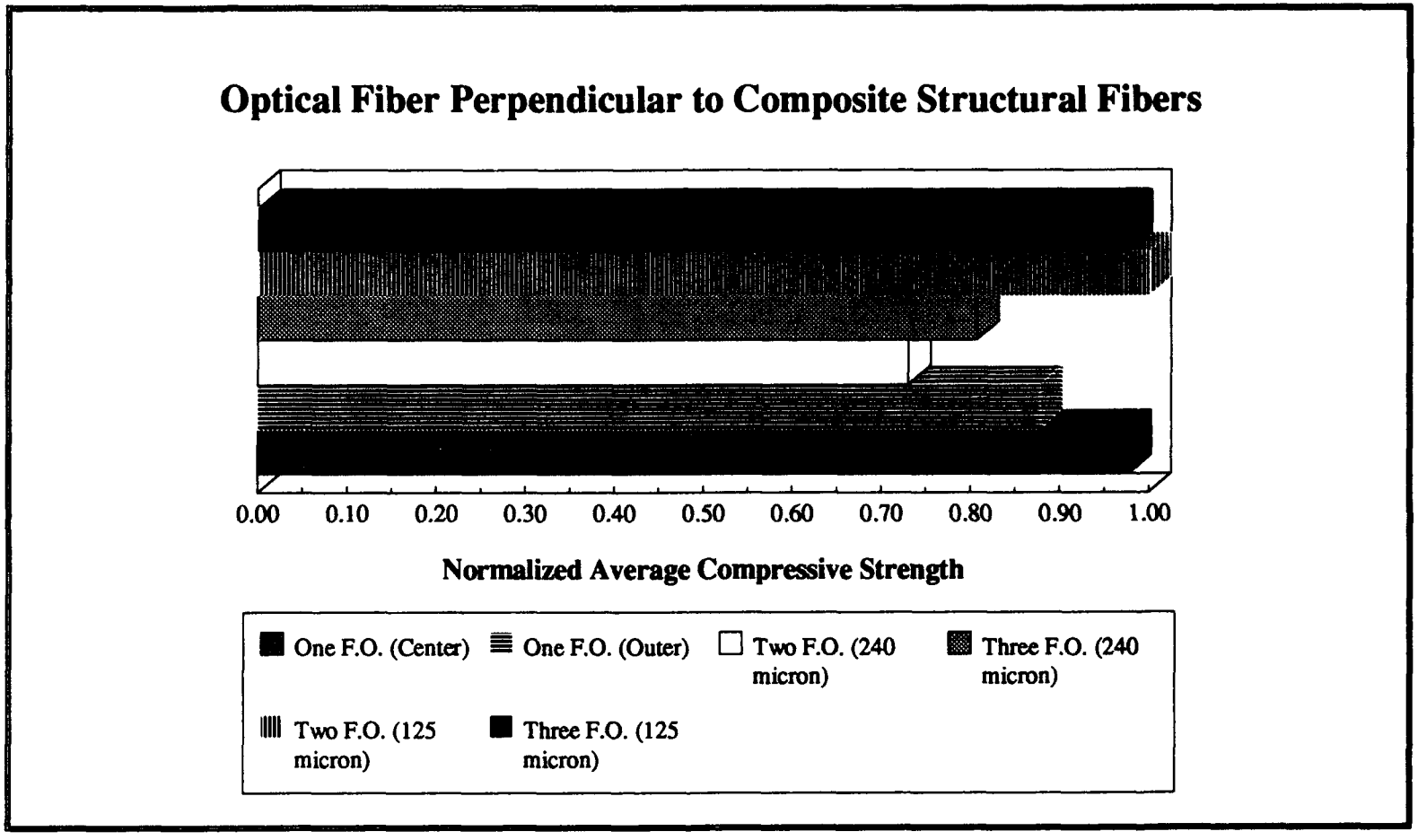

Figure 52 - Normalized Strength of Perpendicular Optical Fibers

whereby the larger optical fiber (240 μm diameter) created greater waviness in the structural fibers. Both Telegades and Hyer [31] and Adams and Hyer [32] have shown that increasing the waviness of structural fibers decreased the strength of the materials studied. This decreased strength results from the structural fibers inability to resist the onset of buckling due to its inherently pre-buckled geometry. The results from this study correlate very well with those given in the above studies. As can be seen from the microphotographs of the laminates in Chapter III, in all cases the larger optical fibers (240 μm) produced substantially greater waviness in the structure than did the smaller optical fibers (125 μm). Correspondingly, in all cases but where the 240 μm diameter optical fiber was placed in the midplane of the structure, lower average strengths resulted. The relatively small 125 μm diameter optical fiber produced only minimal perturbation of the geometry of the structural fibers and, as a result, it did not show any effect on the overall compressive strength of these groups.

Adding to the problem of waviness created by the optical fiber are the stress and strain concentrations created by embedding the optical fiber into composite structures. Although some inconsistencies in results have been noted between the previous studies using FEM and Moiré Interferometry, all of these have shown the stress and strain concentrations around optical fibers. The magnitudes and locations of these concentrations, however, have varied from study to study. Regardless, the overall impact of these results will be considered as having some effect on the overall ability of the laminate to withstand compressive loading. Additional research needs to be accomplished to more accurately quantify and identify these effects, as elaborated next.

One topic that may assist in further determining the stress concentrations and strength effects around optical fibers embedded perpendicular to structural fibers is the incorporation of common failure patterns noted in this study. A vast majority of "resin eyes" failed in the resin rich area in the direction parallel to loading. Two typical

microphotographs can be seen in Figures 42 and 43 of Chapter 4. This would tend to imply that under compressive loading of the laminate, a tensile stress is created in the resin rich area of the "resin eye" by the buckling of the 0° plies surrounding the optical fiber. During testing, this phenomenon was noted during loading of a specimen with polished edges. Figure 53 shows a microphotograph of this specimen at 95% of the ultimate load and clearly shows three matrix cracks in the "resin eye" in the direction parallel to loading. These cracks originated at the coating interface and have propagated outward into the "resin eye". All other areas on this specimen were examined, and no other damage were noted. It would appear that the tensile stress created by the buckling of the 0° plies is sufficient to create matrix cracks in this region and thus initiate failure through crack propagation into the 0° plies surrounding the optical fibers. This would result in the delamination of these plies and generate a failure sequence as described previously.

Figure 53 - Matrix Cracks in "resin eye"

The final topic that warrants consideration in this discussion of the optical fiber perpendicular to the structural fibers is the asymmetric lay-up generated by placing an optical fiber in an outer ply. The lay-up with two optical fibers gave the greatest strength reduction of any of the groups tested in this study. The reduction for this group was substantially greater than the for the group containing three optical fibers (of which two were placed in outer plies). The lay-up with only one optical fiber in an outer ply gave a significantly greater strength reduction than for the lay-up with one optical fiber in the midplane of the structure.

The strength reduction for these asymmetric laminates can again be explained by the waviness of the structural fibers around the optical fiber. In the case where an optical fiber is placed in an asymmetric condition in one of the outer plies of the specimen, fiber waviness results in this location. On the opposite side of the specimen, no optical fiber is present, and therefore, no fiber waviness. This produces a flaw on only one side of the specimen which cannot sustain as high a stress level as the unflawed opposite edge. This results in a premature failure of the outermost plies of the specimen in the area of the embedded optical fiber. Since the IITRI fixture introduces its compressive load through shear transfer from the specimen tabs, this premature failure of the outer plies produces a bending moment on the remaining intact plies. This bending moment results from the fact that the load is applied to the same surfaces as before, however, only one side of the specimen gage section remains intact. The addition of this bending moment to the previously applied compressive load creates a failure of the specimen at the lower stress levels through delamination and global buckling of the specimen. Optical fibers that are placed only in symmetric locations will not undergo this phenomenon due to the inherent symmetry of the specimen and therefore consistent loading develops across the specimen gage section.

5.3 Adhesion

The ability of the optical fiber to accurately sense the changes in its surroundings is the most important feature of smart structure technology. In order for this to occur, the optical fiber coating must be able to transfer the desired sensing function (strain, stress, temperature, etc.) from the composite to the optical fiber core. This requires not only a good bond between the coating and optical fiber core but also between the coating and the composite matrix material. As discussed in Chapter 2, several studies have already been conducted on the adhesive properties of several coatings. DiFranca and Claus [26], and Roberts and Davidson [15] reported findings on these properties. Especially pertinent to this study are the results of Roberts and Davidson who reported that the polyimide coatings they tested adhered well to the optical fiber and failed in the region between the matrix and the coating.

The results from this study suggest the complete opposite from those of Roberts and Davidson [15]. In every case where the specimen failed around the optical fiber, the bond between the coating and the optical fiber core failed. This is apparent in all microphotographs presented in this study and especially in Figures 54 and 55, where the failed area has been magnified to show the intact bond between the coating/matrix interface. As can be seen from this figure, the optical fiber core has stripped away from the coating during the failure sequence, leaving a good interfacial bond between the polyimide coating and the composite matrix. This coating/matrix adhesion gives good indications that the interface will provide an excellent transfer of the sensing function from the composite into the optical fiber coating. The ability of the optical fiber coating to transfer this function to the optical fiber core is in doubt because of the consistently poor adhesive properties seen between these two materials during this study. Additional research must be conducted to determine whether the results indicated from

Figure 54 - Adhesion of Optical Fiber Coating to Epoxy Matrix

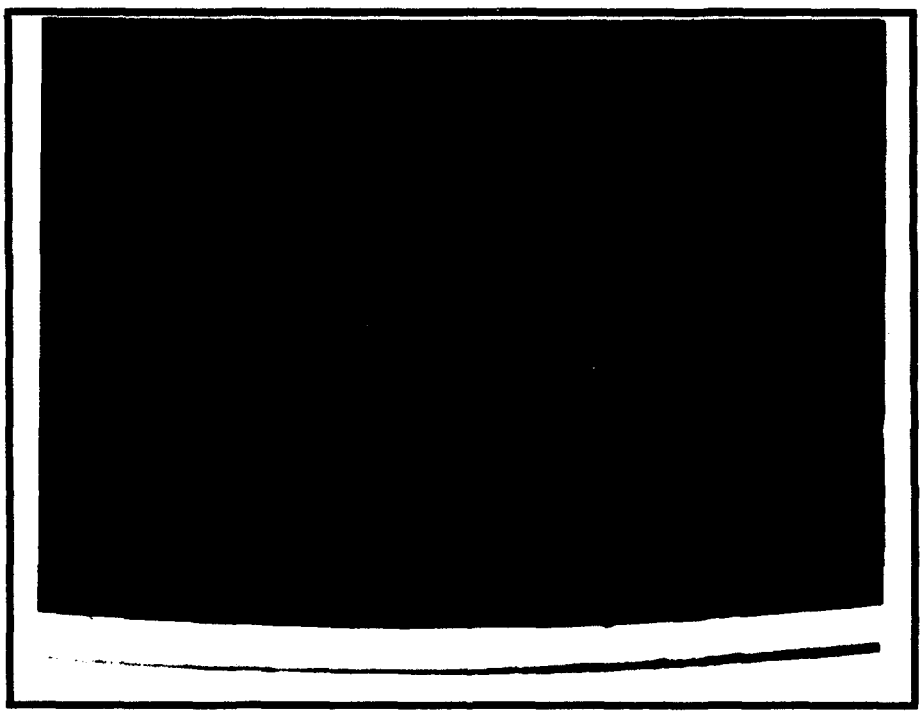

Figure 55 - Adhesion of Optical Fiber Coating to Epoxy Matrix

this study are indicative of all polyimide coatings or are purely dependent on manufacturing specifications of the various optical fibers. It would appear from the results from this study and that of Roberts and Davidson [15] that adhesion is primarily a function of the particular optical fiber and coating system used.

VI. Conclusions and Recommendations

The results from this study show that it is possible to integrate optical fibers into an advanced composite structure without degrading the compressive strength of the structure. By placing the optical fibers in a parallel orientation with the composite's structural fibers, a smart structure can be fabricated that will allow sensing functions to occur without bringing about a weakened structure. This was found to be the case for even relatively large diameter (240 μm) optical fibers which were embedded in multiple cases (two and three) across the midsection of the structure.

Conversely, placing the optical fiber perpendicular to the reinforcing fibers of the composite structure can result in severely reduced compressive strength. As it was shown to be the case for two and three 240 μm optical fibers embedded across the midsection where strength reductions of 27% and 20% can result. However, the results for one 240 μm optical fiber and multiple 125 μm optical fibers located in this arrangement did not provide similar strength reductions. In fact, the smaller optical fibers were shown not to have any deleterious effects even when embedded with two and three across the midsection.

Microphotographs of failed specimens showed that the resin rich area ("resin eye") produced by placing the optical fiber perpendicular to the structural fibers of the composite is vulnerable to failure. Although no completely conclusive evidence was found, it was seen that a tensile stress caused by the buckling of the structural fibers creates cracks in the resin rich area around the optical fiber. These cracks were seen to propagate through the resin and into the surrounding structural fibers and cause delamination of these plies. This delamination led to the formation of sublaminates that caused final failure of the structure by global buckling.

The adhesive properties of this particular optical fiber and polyimide coating were also seen in microphotographs. In contrast to a previous study [15] that

determined that the polyimide coating/optical fiber core interface was the strongest, the results from this study find conclusive evidence that the polyimide coating/composite matrix interface is stronger than the polyimide coating/optical fiber core interface. Almost all failure surfaces that were examined showed optical fiber core pull-out and a good bond between the polyimide coating and the composite matrix.

The results from this study answer several questions regarding the embedment of optical fibers on the compressive strength of the structure. However, very little research has been accomplished on other material properties of these smart structures. For these materials to be accepted into aircraft structures, the fatigue effects of the embedded optical fibers must be understood. Only a handful of studies have been presented in this area and have been inconclusive. This fatigue research is critical to aircraft due to the constant redistribution of loads on an airframe during flight. Greater understanding of any cyclic effects must be understood before smart structures can even be considered for implementation into aircraft structures. The present study provides the first step towards this area of future investigation.

Also, the local interaction mechanics of the optical fiber must be further investigated. Several of the previous studies on micromechanical interaction have not provided results that correspond with failure modes produced in this study. Additional research into the levels of stress and strain concentrations must be accomplished in order to place limits on acceptable concentrations with regard to optical fiber diameters and coating materials. This is required to develop design limits for embedment of these optical fibers into smart structures.

A final topic of investigation needs to be covered addressing a model for embedding optical fibers into composite structures. To date, no models have been presented that can quantify the effects of optical fibers on the compressive strength of

composite materials. Previous models developed for compression of composites without embedded optical fibers are inadequate for this topic.

This study was only able to investigate a small portion of the area of smart structure research. Although the results from this study provide several answers to methods of implementing smart structure technology, this technology is still in its infancy. The research that has been accomplished to date has only scratched the surface on the vast possibilities that this technology offers.

Appendix A: Determination of Critical Buckling Load

For exceedingly high-strength materials, irrespective of modulus, the test is governed by the adhesive strength of the tabs or the interlaminar shear strength of the parent tab material. For low-modulus materials, elastic column buckling may be critical.

The most conservative assumption regarding behavior of a specimen under axial compression is to assume that the specimen acts as a pinned-end column whose length is equal to the unsupported length of the test fixture.

Assuming elastic behavior, the critical buckling load for such a pinned end column is given as:

$$P_{cr} = \frac{\left[\frac{\pi}{L}\right]^2 \cdot D_{11}}{1 + \left[n \cdot \frac{\left[\frac{\pi}{L}\right]^2}{\left[t \cdot w \cdot G_{12}\right]}\right]}$$

where:

- **D = flexural stiffness of the material**
- **G = shear stiffness in the direction of buckling**
- **n = constraint constant (1.2 for rectangular cross-section)**
- **L = gage length of the specimen (12.7 mm)**
- **t = thickness of the specimen (30 plies by .000136 m/ply)**
- **w = width of the specimen (6.35 mm)**

For the laminate used in this testing, the flexural stiffness and shear modulus, calculated in Appendix A is:

$D_{11} := 487.2$ $\quad t := 30 \cdot .136$ $\quad L := 12.7$

$G_{12} := 1.93 \cdot 10^{10}$ $\quad n := 1.2$ $\quad w := 6.35$

$$P := \frac{\left[\frac{\pi}{L}\right]^2 \cdot D_{11}}{1 + \left[n \cdot \frac{\left[\frac{\pi}{L}\right]^2}{\left[t \cdot w \cdot G_{12}\right]}\right]}$$

$P = 29.813$ **Critical Buckling Load (KN)**

$$\sigma := \frac{P}{(w \cdot t)} \cdot 1000$$

$\sigma = 1.151 \cdot 10^3$ **Critical Buckling Stress (MPa)**

Appendix B: Material Properties of the Laminate

Properties obtained from Data Sheet from Hercules, Inc for AS-4/3501

Longitudinal Modulus of Elasticity (Pa): $E_1 = 141 \cdot 10^9$

Transverse Modulus of Elasticity (Pa): $E_2 = 12.5 \cdot 10^9$

Major Poisson's Ratio: $\nu_{12} = 0.27$

Shear Modulus (Pa): $G_{12} = 7.6 \cdot 10^9$

Minor Poisson's Rato:

$$\nu_{21} := E_2 \cdot \frac{\nu_{12}}{E_1} \qquad \nu_{21} = 0.024$$

Ply Thickness (m):

$$Thick := 1.36 \cdot 10^{-4}$$

Evaluate the lamina properties for the Stiffness Matrix:

$$Q_{11} := \frac{E_1}{\left[1 - \nu_{21} \cdot \nu_{12}\right]} \qquad Q_{12} := \frac{E_1}{\left[1 - \nu_{21} \cdot \nu_{12}\right]} \cdot \nu_{21}$$

$$Q_{22} := \frac{E_2}{\left[1 - \nu_{21} \cdot \nu_{12}\right]} \qquad Q_{66} := G_{12}$$

Assemble the lamina Stiffness Matrix:

$$Q := \begin{bmatrix} Q_{11} & Q_{12} & 0 \\ Q_{12} & Q_{22} & 0 \\ 0 & 0 & Q_{66} \end{bmatrix} \quad Q = \begin{bmatrix} 1.419 \cdot 10^{11} & 3.397 \cdot 10^9 & 0 \\ 3.397 \cdot 10^9 & 1.258 \cdot 10^{10} & 0 \\ 0 & 0 & 7.6 \cdot 10^9 \end{bmatrix}$$

Define the Transformation Matrices for each orientation:
(There are four orientations - 0, +45, -45, 90)

$$\theta := \frac{\pi}{4} \qquad \theta 1 := \frac{-\pi}{4} \qquad \theta 2 := \frac{\pi}{2}$$

$$T := \begin{bmatrix} \cos(\theta)^2 & \sin(\theta)^2 & 2 \cdot \sin(\theta) \cdot \cos(\theta) \\ \sin(\theta)^2 & \cos(\theta)^2 & -2 \cdot \sin(\theta) \cdot \cos(\theta) \\ -\sin(\theta) \cdot \cos(\theta) & \sin(\theta) \cdot \cos(\theta) & \cos(\theta)^2 - \sin(\theta)^2 \end{bmatrix} \qquad T = \begin{bmatrix} 0.5 & 0.5 & 1 \\ 0.5 & 0.5 & -1 \\ -0.5 & 0.5 & 0 \end{bmatrix}$$

$$T1 := \begin{bmatrix} \cos(\theta 1)^2 & \sin(\theta 1)^2 & 2 \cdot \sin(\theta 1) \cdot \cos(\theta 1) \\ \sin(\theta 1)^2 & \cos(\theta 1)^2 & -2 \cdot \sin(\theta 1) \cdot \cos(\theta 1) \\ -\sin(\theta 1) \cdot \cos(\theta 1) & \sin(\theta 1) \cdot \cos(\theta 1) & \cos(\theta 1)^2 - \sin(\theta 1)^2 \end{bmatrix} \qquad T1 = \begin{bmatrix} 0.5 & 0.5 & -1 \\ 0.5 & 0.5 & 1 \\ 0.5 & -0.5 & 0 \end{bmatrix}$$

$$T2 := \begin{bmatrix} \cos(\theta 2)^2 & \sin(\theta 2)^2 & 2 \cdot \sin(\theta 2) \cdot \cos(\theta 2) \\ \sin(\theta 2)^2 & \cos(\theta 2)^2 & -2 \cdot \sin(\theta 2) \cdot \cos(\theta 2) \\ -\sin(\theta 2) \cdot \cos(\theta 2) & \sin(\theta 2) \cdot \cos(\theta 2) & \cos(\theta 2)^2 - \sin(\theta 2)^2 \end{bmatrix} \qquad T2 = \begin{bmatrix} 0 & 1 & 0 \\ 1 & 0 & 0 \\ 0 & 0 & -1 \end{bmatrix}$$

Calculate the Q-Bar Matrices for the lamina properties for orientation relative to the zero degree fiber orientation:

$$QB45 := T^{-1}\cdot Q\cdot M\cdot T\cdot M^{-1} \qquad QB45 = \begin{bmatrix} 4.792\cdot10^{10} & 3.272\cdot10^{10} & 3.233\cdot10^{10} \\ 3.272\cdot10^{10} & 4.792\cdot10^{10} & 3.233\cdot10^{10} \\ 3.233\cdot10^{10} & 3.233\cdot10^{10} & 3.693\cdot10^{10} \end{bmatrix}$$

$$QBN45 := T1^{-1}\cdot Q\cdot M\cdot T1\cdot M^{-1} \qquad QBN45 = \begin{bmatrix} 4.792\cdot10^{10} & 3.272\cdot10^{10} & -3.233\cdot10^{10} \\ 3.272\cdot10^{10} & 4.792\cdot10^{10} & -3.233\cdot10^{10} \\ -3.233\cdot10^{10} & -3.233\cdot10^{10} & 3.693\cdot10^{10} \end{bmatrix}$$

$$QB90 := T2^{-1}\cdot Q\cdot M\cdot T2\cdot M^{-1} \qquad QB90 = \begin{bmatrix} 1.258\cdot10^{10} & 3.397\cdot10^{9} & 3.683\cdot10^{-7} \\ 3.397\cdot10^{9} & 1.419\cdot10^{11} & 7.551\cdot10^{-6} \\ 3.683\cdot10^{-7} & 7.551\cdot10^{-6} & 7.6\cdot10^{9} \end{bmatrix}$$

Assemble the [A] matrix for the laminate:

$$A := Thick\cdot(12\cdot Q+6\cdot QB45+6\cdot QBN45+6\cdot QB90)$$

$$A = \begin{bmatrix} 3.201\cdot10^{8} & 6.172\cdot10^{7} & 3.006\cdot10^{-10} \\ 6.172\cdot10^{7} & 2.145\cdot10^{8} & 6.162\cdot10^{-9} \\ 3.006\cdot10^{-10} & 6.162\cdot10^{-9} & 7.887\cdot10^{7} \end{bmatrix}$$

LAMINATE MATERIAL PROPERTIES:

$$E1 := \frac{\left[A_{[0,0]}\cdot A_{[1,1]}-\left[A_{[0,1]}\right]^2\right]}{\left[A_{[1,1]}\cdot Thick\cdot 30\right]} \qquad E1 = 7.41\cdot10^{10}$$ **Longitudinal Modulus**

$$E2 := \frac{\left[A_{[0,0]}\cdot A_{[1,1]}-\left[A_{[0,1]}\right]^2\right]}{\left[A_{[0,0]}\cdot Thick\cdot 30\right]} \qquad E2 = 4.967\cdot10^{10}$$ **Transverse Modulus**

$$\nu_{12} := \frac{A_{[0,1]}}{A_{[1,1]}} \qquad \nu_{12} = 0.288$$ **Major Poisson Ratio**

$$\nu_{21} := \frac{A_{[0,1]}}{A_{[0,0]}} \qquad \nu_{21} = 0.193$$ **Minor Poisson Ratio**

$$G_{12} := \frac{A_{[2,2]}}{(Thick\cdot 30)} \qquad G_{12} = 1.933\cdot10^{10}$$ **Shear Modulus**

Appendix C: Failure Theory Output from GENLAM

Think Composites's GENLAM V

Laminate stiffness matrix

.3201E+09	.6172E+08	.3025E+00	.1968E+00	-.4141E-01	-.5129E-03
.6172E+08	.2145E+09	-.3198E+01	-.4141E-01	-.1147E+00	-.5129E-03
.3025E+00	-.3198E+01	.7887E+08	-.5129E-03	-.5129E-03	-.3941E-01

.1968E+00	-.4141E-01	-.5129E-03	.4872E+03	.6850E+02	.1431E+02
-.4141E-01	-.1147E+00	-.5129E-03	.6850E+02	.2887E+03	.1431E+02
-.5129E-03	-.5129E-03	-.3941E-01	.1431E+02	.1431E+02	.9229E+02

A* B*
3B* D* [GPa]

78.452	15.127	.000	.000	.000	.000
15.127	52.585	.000	.000	.000	.000
.000	.000	19.330	.000	.000	.000

.000	.000	.000	86.075	12.104	2.529
.000	.000	.000	12.104	51.010	2.529
.000	.000	.000	2.529	2.529	16.307

Laminate compliance matrix

.3308E-08	-.9515E-09	-.5126E-16	-.1484E-11	.4398E-12	.1750E-12
-.9515E-09	.4935E-08	.2037E-15	.5739E-12	.1704E-11	-.3312E-12
-.5126E-16	.2037E-15	.1268E-07	-.1162E-12	-.2209E-12	.5466E-11

-.1484E-11	.5739E-12	-.1162E-12	.2129E-02	-.4927E-03	-.2539E-03
.4398E-12	.1704E-11	-.2209E-12	-.4927E-03	.3605E-02	-.4827E-03
.1750E-12	-.3312E-12	.5466E-11	-.2539E-03	-.4827E-03	.1095E-01

a*	b*/3				
b*T	d*	1/[TPa]			
13.495	-3.882	.000	.000	.000	.000
-3.882	20.134	.000	.000	.000	.000
.000	.000	51.732	.000	.000	.000
.000	.000	.000	12.052	-2.788	-1.437
.000	.000	.000	-2.788	20.401	-2.732
.000	.000	.000	-1.437	-2.732	61.971

LAMINATE ENGINEERING CONSTANTS

N O T E ! !

Applies only to SYMMETRIC laminates

Inplane constants

E1o = 74.1006 E2o = 49.6683 E6o = 19.3304 [GPa]

alp1o = 1.4278 alp2o = 4.0137 alp6o = .0000 1/[C]*1E6

bet1o = .0268 bet2o = .0668 bet6o = .0000 [kg/kg]

nu21o = .2877 nu61o = .0000 nu62o = .0000

nu12o = .1928 nu16o = .0000 nu26o = .0000

Flexural constants

E1f = 82.9730 E2f = 49.0174 E6f = 16.1365 [GPa]

nu21f = .2314 nu61f = -.1192 nu62f = -.1339

nu12f = .1367 nu16f = -.0232 nu26f = -.0441

Load Case No 1

eps1	eps2	eps6	k1	k2	k6
-.3365E-02	.7478E-03	.3367E-10	.1567E-05	-.6347E-06	-.1613E-06

eps1o	eps2o	eps6o	eps1f	eps2f	eps6f *1E3
-3.3651	.7478	.0000	.0000	.0000	.0000

N1	N2	N6	M1	M2	M6
-.1000E+07	.0000E+00	.0000E+00	.0000E+00	.0000E+00	.0000E+00

sigma1o	sigma2o	sigma6o	sigma1f	sigma2f	sigma6f [MPa]
-245.10	.00	.00	.00	.00	.00

Temperature difference -134.0 Moisture .0050

Ply strains in 1000:s microstrains

Ply No	eps-1	eps-2	eps-6	eps-x	eps-y	eps-s
30 Top	-3.3651	.7478	.0000	-3.3651	.7478	.0000
30 Bot	-3.3651	.7478	.0000	-3.3651	.7478	.0000
29 Top	-3.3651	.7478	.0000	-3.3651	.7478	.0000
29 Bot	-3.3651	.7478	.0000	-3.3651	.7478	.0000
28 Top	-3.3651	.7478	.0000	-1.3086	-1.3086	4.1130
28 Bot	-3.3651	.7478	.0000	-1.3086	-1.3086	4.1130
27 Top	-3.3651	.7478	.0000	.7478	-3.3651	.0000
27 Bot	-3.3651	.7478	.0000	.7478	-3.3651	.0000
26 Top	-3.3651	.7478	.0000	.7478	-3.3651	.0000
26 Bot	-3.3651	.7478	.0000	.7478	-3.3651	.0000
25 Top	-3.3651	.7478	.0000	-1.3086	-1.3086	-4.1130
25 Bot	-3.3651	.7478	.0000	-1.3086	-1.3086	-4.1130

Ply No	eps-1	eps-2	eps-6	eps-x	eps-y	eps-s
24 Top	-3.3651	.7478	.0000	-3.3651	.7478	. 0000
24 Bot	-3.3651	.7478	.0000	-3.3651	.7478	.0000
23 Top	-3.3651	.7478	.0000	-3.3651	.7478	.0000
23 Bot	-3.3651	.7478	.0000	-3.3651	.7478	.0000
22 Top	-3.3651	.7478	.0000	-1.3086	-1.3086	4.1130
22 Bot	-3.3651	.7478	.0000	-1.3086	-1.3086	4.1130
21 Top	-3.3651	.7478	.0000	-1.3086	-1.3086	-4.1130
21 Bot	-3.3651	.7478	.0000	-1.3086	-1.3086	-4.1130
20 Top	-3.3651	.7478	.0000	-3.3651	.7478	.0000
20 Bot	-3.3651	.7478	.0000	-3.3651	.7478	.0000
19 Top	-3.3651	.7478	.0000	-1.3086	-1.3086	4.1130
19 Bot	-3.3651	.7478	.0000	-1.3086	-1.3086	4.1130
18 Top	-3.3651	.7478	.0000	-3.3651	.7478	.0000
18 Bot	-3.3651	.7478	.0000	-3.3651	.7478	.0000
17 Top	-3.3651	.7478	.0000	-1.3086	-1.3086	-4.1130
17 Bot	-3.3651	.7478	.0000	-1.3086	-1.3086	-4.1130
16 Top	-3.3651	.7478	.0000	.7478	-3.3651	.0000
16 Bot	-3.3651	.7478	.0000	.7478	-3.3651	.0000
15 Top	-3.3651	.7478	.0000	.7478	-3.3651	.0000
15 Bot	-3.3651	.7478	.0000	.7478	-3.3651	.0000
14 Top	-3.3651	.7478	.0000	-1.3086	-1.3086	-4.1130
14 Bot	-3.3651	.7478	.0000	-1.3086	-1.3086	-4.1130
13 Top	-3.3651	.7478	.0000	-3.3651	.7478	.0000
13 Bot	-3.3651	.7478	.0000	-3.3651	.7478	.0000
12 Top	-3.3651	.7478	.0000	-1.3086	-1.3086	4.1130
12 Bot	-3.3651	.7478	.0000	-1.3086	-1.3086	4.1130
11 Top	-3.3651	.7478	.0000	-3.3651	.7478	.0000
11 Bot	-3.3651	.7478	.0000	-3.3651	.7478	.0000
10 Top	-3.3651	.7478	.0000	-1.3086	-1.3086	-4.1130
10 Bot	-3.3651	.7478	.0000	-1.3086	-1.3086	-4.1130
9 Top	-3.3651	.7478	.0000	-1.3086	-1.3086	4.1130
9 Bot	-3.3651	.7478	.0000	-1.3086	-1.3086	4.1130
8 Top	-3.3651	.7478	.0000	-3.3651	.7478	.0000
8 Bot	-3.3651	.7478	.0000	-3.3651	.7478	.0000
7 Top	-3.3651	.7478	.0000	-3.3651	.7478	.0000
7 Bot	-3.3651	.7478	.0000	-3.3651	.7478	.0000
6 Top	-3.3651	.7478	.0000	-1.3086	-1.3086	-4.1130
6 Bot	-3.3651	.7478	.0000	-1.3086	-1.3086	-4.1130
5 Top	-3.3651	.7478	.0000	.7478	-3.3651	.0000
5 Bot	-3.3651	.7478	.0000	.7478	-3.3651	.0000
4 Top	-3.3651	.7478	.0000	.7478	-3.3651	.0000
4 Bot	-3.3651	.7478	.0000	.7478	-3.3651	.0000

Ply No	eps-1	eps-2	eps-6	eps-x	eps-y	eps-s
3 Top	-3.3651	.7478	.0000	-1.3086	-1.3086	4.1130
3 Bot	-3.3651	.7478	.0000	-1.3086	-1.3086	4.1130
2 Top	-3.3651	.7478	.0000	-3.3651	.7478	.0000
2 Bot	-3.3651	.7478	.0000	-3.3651	.7478	.0000
1 Top	-3.3651	.7478	.0000	-3.3651	.7478	.0000
1 Bot	-3.3651	.7478	.0000	-3.3651	.7478	.0000

Ply stresses in MPa

Ply No	sigma-1	sigma-2	sigma-6	sigma-x	sigma-y	sigma-s
30 Top	-475.42	17.54	.00	-475.42	17.54	.00
30 Bot	-475.42	17.54	.00	-475.42	17.54	.00
29 Top	-475.42	17.54	.00	-475.42	17.54	.00
29 Bot	-475.42	17.54	.00	-475.42	17.54	.00
28 Top	-127.21	-64.69	-94.60	-190.55	-1.35	31.26
28 Bot	-127.21	-64.69	-94.60	-190.55	-1.35	31.26
27 Top	-20.24	94.31	.00	94.31	-20.24	.00
27 Bot	-20.24	94.31	.00	94.31	-20.24	.00
26 Top	-20.24	94.31	.00	94.31	-20.24	.00
26 Bot	-20.24	94.31	.00	94.31	-20.24	.00
25 Top	-127.21	-64.69	94.60	-190.55	-1.35	-31.26
25 Bot	-127.21	-64.69	94.60	-190.55	-1.35	-31.26
24 Top	-475.42	17.54	.00	-475.42	17.54	.00
24 Bot	-475.42	17.54	.00	-475.42	17.54	.00
23 Top	-475.42	17.54	.00	-475.42	17.54	.00
23 Bot	-475.42	17.54	.00	-475.42	17.54	.00
22 Top	-127.21	-64.69	-94.60	-190.55	-1.35	31.26
22 Bot	-127.21	-64.69	-94.60	-190.55	-1.35	31.26
21 Top	-127.21	-64.69	94.60	-190.55	-1.35	-31.26
21 Bot	-127.21	-64.69	94.60	-190.55	-1.35	-31.26
20 Top	-475.42	17.54	.00	-475.42	17.54	.00
20 Bot	-475.42	17.54	.00	-475.42	17.54	.00
19 Top	-127.21	-64.69	-94.60	-190.55	-1.35	31.26
19 Bot	-127.21	-64.69	-94.60	-190.55	-1.35	31.26
18 Top	-475.42	17.54	.00	-475.42	17.54	.00
18 Bot	-475.42	17.54	.00	-475.42	17.54	.00
17 Top	-127.21	-64.69	94.60	-190.55	-1.35	-31.26
17 Bot	-127.21	-64.69	94.60	-190.55	-1.35	-31.26
16 Top	-20.24	94.31	.00	94.31	-20.24	.00
16 Bot	-20.24	94.31	.00	94.31	-20.24	.00

Ply No	eps-1	eps-2	eps-6	eps-x	eps-y	eps-s
15 Top	-20.24	94.31	.00	94.31	-20.24	.00
15 Bot	-20.24	94.31	.00	94.31	-20.24	.00
14 Top	-127.21	-64.69	94.60	-190.55	-1.35	-31.26
14 Bot	-127.21	-64.69	94.60	-190.55	-1.35	-31.26
13 Top	-475.42	17.54	.00	-475.42	17.54	.00
13 Bot	-475.42	17.54	.00	-475.42	17.54	.00
12 Top	-127.21	-64.69	-94.60	-190.55	-1.35	31.26
12 Bot	-127.21	-64.69	-94.60	-190.55	-1.35	31.26
11 Top	-475.42	17.54	.00	-475.42	17.54	.00
11 Bot	-475.42	17.54	.00	-475.42	17.54	.00
10 Top	-127.21	-64.69	94.60	-190.55	-1.35	-31.26
10 Bot	-127.21	-64.69	94.60	-190.55	-1.35	-31.26
9 Top	-127.21	-64.69	-94.60	-190.55	-1.35	31.26
9 Bot	-127.21	-64.69	-94.60	-190.55	-1.35	31.26
8 Top	-475.42	17.54	.00	-475.42	17.54	.00
8 Bot	-475.42	17.54	.00	-475.42	17.54	.00
7 Top	-475.42	17.54	.00	-475.42	17.54	.00
7 Bot	-475.42	17.54	.00	-475.42	17.54	.00
6 Top	-127.21	-64.69	94.60	-190.55	-1.35	-31.26
6 Bot	-127.21	-64.69	94.60	-190.55	-1.35	-31.26
5 Top	-20.24	94.31	.00	94.31	-20.24	.00
5 Bot	-20.24	94.31	.00	94.31	-20.24	.00
4 Top	-20.24	94.31	.00	94.31	-20.24	.00
4 Bot	-20.24	94.31	.00	94.31	-20.24	.00
3 Top	-127.21	-64.69	-94.60	-190.55	-1.35	31.26
3 Bot	-127.21	-64.69	-94.60	-190.55	-1.35	31.26
2 Top	-475.42	17.54	.00	-475.42	17.54	.00
2 Bot	-475.42	17.54	.00	-475.42	17.54	.00
1 Top	-475.42	17.54	.00	-475.42	17.54	.00
1 Bot	-475.42	17.54	.00	-475.42	17.54	.00

Quadratic Failure Criterion

Ply	Angle	Matr	h*1000	R-int/t	R-int/b	R-deg/t	R-deg/b
30	.0	3	.136	2.89	2.89	2.66	2.66
29	.0	3	.136	2.89	2.89	2.66	2.66
28	45.0	3	.136	4.76	4.76	8.22	8.22
27	90.0	3	.136	5.54	5.54	12.2	12.2
26	90.0	3	.136	5.54	5.54	12.2	12.2
25	-45.0	3	.136	4.76	4.76	8.22	8.22

Ply	Angle	Matr	h*1000	R-int/t	R-int/b	R-deg/t	R-deg/b
24	.0	3	.136	2.89	2.89	2.66	2.66
23	.0	3	.136	2.89	2.89	2.66	2.66
22	45.0	3	.136	4.76	4.76	8.22	8.22
21	-45.0	3	.136	4.76	4.76	8.22	8.22
20	.0	3	.136	2.89	2.89	2.66	2.66
19	45.0	3	.136	4.76	4.76	8.22	8.22
18	.0	3	.136	2.89	2.89	2.66	2.66
17	-45.0	3	.136	4.76	4.76	8.22	8.22
16	90.0	3	.136	5.54	5.54	12.2	12.2
15	90.0	3	.136	5.54	5.54	12.2	12.2
14	-45.0	3	.136	4.76	4.76	8.22	8.22
13	.0	3	.136	2.89	2.89	2.66	2.66
12	45.0	3	.136	4.76	4.76	8.22	8.22
11	.0	3	.136	2.89	2.89	2.66	2.66
10	-45.0	3	.136	4.76	4.76	8.22	8.22
9	45.0	3	.136	4.76	4.76	8.22	8.22
8	.0	3	.136	2.89	2.89	2.66	2.66
7	.0	3	.136	2.89	2.89	2.66	2.66
6	-45.0	3	.136	4.76	4.76	8.22	8.22
5	90.0	3	.136	5.54	5.54	12.2	12.2
4	90.0	3	.136	5.54	5.54	12.2	12.2
3	45.0	3	.136	4.76	4.76	8.22	8.22
2	.0	3	.136	2.89	2.89	2.66	2.66
1	.0	3	.136	2.89	2.89	2.66	2.66

Loadcase	FPF	Ultimate	Safety	Limit*	Limit
1	2.89	2.89	1.00	2.89	2.89

Computed First Ply Failure: 708.33 MPa
Computed Ultimate Strength: 708.33 MPa

Max-Strain Failure Criterion

Ply	Angle	Matr	h*1000	R-int/t	R-int/b	R-deg/t	R-deg/b
30	.0	3	.136	3.67	3.67	3.02	3.02
29	.0	3	.136	3.67	3.67	3.02	3.02
28	45.0	3	.136	3.99	3.99	8.67	8.67
27	90.0	3	.136	5.97	5.97	13.9	13.9

Ply	Angle	Matr	h*1000	R-int/t	R-int/b	R-deg/t	R-deg/b
26	90.0	3	.136	5.97	5.97	13.9	13.9
25	-45.0	3	.136	3.99	3.99	8.67	8.67
24	.0	3	.136	3.67	3.67	3.02	3.02
23	.0	3	.136	3.67	3.67	3.02	3.02
22	45.0	3	.136	3.99	3.99	8.67	8.67
21	-45.0	3	.136	3.99	3.99	8.67	8.67
20	.0	3	.136	3.67	3.67	3.02	3.02
19	45.0	3	.136	3.99	3.99	8.67	8.67
18	.0	3	.136	3.67	3.67	3.02	3.02
17	-45.0	3	.136	3.99	3.99	8.67	8.67
16	90.0	3	.136	5.97	5.97	13.9	13.9
15	90.0	3	.136	5.97	5.97	13.9	13.9
14	-45.0	3	.136	3.99	3.99	8.67	8.67
13	.0	3	.136	3.67	3.67	3.02	3.02
12	45.0	3	.136	3.99	3.99	8.67	8.67
11	.0	3	.136	3.67	3.67	3.02	3.02
10	-45.0	3	.136	3.99	3.99	8.67	8.67
9	45.0	3	.136	3.99	3.99	8.67	8.67
8	.0	3	.136	3.67	3.67	3.02	3.02
7	.0	3	.136	3.67	3.67	3.02	3.02
6	-45.0	3	.136	3.99	3.99	8.67	8.67
5	90.0	3	.136	5.97	5.97	13.9	13.9
4	90.0	3	.136	5.97	5.97	13.9	13.9
3	45.0	3	.136	3.99	3.99	8.67	8.67
2	.0	3	.136	3.67	3.67	3.02	3.02
1	.0	3	.136	3.67	3.67	3.02	3.02

Loadcase	FPF	Ultimate	Safety	Limit*	Limit
1	3.67	3.67	1.00	3.67	3.67

Computed First Ply Failure: 899.51 MPa
Computed Ultimate Strength: 899.51 MPa

Fiber-Strain Failure Criterion

Ply	Angle	Matr	h*1000	R-int/t	R-int/b	R-deg/t	R-deg/b
30	.0	3	.136	3.67	3.67	3.02	3.02
29	.0	3	.136	3.67	3.67	3.02	3.02
28	45.0	3	.136	10.2	10.2	8.67	8.67

Ply	Angle	Matr	h*1000	R-int/t	R-int/b	R-deg/t	R-deg/b
27	90.0	3	.136	16.2	16.2	13.9	13.9
26	90.0	3	.136	16.2	16.2	13.9	13.9
25	-45.0	3	.136	10.2	10.2	8.67	8.67
24	.0	3	.136	3.67	3.67	3.02	3.02
23	.0	3	.136	3.67	3.67	3.02	3.02
22	45.0	3	.136	10.2	10.2	8.67	8.67
21	-45.0	3	.136	10.2	10.2	8.67	8.67
20	.0	3	.136	3.67	3.67	3.02	3.02
19	45.0	3	.136	10.2	10.2	8.67	8.67
18	.0	3	.136	3.67	3.67	3.02	3.02
17	-45.0	3	.136	10.2	10.2	8.67	8.67
16	90.0	3	.136	16.2	16.2	13.9	13.9
15	90.0	3	.136	16.2	16.2	13.9	13.9
14	-45.0	3	.136	10.2	10.2	8.67	8.67
13	.0	3	.136	3.67	3.67	3.02	3.02
12	45.0	3	.136	10.2	10.2	8.67	8.67
11	.0	3	.136	3.67	3.67	3.02	3.02
10	-45.0	3	.136	10.2	10.2	8.67	8.67
9	45.0	3	.136	10.2	10.2	8.67	8.67
8	.0	3	.136	3.67	3.67	3.02	3.02
7	.0	3	.136	3.67	3.67	3.02	3.02
6	-45.0	3	.136	10.2	10.2	8.67	8.67
5	90.0	3	.136	16.2	16.2	13.9	13.9
4	90.0	3	.136	16.2	16.2	13.9	13.9
3	45.0	3	.136	10.2	10.2	8.67	8.67
2	.0	3	.136	3.67	3.67	3.02	3.02
1	.0	3	.136	3.67	3.67	3.02	3.02

Loadcase	FPF	Ultimate	Safety	Limit*	Limit
1	3.67	3.67	1.00	3.67	3.67

Computed First Ply Failure: 899.51 MPa
Computed Ultimate Strength: 899.51 MPa

Appendix D: Test Data

Plate 1 (Control Group)

Specimen Number	Area (mm^2)	Failure Load (kN)	Longitudinal Modulus (GPa)	Ultimate Strength (MPa)
1-CON-1	26.59	19.38	57.69	728.95
2-CON-1	26.31	18.68	---	709.94
3-CON-1	26.42	20.26	56.53	766.78
4-CON-1	26.68	20.79	---	779.06
5-CON-1	26.52	19.33	53.37	729.08
6-CON-1	26.47	20.65	---	780.04
7-CON-1	26.85	18.61	---	693.21
8-CON-1	26.74	20.64	---	771.89
9-CON-1	26.68	19.54	---	732.47
10-CON-1	26.52	20.32	---	766.28
AVERAGE	---	---	**55.86**	**745.77**
STD DEV	---	---	**2.24**	**31.91**
% DEV	---	---	**4.00%**	**4.28%**

Plate 1 (Central Optical Fiber Group)

Specimen Number	Area (mm^2)	Failure Load (kN)	Longitudinal Modulus (GPa)	Ultimate Strength (MPa)
1-CEN-1	26.59	18.96	54.34	708.00
2-CEN-1	26.91	18.57	---	690.16
3-CEN-1	26.31	17.93	55.60	681.33
4-CEN-1	26.53	18.33	---	690.77
5-CEN-1	26.68	19.74	53.98	739.93
6-CEN-1	26.74	18.62	---	696.45
7-CEN-1	25.49	18.34	---	706.75
8-CEN-1	25.57	19.43	---	759.87
9-CEN-1	26.46	19.10	---	722.17
10-CEN-1	26.47	18.88	---	713.24
AVERAGE	---	---	**54.64**	**712.93**
STD DEV	---	---	**0.85**	**25.94**
% DEV	---	---	**1.55%**	**3.64%**

Plate 1 (Outer Optical Fiber Group)

Specimen Number	Area (mm^2)	Failure Load (kN)	Longitudinal Modulus (GPa)	Ultimate Strength (MPa)
1-OUT-1	26.59	19.15	56.78	720.26
2-OUT-1	26.58	18.74	---	704.88
3-OUT-1	26.31	18.76	57.38	713.08
4-OUT-1	26.64	19.19	---	720.56
5-OUT-1	26.12	19.85	54.87	760.10
6-OUT-1	26.37	18.75	---	711.19
7-OUT-1	24.62	18.01	---	677.65
8-OUT-1	24.59	20.31	---	761.24
9-OUT-1	26.47	19.37	---	731.70
10-OUT-1	26.68	18.72	---	701.46
AVERAGE	---	---	**56.35**	**720.21**
STD DEV	---	---	**1.31**	**26.33**
% DEV	---	---	**2.32%**	**3.66%**

Plate 2 (Control Group)

Specimen Number	Area (mm^2)	Failure Load (kN)	Longitudinal Modulus (GPa)	Ultimate Strength (MPa)
1-CON-2	26.70	18.07	55.05	676.85
2-CON-2	26.68	17.67	---	662.32
3-CON-2	26.85	20.15	---	750.64
4-CON-2	26.85	20.43	54.39	760.91
5-CON-2	26.85	18.91	---	704.31
6-CON-2	26.59	20.73	---	779.59
7-CON-2	27.18	21.76	---	800.80
8-CON-2	26.85	19.82	55.29	743.36
9-CON-2	26.74	19.82	---	741.31
10-CON-2	27.01	18.56	---	687.03
AVERAGE	---	---	**54.91**	**730.71**
STD DEV	---	---	**0.47**	**46.03**
% DEV	---	---	**0.85%**	**6.30%**

Plate 2 (Central Optical Fiber Group)

Specimen Number	Area (mm^2)	Failure Load (kN)	Longitudinal Modulus (GPa)	Ultimate Strength (MPa)
1-CEN-2	26.68	18.27	56.79	684.64
2-CEN-2	26.68	20.88	---	782.56
3-CEN-2	26.64	19.30	54.78	724.57
4-CEN-2	26.11	18.46	---	707.14
5-CEN-2	27.34	19.17	54.65	701.07
6-CEN-2	27.07	18.00	---	665.07
7-CEN-2	27.12	18.85	---	694.99
8-CEN-2	26.68	21.46	---	804.04
9-CEN-2	27.23	18.62	---	683.77
10-CEN-2	27.06	18.79	---	694.36
AVERAGE	---	---	**55.41**	**714.22**
STD DEV	---	---	**1.20**	**46.92**
% DEV	---	---	**2.16%**	**6.57%**

Plate 2 (Outer Optical Fiber Group)

Specimen Number	Area (mm^2)	Failure Load (kN)	Longitudinal Modulus (GPa)	Ultimate Strength (MPa)
1-OUT-2	26.68	18.71	---	701.29
2-OUT-2	26.68	17.19	59.66	644.17
3-OUT-2	26.91	18.25	52.36	678.19
4-OUT-2	26.53	15.72	---	592.62
5-OUT-2	27.01	16.51	53.29	611.35
6-OUT-2	27.34	18.40	---	673.12
7-OUT-2	27.50	18.02	---	655.37
8-OUT-2	27.18	16.21	---	596.55
9-OUT-2	26.91	15.11	---	561.41
10-OUT-2	27.01	19.06	---	705.46
AVERAGE	---	---	**55.10**	**641.95**
STD DEV	---	---	**3.97**	**46.72**
% DEV	---	---	**7.21%**	**7.28%**

Plate 3 (Control Group)

Specimen Number	Area (mm^2)	Failure Load (kN)	Longitudinal Modulus (GPa)	Ultimate Strength (MPa)
1-CON-3	25.50	21.92	56.19	859.52
2-CON-3	25.44	20.46	---	804.14
3-CON-3	24.98	19.55	---	782.92
4-CON-3	25.08	18.65	54.69	743.64
5-CON-3	25.41	19.76	---	777.58
6-CON-3	24.85	17.93	---	721.58
7-CON-3	25.41	20.20	---	795.07
8-CON-3	25.11	19.32	57.63	769.28
9-CON-3	25.41	20.62	---	811.68
10-CON-3	25.11	19.60	---	780.60
AVERAGE	---	---	**56.17**	**784.60**
STD DEV	---	---	**1.47**	**39.96**
% DEV	---	---	**2.62%**	**5.09%**

Plate 3 (Two Optical Fiber Group)

Specimen Number	Area (mm^2)	Failure Load (kN)	Longitudinal Modulus (GPa)	Ultimate Strength (MPa)
1-TWO-3	25.81	21.49	56.42	832.60
2-TWO-3	25.08	18.54	---	739.39
3-TWO-3	25.87	18.60	58.96	718.78
4-TWO-3	24.81	19.09	---	769.20
5-TWO-3	25.37	18.53	56.69	730.34
6-TWO-3	24.49	20.18	---	823.95
7-TWO-3	25.54	20.31	---	795.17
8-TWO-3	24.49	18.61	---	759.72
9-TWO-3	25.04	20.72	---	827.40
10-TWO-3	24.53	19.23	---	784.05
AVERAGE	---	---	**57.36**	**778.06**
STD DEV	---	---	**1.39**	**44.02**
% DEV	---	---	**2.43%**	**5.66%**

Plate 3 (Three Optical Fiber Group)

Specimen Number	Area (mm^2)	Failure Load (kN)	Longitudinal Modulus (GPa)	Ultimate Strength (MPa)
1-THR-3	25.34	20.04	57.86	791.02
2-THR-3	26.04	19.76	---	758.89
3-THR-3	25.08	20.67	53.17	824.46
4-THR-3	25.97	19.26	---	741.34
5-THR-3	25.71	19.66	---	764.94
6-THR-3	24.65	19.24	55.62	780.35
7-THR-3	25.28	19.46	---	769.74
8-THR-3	24.69	18.51	---	749.73
9-THR-3	25.28	20.42	---	808.07
10-THR-3	24.75	20.82	---	841.34
AVERAGE	---	---	**55.55**	**782.99**
STD DEV	---	---	**2.35**	**27.31**
% DEV	---	---	**4.23%**	**3.49%**

Plate 4 (Control Group)

Specimen Number	Area (mm^2)	Failure Load (kN)	Longitudinal Modulus (GPa)	Ultimate Strength (MPa)
1-CON-4	24.23	20.09	59.87	829.23
2-CON-4	24.65	17.52	---	710.77
3-CON-4	24.23	19.88	57.83	820.42
4-CON-4	24.23	18.45	---	761.55
5-CON-4	23.88	18.60	57.13	778.95
6-CON-4	24.32	19.18	---	788.34
7-CON-4	23.97	17.32	---	722.67
8-CON-4	24.16	18.15	---	751.21
9-CON-4	24.72	18.15	---	734.19
10-CON-4	23.88	19.66	---	823.25
AVERAGE	---	---	**58.28**	**772.06**
STD DEV	---	---	**1.42**	**41.54**
% DEV	---	---	**2.44%**	**5.38%**

Plate 4 (Two Optical Fiber Group)

Specimen Number	Area (mm^2)	Failure Load (kN)	Longitudinal Modulus (GPa)	Ultimate Strength (MPa)
1-TWO-4	24.10	13.76	59.23	570.97
2-TWO-4	23.62	12.78	---	541.12
3-TWO-4	23.78	13.28	61.18	558.37
4-TWO-4	25.21	13.03	---	516.92
5-TWO-4	24.44	14.19	56.72	560.27
6-TWO-4	24.27	13.11	---	540.43
7-TWO-4	25.54	14.31	---	560.27
8-TWO-4	24.04	15.14	---	629.86
9-TWO-4	25.20	13.03	---	516.94
10-TWO-4	25.21	15.78	---	625.87
AVERAGE	---	---	**59.04**	**564.14**
STD DEV	---	---	**2.24**	**35.02**
% DEV	---	---	**3.79%**	**6.21%**

Plate 5 (Control Group)

Specimen Number	Area (mm^2)	Failure Load (kN)	Longitudinal Modulus (GPa)	Ultimate Strength (MPa)
1-CON-5	26.19	20.05	57.28	765.34
2-CON-5	26.52	19.85	---	748.35
3-CON-5	26.19	20.46	---	780.95
4-CON-5	26.36	20.18	56.26	765.47
5-CON-5	26.46	20.55	---	776.58
6-CON-5	25.82	20.30	---	786.24
7-CON-5	26.19	19.58	---	747.69
8-CON-5	26.25	21.78	54.67	829.78
9-CON-5	26.09	20.27	---	777.05
10-CON-5	26.36	19.91	---	755.53
AVERAGE	---	---	**56.07**	**773.30**
STD DEV	---	---	**1.31**	**24.52**
% DEV	---	---	**2.34%**	**3.17%**

Plate 5 (Three Optical Fiber Group)

Specimen Number	Area (mm^2)	Failure Load (kN)	Longitudinal Modulus (GPa)	Ultimate Strength (MPa)
1-THR-5	25.97	15.70	55.84	604.62
2-THR-5	26.03	15.07	---	578.94
3-THR-5	26.46	14.72	54.56	556.24
4-THR-5	26.36	18.60	---	705.79
5-THR-5	26.13	16.64	55.91	636.87
6-THR-5	26.03	15.43	---	592.60
7-THR-5	26.46	16.85	---	636.85
8-THR-5	25.76	16.76	---	650.62
9-THR-5	26.30	16.37	---	622.58
10-THR-5	26.52	17.44	---	657.70
AVERAGE	---	---	**55.44**	**624.28**
STD DEV	---	---	**0.76**	**44.17**
% DEV	---	---	**1.37%**	**7.08%**

Plate 6 (Control Group)

Specimen Number	Area (mm^2)	Failure Load (kN)	Longitudinal Modulus (GPa)	Ultimate Strength (MPa)
1-CON-6	27.94	21.73	---	777.62
2-CON-6	27.88	20.58	---	737.88
3-CON-6	27.88	21.26	---	762.27
4-CON-6	27.88	20.70	---	742.51
5-CON-6	27.83	19.25	---	691.80
6-CON-6	27.88	21.56	---	773.11
7-CON-6	27.88	21.28	---	763.07
8-CON-6	27.88	21.25	---	762.11
9-CON-6	27.88	20.51	---	735.66
10-CON-6	27.99	21.69	---	774.86
AVERAGE	---	---	---	**752.09**
STD DEV	---	---	---	**26.36**
% DEV	---	---	---	**3.50%**

Plate 6 (Two Optical Fiber Group)

Specimen Number	Area (mm^2)	Failure Load (kN)	Longitudinal Modulus (GPa)	Ultimate Strength (MPa)
1-TWO-6	27.55	19.90	---	722.05
2-TWO-6	27.66	21.51	---	777.55
3-TWO-6	27.72	20.47	---	738.59
4-TWO-6	27.88	22.59	---	810.45
5-TWO-6	27.72	21.90	---	789.89
6-TWO-6	27.94	23.27	---	833.08
7-TWO-6	27.39	20.73	---	756.90
8-TWO-6	27.94	20.60	---	737.48
9-TWO-6	27.60	22.03	---	798.04
10-TWO-6	27.50	19.56	---	711.45
AVERAGE	---	---	---	**767.55**
STD DEV	---	---	---	**37.48**
% DEV	---	---	---	**4.88%**

Plate 6 (Three Optical Fiber Group)

Specimen Number	Area (mm^2)	Failure Load (kN)	Longitudinal Modulus (GPa)	Ultimate Strength (MPa)
1-THR-6	27.56	19.81	---	718.74
2-THR-6	27.88	20.86	---	748.43
3-THR-6	28.10	21.46	---	763.63
4-THR-6	27.44	20.57	---	749.75
5-THR-6	27.12	19.62	---	723.67
6-THR-6	27.94	21.41	---	766.43
7-THR-6	27.50	19.95	---	725.34
8-THR-6	27.18	19.61	---	721.65
9-THR-6	27.83	20.02	---	719.59
10-THR-6	27.34	19.96	---	730.17
AVERAGE	---	---	---	**736.74**
STD DEV	---	---	---	**19.53**
% DEV	---	---	---	**2.65%**

Bibliography

[1] Lees, J. K., "Advanced Composites are Earning Their Wings", Mechanical Engineering, April 1988, pp 50-53.

[2] Green, S., "Aspects of Compression in Aerospace Composites - Future Requirements", AGARD, 1991.

[3] Talat, K., "Smart Skins and Fiber Optic Sensor Application and Issues", Fiber Optic Smart Structures and Skins III, SPIE Volume 1370, 1990, pp 103-114.

[4] Rogers, C. A., "Intelligent Material Systems and Structures", US/Japan Workshop on Smart/Intelligent Materials and Systems, 1990, pp 11-18.

[5] Barrick, M. D., "Producibility and Life Cycle Cost Issues in Applications of Embedded Fiber Optic Sensors in Smart Skins", Fiber Optic Smart Structures and Skins, SPIE Volume 986, 1988, pp 171-179.

[6] Sendeckyj, G. P. and Paul, C. A., "Some Smart Structures Concepts", Fiber Optic Smart Structures and Skins II, SPIE Volume 1170, 1989, pp 2-10.

[7] Australian Defense Report, Technical Report 607, Aeronautical Research Laboratory, Melbourne, Australia, 1991, pp 7-8.

[8] Measures, R. M., "Fiber Optic Smart Structures Program at UTIAS", Fiber Optic Smart Structures and Skins II, SPIE Volume 1170, 1989, pp 92-108.

[9] Measures, R. M., "Advances Toward Fiber Optic Based Smart Structures", Optical Engineering, Volume 31, Number 1, 1992, pp 34-46.

[10] Carman, G. P. and Sendeckyj, G. P., "Review of the Mechanics of Embedded Optical Sensors", unpublished, 1993

[11] Claus, R. O., Bennett, K. D. and Jackson, B. S., "Nondestructive Evaluation of Composite Materials by Pulsed Time Domain Methods in Imbedded Optical Fibers", Review of Progress in Quantitative Nondestructive Evaluation, Volume 5B, 1985, pp 1149-1156.

[12] Measures, R. M. , Glossop, N. D. W., Lymer, J., Leblanc, M., West, J., Dubois, S., Tsaw, W. and Tennyson, R. C., "Structurally Integrated Fiber Optic Damage Assessment Systems for Composite Materials", Applied Optics, Volume 28, 1989, pp 2626-2633.

[13] Jensen, D. W., Pascual, J. and August, J. A., "Performance of Graphite/ Bismaleimide Laminates with Embedded Fiber Optic Sensors. Part 1: Uniaxial Tension", Smart Materials and Structures, Volume 1, 1992, pp 24-30.

[14] Jensen, D. W., Pascual, J. and August, J. A., "Performance of Graphite/ Bismaleimide Laminates with Embedded Fiber Optic Sensors. Part 2: Uniaxial Compression", Smart Materials and Structures, Volume 1, 1992, pp 31-35.

[15] Roberts, S. S. and Davidson, R., "Mechanical Properties of Composite Materials Containing Embedded Fibre Optic Sensors", Fiber Optic Smart Structures and Skins IV, SPIE Volume 1588, 1991, pp 326-341.

[16] Holl, M. and Boyd, S., "The Effect of Embedded Fiber Optics on the Mechanical Properties of a Composite Host Material", Smart Materials, SPIE Volume 1916, 1993.

[17] Dasgupta, A., Wan, Y., Sirkis, J. S., and Singh, H., "Micro-mechanical Investigation of an Optical Fiber Embedded in a Laminated Composite", Fiber Optic Smart Structures and Skins III, SPIE Volume 1370, 1990, pp 119-128.

[18] Leka, L. G. and Bayo, E., "A Close Look at the Embedment of Optical Fibers into Composite Structures", Journal of Composites Technology and Research, Volume 11, Number 3, 1989, pp 106-112.

[19] Czarnek, R., Guo, Y. F., Bennett, K. D., and Claus, R. O., "Interferometric Measurements of Strain Concentrations Induced by and Optical Fiber Embedded in a Fiber Reinforced Composite", Fiber Optic Smart Structures and Skins, SPIE Volume 986, 1989, pp 43-54

[20] Salehi, A., Tay, A., Wilson, D. A., and Smith, D. G., "Strain Concentrations Around Embedded Optical Fibers by FEM and Moiré Interferometry", Design and Manufacturing of Advanced Composites, 5th ASM/ESD Conference, 1989, pp 11-19.

[21] Singh, H., Sirkis, J. S. and Dasgupta, A., "Micro-Interaction of Optical Fibers Embedded in Laminated Composites", Fiber Optic Smart Structures and Skins IV, SPIE Volume 1588, 1991, pp 76-85.

[22] Davidson, R. and Roberts, S. S. J., "Finite Element Analysis of Composite Laminates Containing Transversely Embedded Optical Fiber Sensors", First European Conference on Smart Structures and Materials, SPIE Volume 1777, 1992, pp 115-122.

[23] Martin, D. A., "Optical Fiber Coating Evaluations for Composites Embedment Applications", Materials Research Society Symposium Proceedings, Volume 88, 1987, pp 19-26.

[24] Urruti, E. H., Hawk, R. M., and Blaszyk, P. E., "Optical Fibers for Structural Sensing Applications", Fiber Optic Smart Structures and Skins, SPIE Volume 986, 1988, pp 158-163.

[25] Nath, D. K., Nelson, G. W., Griffin, S. E., Harrington, C. T., He, Y., Reinhart, L. J., Paine, D. C., and Morse, T. F., "Polyimide Coated Embedded Optical Fiber Sensors", Structures Sensing and Control, SPIE Volume 1489, 1991, pp 17-32.

[26] DiFranca, C. and Claus, R. O., "Structure/Property Correlation of Several Polyimide Optical Fiber Coatings for Embedding in an Epoxy Matrix", Fiber Optic Smart Structures and Skins II, SPIE Volume 1170, 1989, pp 505-512.

[27] Camponeschi, E. T., "Compression of Composite Materials: A Review", Composite Materials: Fatigue and Fracture (Third Volume), ASTM STP 1110, 1991, pp 550-578.

[28] Colvin, G. E., and Swanson, S. R., "In-Situ Compressive Strength of Carbon/ Epoxy AS4/3501-6 Laminates", Journal of Engineering Materials and Technology, Volume 115, January 1993, pp 122-128.

[29] Ha, J. B., and Nairn, J. A., "Compression Failure Mechanisms of Single-Ply, Unidirectional, Carbon-Fiber Composites", SAMPE Quarterly, April 1992, pp 29-36.

[30] Sohi, M. M., Hahn, H. T., and Williams, J. G., "The Effect of Resin Toughness and Modulus on Compressive Failure Modes of Quasi-Isotropic Graphite/Epoxy Laminates", Toughened Composites, ASTM STP 937, 1985, pp 37-60.

[31] Telegades, H. K., and Hyer, M. W., "The Influence of Layer Waviness on the Stress State and Failure in Composite Laminates", Journal of Reinforced Plastics and Composites, Volume 9, Number 5, 1990, pp 503-518.

[32] Adams, D. O., and Hyer, M. W., "Fabrication and Compression Testing of Layer Waviness in Thermoplastic Composite Laminates", 36th International SAMPE Symposium, pp 1094-1108.

[33] ASTM Standard D3410-88, "Standard Test Method for Compressive Properties of Unidirectional or Crossply Fiber-Resin Composites", American Society for Testing and Materials, 1989.

[34] Timoshenko, S. P. and Gere, J. M., Theory of Elastic Stability, McGraw Hill Book Company Inc., New York, 1961, pp 132.

[35] Jones, Robert M., Mechanics of Composite Materials, Hemisphere Publishing Corporation, 1975.

[36] Agarwal, Bhagwan D. and Broutman, Lawrence J., Analysis and Performance of Fiber Composites, Second Edition, John Wiley and Sons Inc., 1990.

[37] Lee, S., "Lamination Theory", International Encyclopedia of Composites, Volume 3, pp 44-55, 1991.

[38] Tsai, Stephen W., Composites Design, 4th Edition, Think Composites, Dayton, Ohio, 1988.

[39] Hercules Advanced Materials and Systems Company, "Hercules Carbon Prepreg Tape AS4/3501-6 Product Data Sheet", Number 843-4, August 1991.

[40] ASTM Standard D3171-82, "Standard Test Method for Fiber Content of Resin-Matrix Composites by Matrix Digestion", American Society for Testing and Materials, 1982.

[41] Bearden, Keith L., "Behavior of a Titanium Matrix Composite under Quasi-Static Tensile and Compressive Loading, Masters Thesis, AFIT/GAE/ENY/92D-07, School of Engineering, Air Force Institute of Technology, Wright-Patterson AFB, Ohio, December 1992.

[42] Sirkis, J. S. and Dasgupta, A., "The Role of Local Interaction Mechanics in Fiber Optic Smart Structures", Journal of Intelligent Material Systems and Structures, Volume 4, April 1993.

Vita

Captain Stefan B. Dosedel was born on 5 April 1966 in Vicenza, Italy. He graduated from Lakenheath American High School, RAF Lakenheath, England in June 1984. He was awarded a four year Air Force ROTC Scholarship and attended the University of Notre Dame from 1984 through 1988 and graduated with a Bachelor of Science Degree in Mechanical Engineering. Upon completing his undergraduate degree, he was commissioned into the Air Force.

Captain Dosedel was assigned to the Western Space and Missile Center (WSMC) at Vandenberg AFB, California. His initial duties included designing and constructing $5M in modifications to the only operational hypergolic rocket propellant storage facility in the United States. After completion of these modifications, he assumed the management of a $27M contract for operations and maintenance of these facilities. These facilities were critical to the successful staging and launch of several Titan and Delta rockets from this west coast facility during Captain Dosedel's tenure at Vandenberg AFB.

Captain Dosedel entered the School of Engineering, Air Force Institute of Technology, in May 1992.

REPORT DOCUMENTATION PAGE

Form Approved
OMB No. 0704-0188

Public reporting burden for this collection of information is estimated to average 1 hour per response, including the time for reviewing instructions, searching existing data sources, gathering and maintaining the data needed, and completing and reviewing the collection of information. Send comments regarding this burden estimate or any other aspect of this collection of information, including suggestions for reducing this burden to Washington Headquarters Services, Directorate for Information Operations and Reports, 1215 Jefferson Davis Highway, Suite 1204, Arlington, VA 22202-4302, and to the Office of Management and Budget, Paperwork Reduction Project (0704-0188), Washington, DC 20503

1. AGENCY USE ONLY (Leave blank)	2. REPORT DATE	3. REPORT TYPE AND DATES COVERED
	December 1993	Master's Thesis

4. TITLE AND SUBTITLE

THE INFLUENCE OF EMBEDDED OPTICAL FIBERS ON COMPRESSIVE STRENGTH OF ADVANCED COMPOSITES

5. FUNDING NUMBERS

6. AUTHOR(S)

Stefan B. Dosedel, Captain, USAF

7. PERFORMING ORGANIZATION NAME(S) AND ADDRESS(ES)

Air Force Institute of Technology, WPAFB OH 45433-6583

8. PERFORMING ORGANIZATION REPORT NUMBER

AFIT/GAE/ENY/93D-12

9. SPONSORING/MONITORING AGENCY NAME(S) AND ADDRESS(ES)

Michael Holl, Captain, USAF
WL/MLBC
Wright Patterson AFB, OH 45433

10. SPONSORING/MONITORING AGENCY REPORT NUMBER

11. SUPPLEMENTARY NOTES

12a. DISTRIBUTION/AVAILABILITY STATEMENT

Approved for public release; distribution unlimited

12b. DISTRIBUTION CODE

13. ABSTRACT *(Maximum 200 words)*

This study investigated the effects of embedding optical fibers into advanced composite materials. This combination was meant to simulate "smart structures" that have been shown to sense several different variables in the composite including strain, temperature, and damage. A laminate orientation taken from an existing aircraft structure was used to fabricate sixteen groups of specimens which were subjected to compression testing in an IITRI fixture to determine the ultimate compressive strength and modulus of elasticity. Ten of these groups were fabricated with optical fibers while the other six were control groups and contained no optical fibers. This study showed that varying the number of embedded optical fibers, optical fiber size, optical fiber orientation, and optical fiber location in the composite structure can reduce the compressive strength of the structure by up to 27%. This maximum degradation occurred when multiple optical fibers were placed perpendicular to the composite structural fibers. No deleterious effects were seen when the optical fiber was placed parallel to the composite structural fibers. No change in modulus of elasticity was seen for any of the groups tested.

14. SUBJECT TERMS

Smart Structures, Smart Materials, Compression, Fiber Waviness, Composites, Optical Fibers, Graphite/Epoxy, AS4/3501-6, Adhesion, Resin eye

15. NUMBER OF PAGES

130

16. PRICE CODE

17. SECURITY CLASSIFICATION OF REPORT	18. SECURITY CLASSIFICATION OF THIS PAGE	19. SECURITY CLASSIFICATION OF ABSTRACT	20. LIMITATION OF ABSTRACT
Unclassified	Unclassified	Unclassified	UL